Control of photophysical properties of porphyrin derivatives by localized surface plasmon resonance of metal nanoparticles

金属ナノ粒子の局在表面プラズモン共鳴による

ポルフィリン誘導体の光物理特性制御

Dissertation

Department of Materials and Applied Chemistry,
Graduate School of Science and Technology,
Nihon University

2020

Naoto Takeshima
Supervised by Prof. Joe Otsuki

Contents

Abbreviations

Name	Abbreviation
Ammonia	NH_3
Atomic force microscopy	AFM
Boundary element method	BEM
Dimethylformamide	DMF
Dye-sensitized solar cell	DSSC
Enhancement factor	EF
Hydrogen peroxide	H_2O_2
Incident photon to current efficiency	IPCE
Induced transparency	IT
Internal conversion	IC
Intersystem crossing	ISC
Light-emitting diode	LED
Localized surface plasmon	LSP
Metal nanoparticle	MNP
Near-infrared region	NIR
Photodynamic therapy	PDT
Poly(vinyl pyrrolidone)	PVP
Polyethylene imine	PEI
Polymethyl methacrylate	PMMA
Polystyrene sulfonate	PSS
Scanning electron microscopy	SEM
Silver nanoprism	AgPR
Silver nitrate	$AgNO_3$
Sodium borohydride	$NaBH_4$
Sodium hydroxide	NaOH
Tetraphenyl porphyrin	TPP
Transmission electron microscopy	TEM
Triplet-triplet annihilation	TTA

Chapter 1

Introduction

1-0. General Introduction

Society faces the unprecedented environmental issues including the global warming and the depletion of the fossil fuel, thus, utilizing the optoelectronic devices driven under the sun, which is an inexhaustible energy source, has been focused. Scientists have designed and synthesized photofunctional materials for the high-performance devices. To control photoreactions at a nanoscale dimension freely has been recognized as one of the approaches for the improvement of the performance of the devices further. Under such the background, metal nanoparticles have attractive much attention owing to their peculiar ability that confine the light at a nanospace below diffraction limit. Significant improvement of the optoelectronic devices has been demonstrated by introducing the metal nanoparticles into them. In recent years, it has been shown that the hybridization of the photofunctional materials and the metal nanoparticles exhibit newly photochemical reactions. By utilizing the metal nanoparticles, the modern society will exceed the technological limits in the future.

1-1. Photophysical Process of Porphyrins as Photosensitizers

Porphyrins have a structure similar to chlorophylls used in the natural photosynthesis and are widely used as photosensitizers in optoelectronic devices including solar cells, [1] photocatalysts, [2] and in photochemical reactions including photodynamic therapy (PDT) [3] and photon up-conversion via triplet-triplet annihilation (TTA). [4] These light-driven systems depend on basic photophysical processes of porphyrins including a photoexcitation, an internal conversion (IC), an emission (fluorescence or phosphorescence) and an intersystem crossing (ISC). These processes can be described in Jablonski diagram (**Figure 1-1**).
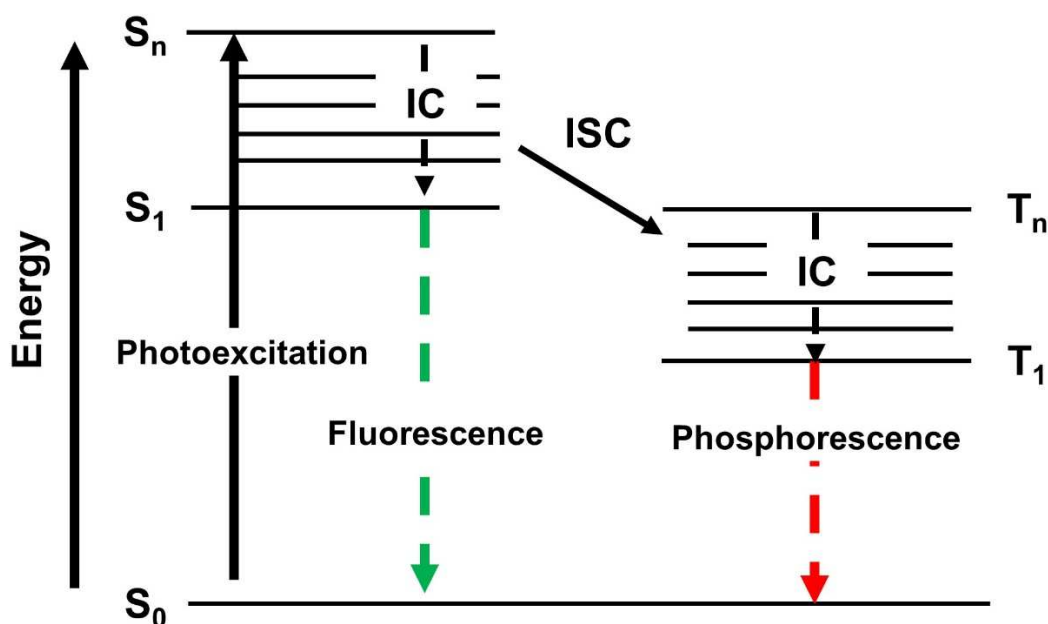

Figure 1-1. Jablonski diagram for basic photophysical processes.

Porphyrins absorb irradiated photons corresponding to their energy gap, leading to the photoexcitation from the energetically lower singlet ground state (S_0) to the higher excited singlet state (S_n). The higher excited state is rapidly deactivated non-radiatively via IC and transit to the lowest excited singlet state (S_1), followed by emitting photons (fluorescence). Series of these energy flows occur in the several to several ten nanoseconds generally. If a rate of ISC, which is a spin-forbidden transition, is fast decay process, the transition from S_n to T_n becomes possible. Likewise, higher energies of T_n are deactivated via IC, followed by emitting phosphorescence from the lowest excited triplet state (T_1). In general, the transition from the singlet state to the triplet state is a very slow process because this process leads a change in spin-multiplicity of electrons.

However, if a heavy metal such as ruthenium, palladium, and platinum is introduced into the center of the porphyrin skeleton, ISC becomes fast process owing to the strong spin-orbit coupling by the heavy metal effect. Since the transition from the triplet state to the singlet state is also the spin-forbidden, the lifetime of the excited triplet state is longer (several millisecond) than that of the excited singlet state (several nanosecond).

An optical property of porphyrins has been known to be affected by various factors including a length of π-conjugated chain, [5] a polarity in the solvent, [6] an aggregation state, [7] a kind of the heavy metal in the core, [8] and so on. In fact, an incident photon to current efficiency (IPCE) was improved from dye-sensitized solar cells (DSSCs) based on porphyrins bearing π-conjugated cyclic aromatic hydrocarbons. [9] An extension of π-conjugation makes an absorption wavelength of porphyrins to longer and wider wavelength regions. Therefore, solar cells can harvest photons on broadband wavelength regions, leading to an increase in photocurrents. Controlling the optical property of porphyrins is an important research subject for the development of high-efficiency light driven devices.

1-2. Localized Surface Plasmon Resonance of Noble Metal Nanoparticles

Unlike a bulk metal, noble metal nanoparticles (MNPs) exhibit a unique optical property. [10] When the MNPs resonant with an external electromagnetic field such as the light, a collective oscillation of free electrons in the conduction band results from an excitation of a LSP resonance (**Figure 1-2**).
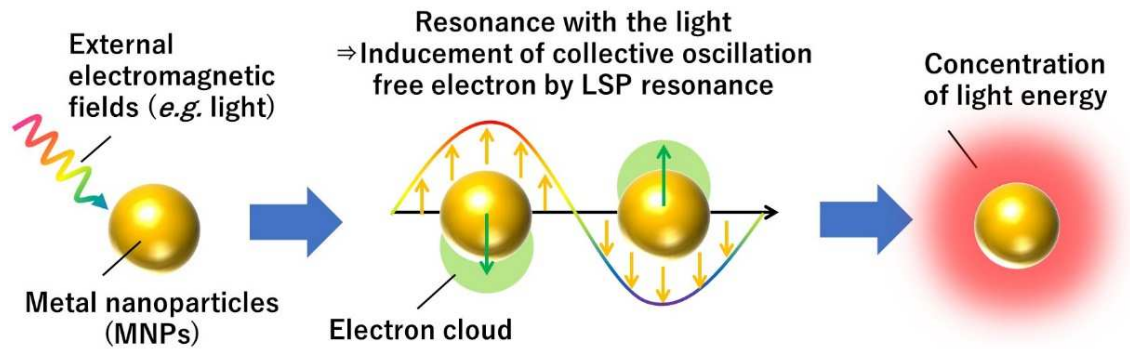

Figure 1-2. Cartoon of the electromagnetic fields induced by the LSP resonance.

Irradiated photons are confined to a space below several nanometer on the surface of the MNPs, thus, strength of these electromagnetic fields (E-fields) induced by the LSP gets stronger than that of the external fields.

Now, by using a wavelength-dependent dielectric constant of the MNPs (ε_1) and a surrounding medium (ε_2), the polarizability ($\boldsymbol{\alpha}$) of the MNPs with the radius a can be written as equation (1,2) [10,11]

$$\boldsymbol{\alpha} = g_d a^3 \cdot \cdot \cdot (1)$$

$$g_d = \frac{\varepsilon_1(\omega) - \varepsilon_2}{\varepsilon_1(\omega) + 2\varepsilon_2} \cdot \cdot \cdot (2)$$

Also, the electric field of the incident electromagnetic wave can be denoted by the vector E_0 in the x direction, leading to $E_0 = E_0 \hat{\boldsymbol{x}}$, where $\hat{\boldsymbol{x}}$ is a unit vector. If a is much smaller than the wavelength, by solving Maxwell's equations, the E-field around the surface of the MNP is given by equation (3) [10, 11]

$$E_{out} = E_0\hat{x} - \alpha E_0\left[\frac{\hat{x}}{r^3} - \frac{3x}{r^5}(x\hat{x} + y\hat{y} + z\hat{z})\right] \cdot \cdot \cdot (3)$$

Furthermore, by using the eq.1, absorption cross section (C_{abs}) and scattering cross section (C_{scat}) can be written in equations (4) and (5), respectively,

$$C_{abs} = 4x\text{Im}(g_d) \cdot \cdot \cdot (4)$$

$$C_{sca} = \frac{8}{3}x^4|g_d|^2 \cdot \cdot \cdot (5)$$

Here, $x = 2\pi a(\varepsilon_0)^{1/2}/\lambda$, where ε_0 is the dielectric constant in a vacuum. From these equations, it can be seen that the dielectric constants and polarizability are important parameters to determine the property of absorption and scattering and the strength of the E-fields around the MNPs.

It has been discovered that the optical property of photofunctional materials, which are positioned in the fields induced by the LSP resonance, can be variously altered. By regarding this strong E-fields as the strong light-matter interaction space, an attempt to control and improve the optical property of photofunctional materials has been conducting.

1-3. Plasmonic Materials

1-3-1. Anisotropic Silver Nanoplate

The E-field intensity, induced by the LSP excitation, is affected by several structural parameters such as the shape (sphere, rod, cube, star, and prism), the size (small and large), and the kind of metals (Au, Ag, Cu and Al) (**Figure 1-3**). [10]
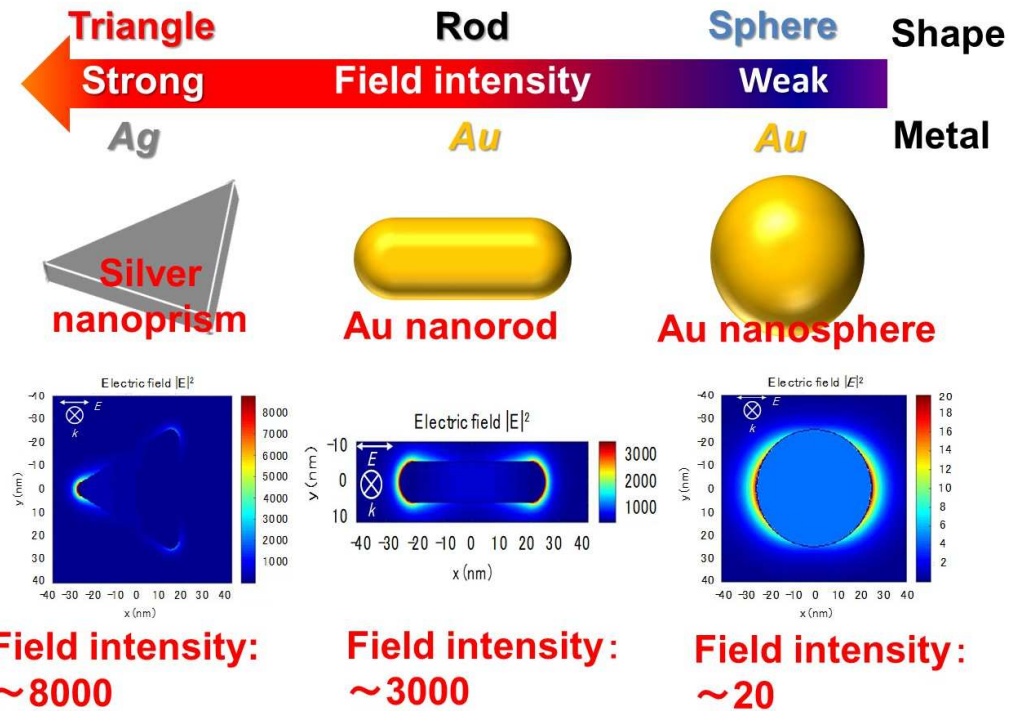
Figure 1-3. Dependence of the field intensity on several structural parameters.

The E-field has been confined and the intensity of that has been strengthened at a point having higher curvature (lightning rod effect). [10] Among various plasmonic materials, an anisotropic silver nanoplate, silver nanoprisms (AgPRs) show very intense E-fields at its corners (**Figure 1-3**). [12] In addition, the LSP of AgPRs can be excited over broad wavelength regions from visible to near-infrared region (NIR) by changing an aspect ratio of an edge length to a thickness of AgPRs (**Figure 1-4**). [13] These facts derived from the small imaginary part (which hinder the electron motion, leading to Ohmic loss) of the dielectric function of silver in the wavelength regions. [14]
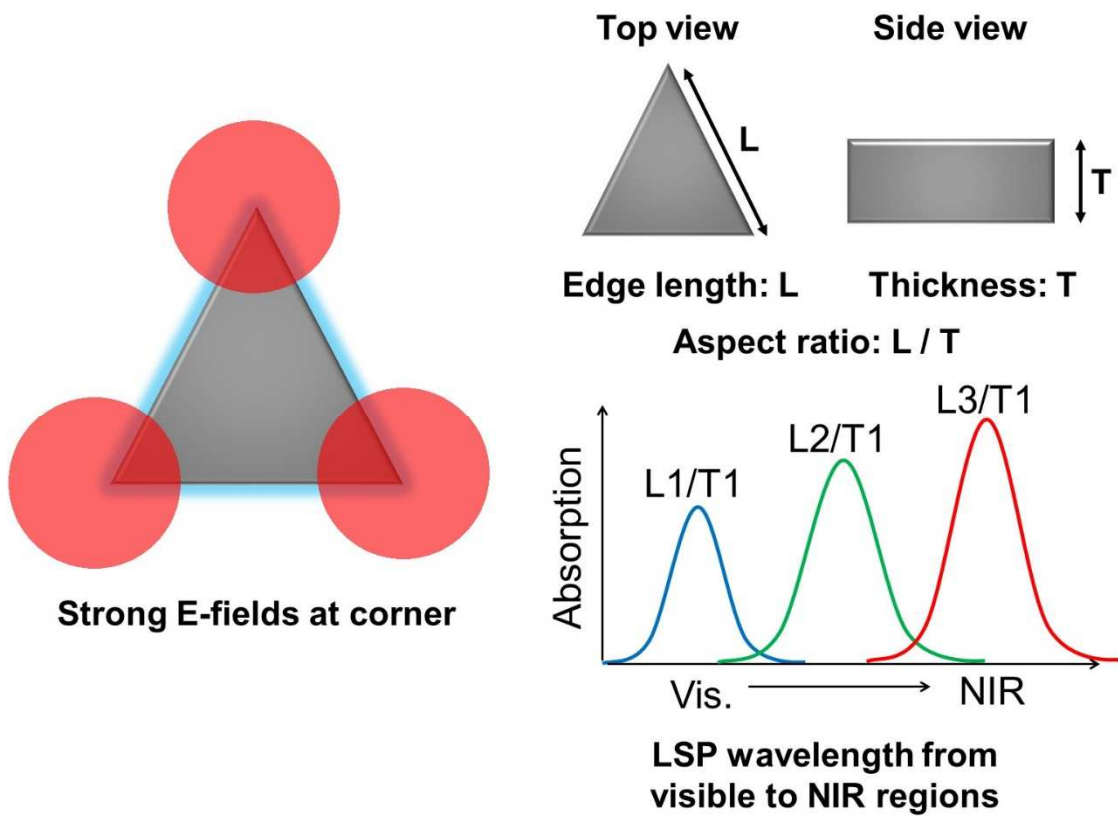
Figure 1-4. Morphological and optical feature of AgPRs.

1-3-2. Chemical Synthesis

The LSP expression wavelength of AgPRs can be controlled by changing the aspect ratio. [12] Thus, excellent synthetic methods focused on controlling the shape of AgPRs have been reported in the field of colloidal chemistry. Xinyi et al. developed a stepwise reduction method by using sodium borohydride (NaBH₄) and trisodium citrate, in which strict surfactants and capping agents were not required. [15] However, their synthetic approach could not control the size of AgPRs and the LSP band was broad. These facts were detrimental to be used in the application. Aherne et al. demonstrated a highly reproducible and rapid preparation method of AgPRs. [16] First, silver seeds are prepared in an aqueous media by combining trisodium citrate (as a stabilizer), poly(sodium styrenesulphonate) (as a stabilizer), sodium borohydride (as a reducing agent), and silver nitride (as a silver source). Next, various quantities of seed solution containing ascorbic acid are added to an aqueous solution of silver nitride, leading to the formation of the various AgPRs with different edge length (**Figure 1-5**). Haber et al. reported that a scalable and refined protocol for the synthesis of AgPRs with different sizes by optimizing the experimental condition. [17] Also, Pastoriza-Santos et al. synthesized the AgPRs using poly(vinyl pyrrolidone) (PVP) in N, N-dimethylformamide (DMF). [18] This method makes AgPRs possible to disperse in different organic solvents. Various synthesis methods enable AgPRs to use in the wide applications.
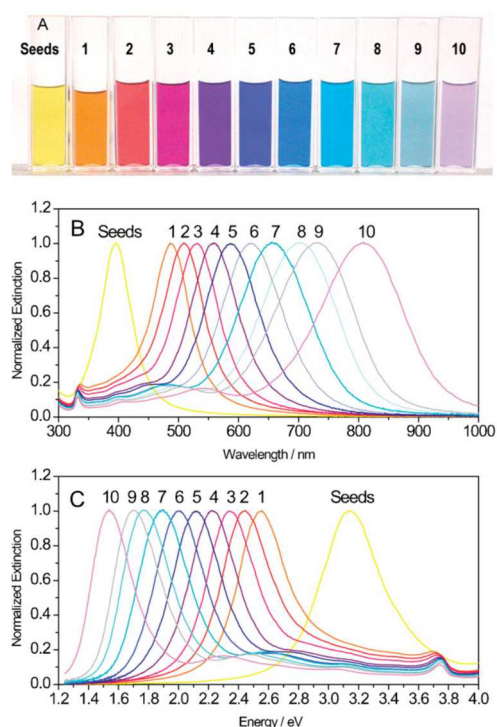

Figure 1-5. Photograph and normalized extinction spectra reported by Ref. [17].

1-3-3. Plasmon-Mediated Photochemical Synthesis

In 2001, Jin et al. developed a photoinduced synthesis of AgPRs for the first time. [19] They found that when an aqueous solution of citrate-stabilized Ag nanospheres with a diameter below 10 nm was irradiated with a conventional light, its spherical shape turned to triangle one. Also, it has been demonstrated that LSP excitation is an important role in the photoinduced synthesis. Procedure of the plasmon-mediated photochemical synthesis have been proposed as below. [20-22]

Step 1: An aqueous solution of citrate-stabilized Ag nanospheres with a diameter 10 nm is irradiated with the light which the LSP can be excited.

Step 2: After the deactivation of the LSP, hot holes and hot electrons are generated in the Ag nanosphere. The hot holes oxidize capping agents adsorbed on the surface of the Ag nanosphere, which makes the Ag nanosphere to an electron rich state. At the same stage, a part of the Ag nanosphere is also photo-oxidized by dissolved oxygen species, resulting in Ag^+ ($Ag + 1/2\ O_2 + H_2O \rightarrow Ag^+ + 2OH^-$).

Step 3: Excess amounts of electrons reduce Ag+, subsequently, Ag^0 are formed and consumed by an anisotropic growth, resulting in the formation of AgPRs.

Xue and Mirkin controlled the size of AgPRs by changing the pH of colloidal aqueous solution of Ag and selecting the wavelength of the irradiation light. [23] By adding an aqueous solution of sodium hydroxide (NaOH) into the Ag colloidal aqueous solution to make hard acidic condition, interparticle electrostatic repulsion becomes strong. This suppresses a fusion process of AgPRs, resulting in the formation of smaller sized AgPRs. In contrast, in the case without adjusting the pH, AgPRs growth slowly until they cannot absorb photons, resulting in the formation of larger sized AgPRs. Furthermore, they found that the correlation in the irradiation wavelength and the size of AgPRs formed by corresponding irradiation light. This excellent approach enables us to synthesize AgPRs showing LSP band on wide wavelength range from 500 to over 1200 nm.

The plasmon-mediated photochemical synthesis method have advantageous including high reproducibility, narrow particle size distribution. In addition to that, no need to use the strong stabilizer such as cetyltrimethylammonium bromide is important. It is because the stabilizer strongly binds to the surface of AgPRs, making the modification of the surface functionality of AgPRs difficult. [24] AgPRs will be widely used for the improvement of device performances and for the study of light-matter interaction.

1-4. Effect of LSP on Optical Property

When fluorophores (*e.g.* quantum dots, organic molecules, carbon materials) are positioned in the E-fields induced by the LSP, as well as the LSP bands overlap with the absorption or emission bands of the fluorophores, leading to the modification of an excitation efficiency and a radiative decay process. [25] These mechanisms can be described as shown in **Figure 1-6** and are depicted in **Figure 1-7.** [26]
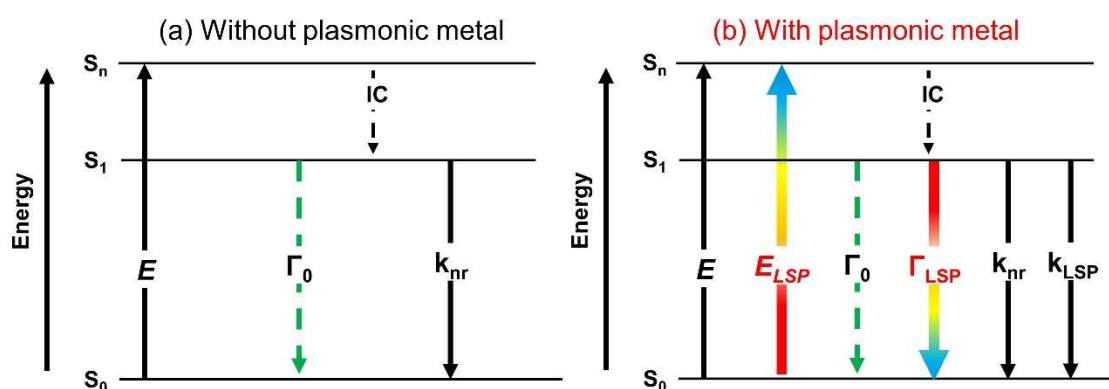
Figure 1-6. Effects of in the presence or absence of the plasmonic metal nanoparticle of the optical process of fluorophores positioned in the E-fields.

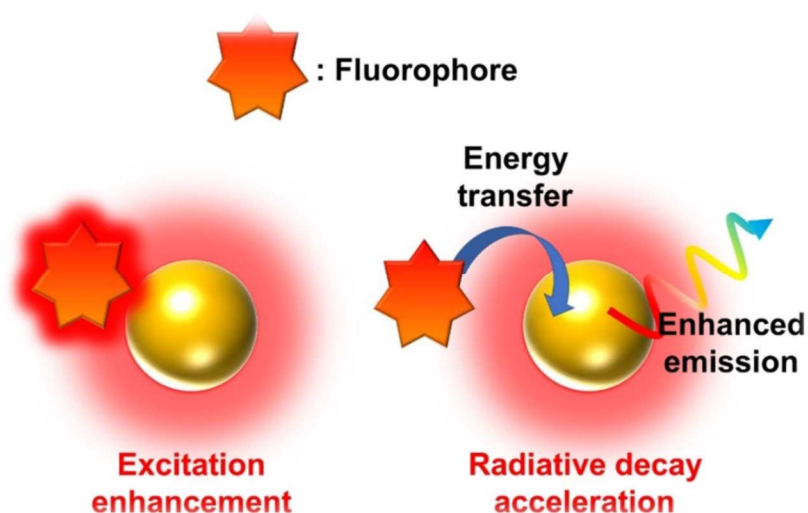**Figure 1-7.** Cartoon of the effect of the LSP resonance on the optical property of fluorophores positioned in the E-fields.

E, Γ_0 and k_{nr} represent the rate of excitation, radiative decay and non-radiative decay in the absence of the plasmonic metal, while E_{LSP}, Γ_{LSP} and k_{LSP} are those in the presence of plasmonic metal. Fluorescence emission quantum yields, in the absence or presence of

the LSP effect, can be written in equation (4) and (5), respectively. [26]

$$Q = \frac{\Gamma_0}{\Gamma_0 + k_{nr}} \cdots (4) \ (Absence \ of \ the \ plasmonic \ metal)$$

$$Q_{LSP} = \frac{\Gamma_0 + \Gamma_{LSP}}{\Gamma_0 + \Gamma_{LSP} + k_{nr} + k_{LSP}} \cdots (5) \ (Presence \ of \ the \ plasmonic \ metal)$$

From **Figure 1-6** and equations (4 and 5), it is understood that the excitation enhancement results in the increase in the amounts of the excited state species, and the LSP-induced radiative decay acceleration is of particular effective to the fluorophores with intrinsically low emission quantum yield.

The enhancement mechanisms by the LSP has been supported experimentally and theoretically by many researchers. For example, in the case of the excitation enhancement, since the E-field can act as a light-harvesting antenna, fluorophores in the fields can experience the concentrated photon flux. Zasedatelev et al. demonstrated the enhancement of an absorption coefficient of a phthalocyanine layer on plasmonic gold nanoparticle and revealed that the enhancement has resulted from the intense plasmonic field (**Figure 1-8**). [27]
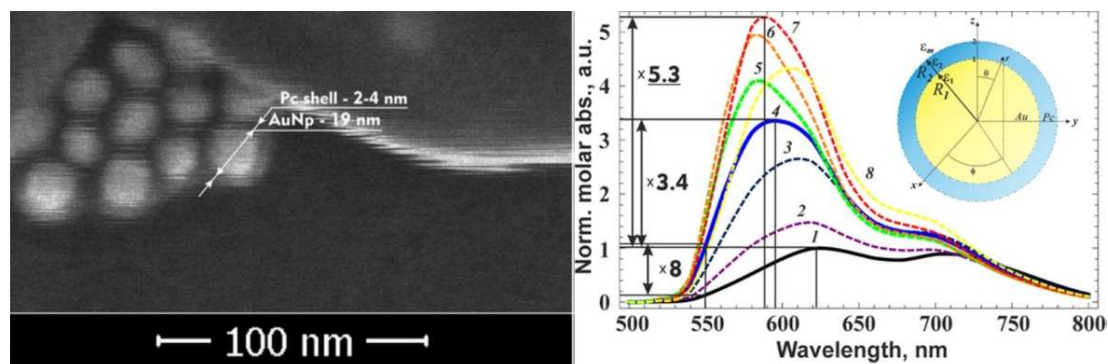
Figure 1-8. SEM image of the nanocomposite of phthalocyanine and gold nanoparticle and theoretical calculation by Ref [27].

In the case of the radiative decay acceleration, this is achieved by an energy transfer from the energy of the excited singlet state of fluorophores to the MNPs. After the deactivation of the LSP, the MNPs scatter photons with the same spectral shape of fluorophores. The enhancement of an emission intensity can be achieved, since the energy supposed to be decayed non-radiatively is transferred to the MNPs which leads to an increase in the

radiative decay rate. Zhang et al. reported the fluorophore's structured emission which is coupled to plasmon of silver island films. [28] Also, Munechika et al. achieved the fluorescence enhancement with spectral dependences from quantum dots near AgPRs by measuring a dark field scattering. [29] This result clearly showed an importance of spectral overlapping of the LSP wavelength with the emission wavelength of fluorophores for efficient emission enhancement.

Like fluorescence enhancement mechanism, the radiative decay process from the triplet excited state, which emits phosphorescence, can also be modified by the LSP. Pan et al. observed 200-fold enhancement in the phosphorescence intensity from a phosphorescent porphyrin derivative with a silver nanotextured film. [30] By analyzing the results, they found that the phosphorescence enhancement contained the increase in the absorption, the acceleration of the radiative decay rate, and a metallic quenching which is detrimental to the emission enhancement. The dependence of the film thickness on an enhancement factor was observed owing to the presence of the metallic quenching, suggesting an exist of the optimized spatial distance of fluorophores and plasmonic materials.

In recent years, new aspects of light-matter interaction has been attracted much attention. When the LSP band well-overlapped with the resonance band of the exciton, the plasmon (LSP) - exciton coupling state is formed. [31-34] Coupling strength represents the degree of energy transfer between LSP and exciton of emitters, and depending on its strength, the coupling state is classified into three; weak, intermediate and strong coupling regime. The system shows different optical property corresponding to respective coupling regimes.

In the weak coupling regime, spectral dips on the scattering spectra of the LSP - exciton system is generated, but that is not observed on the absorption spectra. [35-37] These spectral features suggest an enhanced absorption. Absorption enhancement of excitonic components is occurred whereas the energy of plasmonic components is damped. The enhanced absorption component of excitonic materials offset the damped energy generated on LSP, thus, extinction (absorption + scattering) spectra almost unchanged (**Figure 1-9, upper**). Balci et al. observed the 15-fold absorption enhancement of organic molecules coupled to surface plasmon polariton. [38] They attributed the enhancement to the weak coupling regime.

In the strong coupling regime, the coherent energy transfer between plasmon and exciton results in the hybridization of respective eigenmodes. Thus, the plasmon-exciton system behaves quasi-particle. Absorption and scattering spectra of the system under the strong coupling regime is energetically splitted into a higher and lower energy state

(**Figure 1-9, bottom**). [30-33] This splitting is called a Rabi splitting. Wersall et al. synthesized the core (AgPRs) - shell (J-aggregates of cyanine dyes) geometry and observed splitting in the scattering as well as photoluminescence spectra. [39] The result indicated the LSP of AgPRs strongly interacted with an exciton of cyanine dyes, and the photons scattered from the hybridized energy states produced by the strong coupling. In the intermediate coupling regime, changes in its optical property show "intermediate" between weak and strong coupling. [37] Spectral dips can be observed on both absorption and scattering spectra, but that is not generated on emission spectra (**Figure 1-9, middle**). This spectral dip is attributed to an induced transparency (IT). Zhao et al. reported that photoluminescence enhancement from transition metal dichalcogenides hybridized with silver nanoparticles, which showed the IT. [40] Although the plasmon - exciton coupling has a great potential to manipulate light - matter interaction further, the interpretation of effect of respective coupling regime on photophysical property still remain complicated and unclear.
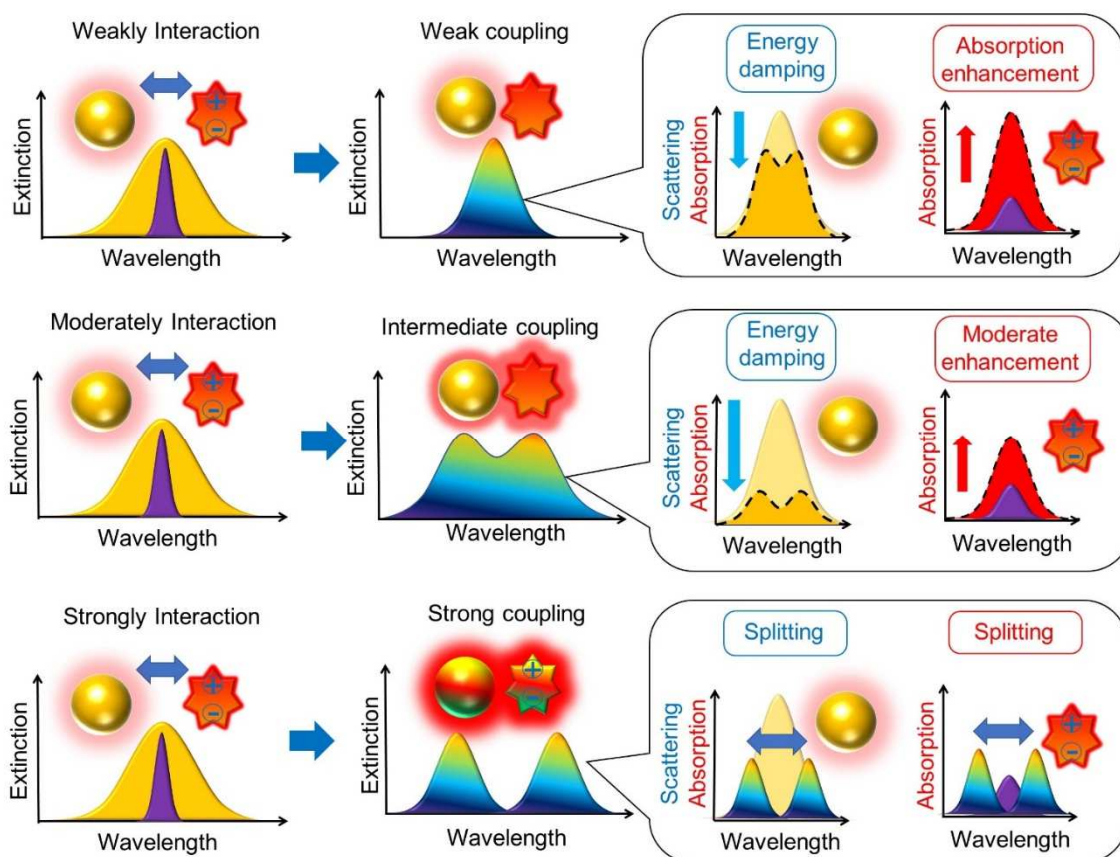

Figure 1-9. Change in the extinction, absorption and scattering spectra under the different coupling regime.

1-5. Application of LSP Resonance

Myriad investigations not only for the effect of the LSP on basic optical property but also the applications utilizing the LSP, have been reported.

Application 1: Photoelectric conversion

Akiyama et al. observed photocurrent enhancements from nanostructured assembly of porphyrin and plasmonic gold nanoparticles. [41] The enhanced photocurrent was ascribed to the increased excitation efficiency of porphyrin molecules by the E-field of the LSP. We have also reported previously the photocurrent enhancement attributed to the photoexcitation enhancement of porphyrins by using different plasmonic materials and geometries such as 2D half shell arrays composed of Au, Ag and Cu, and AgPRs monodispersed onto an electrode (**Figure 1-10**). [42-45]
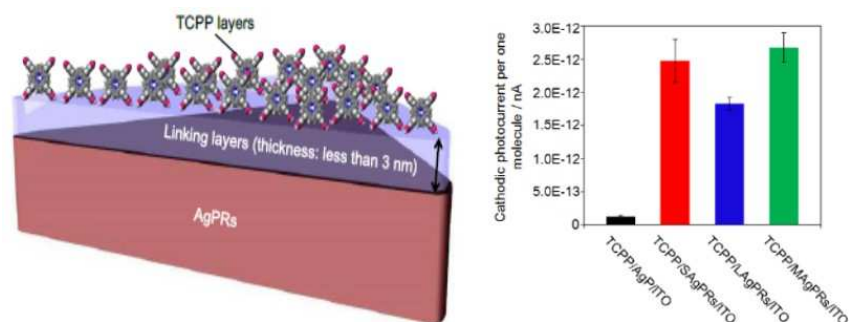
Figure 1-10. Schematic diagram of photo-electric conversion system composed of porphyrin derivative and AgPRs, and photocurrent values by Ref [45].

Also, Kawawaki et al. developed the high-efficiency solar cell, which is comprised of PbS quantum dot and ZnO nanowire, incorporated plasmonic silver nanocubes (**Figure 1-11**). [46] They improved the energy conversion efficiency of the solar cell from 4.45 % to 6.03%.

Figure 1-11. Plasmonic solar cell comprised of PbS quantum dot / ZnO nanowire by Ref [46].

15

Solar cells incorporated plasmonic materials are called plasmonic solar cells in recent years. The related research will attract much attention further for solving the energy problem.

Application 2: Emission device

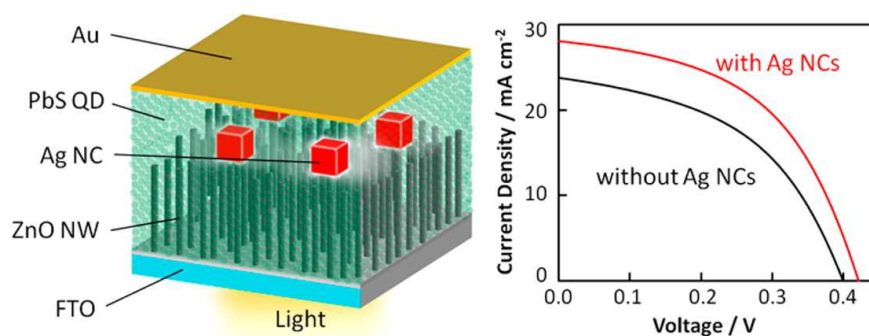Kwon et al. demonstrated the plasmon-enhanced photoluminescence intensity from light-emitting diodes (LEDs) combined with silver nanoparticles (**Figure 1-12**). [47] They attributed the enhanced emission intensity to the increase in the spontaneous emission rate.
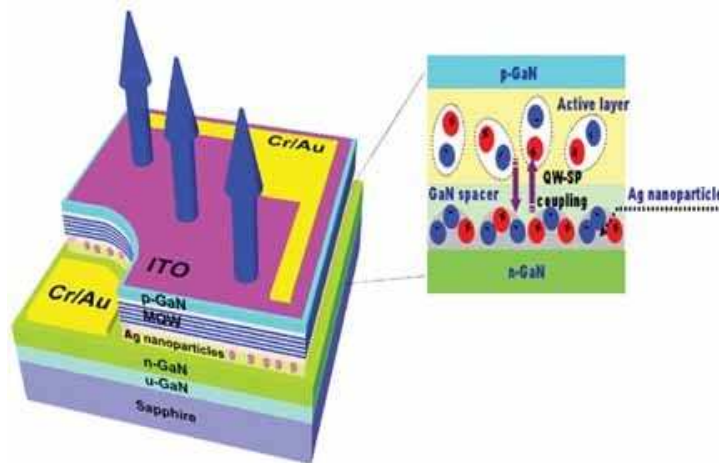
Figure 1-12. Schematic 3D representation of a InGaN/GaN LED with embedded Ag nanoparticles from Ref [47].

Fu et al. synthesized the hybrid nanocomplex of a dye labeled single stranded DNA and a biotin end-capped gold plasmonic nanorod and observed 40-fold emission enhancement. [48] Kinkhabwala et al. observed a huge fluorescence enhancement up to 1340-fold from single dye molecules positioned at the points where the hot spot generated between adjacent plasmonic nanoparticles (**Figure 1-13**). [49] These results have a great potential in the sensor applications including a label free detection, [50] a single molecule imaging. [51]
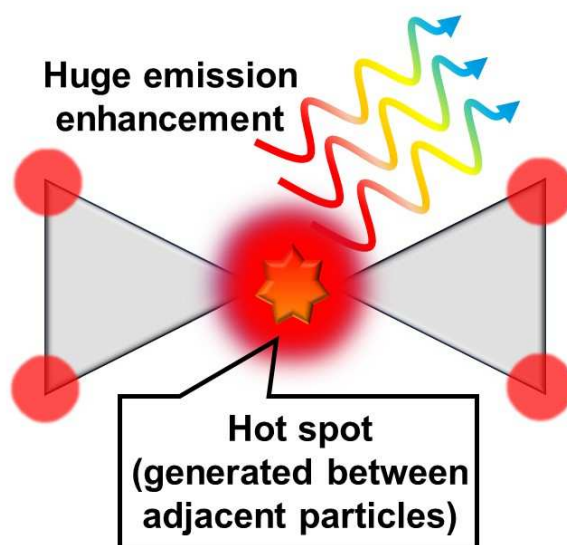
Figure 1-13. Schematic diagram for the hot spot generated between adjacent interparticle.

Application 3: Manipulation of photochemical dynamics

In the strong coupling regime, unexpected photochemical reaction never reported have been observed. Munkhbat et al. reported a suppression of a photobleaching of hybrids comprised of J-aggregates and AgPRs under the strong coupling, and they concluded the change in photobleaching dynamics, which attributed to the drastic modification of the relaxation pathway by the strong coupling. [52] Berghuis et al. demonstrated the enhanced delayed fluorescence via singlet fission in tetracene crystals deposited on plasmonic nanoparticle arrays. [53] Splitting in the extinction spectra and emission enhancement was observed from the strongly coupled system. Interestingly, the wavelength, at which emission enhancement occurred, coincided to splitting peak. They suggested that the triplet excited state was harvested in the separated energy state, resulting in the enhanced emission (**Figure 1-14**).

Figure 1-14. Jablonski diagram for tetracene crystals (a) uncoupled and (b) strongly coupled with plasmonic arrays by Ref [53].
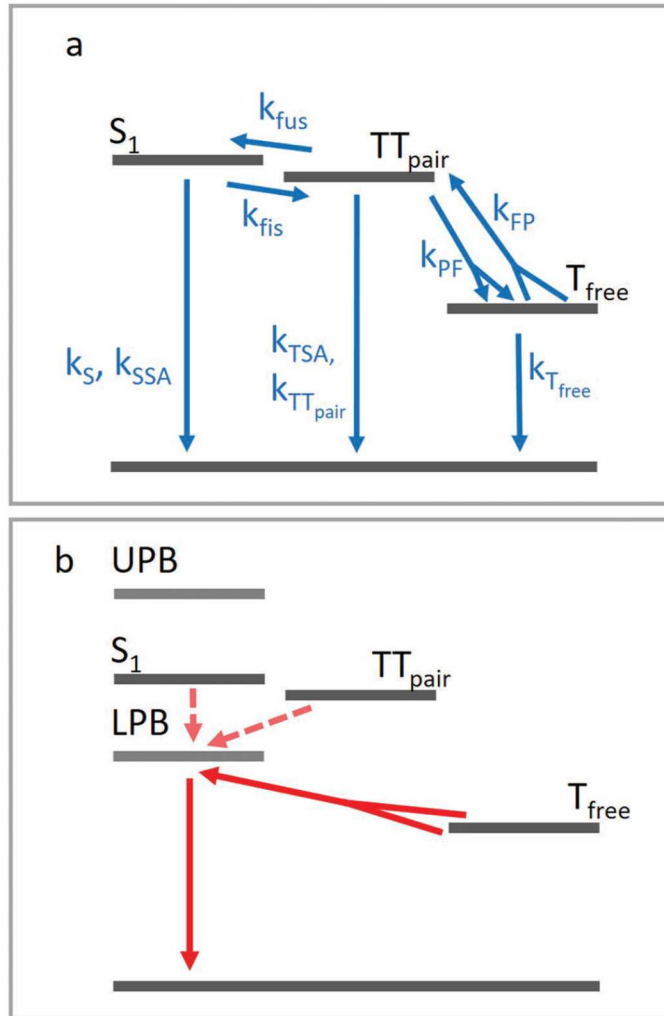
1-6. Object and Outline of This Dissertation

Modification of the optical property of porphyrins as photosensitizers has been attempted by many researchers for the high-performance light driven devices. Recently, it has been known that the LSP of the MNPs can significantly alter the optical property of photofunctional materials as the result of LSP - exciton interactions. The LSP-induced excitation and emission enhancement phenomena have been recognized to useful for the improvement of the device performance. Furthermore, it has been found that the interaction between LSP and exciton of photofunctional materials leads to the strong coupling state, which shows unexpected photochemical phenomena. However, the effects of the LSP on the optical property of photofunctional materials containing the complicated photoelement process such as ISC, is still unclear. In addition, the attempt utilizing the interaction of LSP and exciton to the real application have not much progressed.

Under such the background, we established the synthesis method of precisely-tuned LSP wavelength of AgPRs and investigated the optical property of the hybrids comprised of phosphorescent porphyrin derivatives with AgPRs by various spectroscopic measurement. Furthermore, as a first step for the real application utilizing the LSP - exciton interaction, we tried to construct the structure comprised of tetraphenyl porphyrin and AgPRs showing LSP - exciton interaction at multiple wavelengths in visible region.

This thesis is based on the results obtained in Chapters 2 and 3.

In Chapter 2, we investigated the change in the optical property of the hierarchical structure composed of phosphorescent palladium derivative and AgPRs. Although the significant phosphorescence intensity was obtained owing to rate of ISC of the metalloporphyrin is nearly 1, very high fluorescence intensity was observed by the regulation of LSP expression wavelength. By the lifetime measurement, it was revealed that intrinsically slow process of fluorescence radiation was drastically accelerated by the LSP. And, the results suggested that the accelerated process competes with intrinsically very fast process, ISC. Furthermore, we found that these changes in the optical property depended on not only the LSP expression wavelength, but also, the spatial distance between nanoparticles and molecules.

In Chapter 3, we investigated the optical property of hybrids comprised of tetraphenylporphyrin and AgPRs showing strictly-tuned LSP wavelength and achieved the absorption enhancement based on the LSP-exciton interaction over wide visible wavelength regions. Moreover, by investigating the fluorescence enhancement phenomena of the hybrids, we succeeded in the quantitative evaluation of enhanced -light absorption property.

In Chapter 4, this thesis was summarized. We found that the complicated photoelement process including ISC could be affected strongly by the LSP, which will lead to the development of biosensing and light emitting device. And, it was demonstrated that the enhanced light absorption property based on the LSP-exciton interaction over wide wavelength regions, suggesting the usefulness of utilizing the LSP-exciton interaction for the development of the solar energy converting device.

1-7. References

1. Song, H.; Liu, Q.; Xie, Y. Porphyrin-sensitized solar cells: systematic molecular optimization, coadsorption and cosensitization. *Chem. Commun.* **2018**, *54*, 1811-1824.

2. Yadav, R. K.: Oh, G. H.; Park, No-J.; Kumar, A.; Kong, Ki-J.; Baeg, Jin-O. Highly Selective Solar- Driven Methanol from CO_2 by a Photocatalyst/Biocatalyst Integrated System. *J. Am. Chem. Soc.* **2014**, *134*(48), 16728-16731.

3. Kirar, S.; Thakur, N. S.; Laha, J. K.; Baberjee, U. C. Porphyrin Functionalized Gelatin Nanoparticle-Based Biodegradable Phototheranostics: Potential Tools for Antimicrobial Photodynamic Therapy. *ACS Appl. Bio. Mater.* **2019**, *2*, 4202-4212.

4. Islangulov, R. R.; Lott, J.; Weder, C.; Castellano F. N. Noncoherent Low-Power Upconversion in Solid Polymer Films. *J. Am. Chem. Soc.* **2007**, *129*(42), 12652-12653.

5. Ventura, B.; Flamigni, L.; Marconi, G.; Lodato, F.; Offiver, D. L. Extending the porphyrin core: synthesis and photophysical characterization of porphyrins with π-conjugated β-substituents. *New J. Chem.* **2008**, *32*, 166-178.

6. Ghosh, M.; Mora, A. K.; Nath, S.; Chandra, A. K.; Hajra, A.; Sinha, S. Photophysics of Soret-excited free base tetraphenylporphyrin and its zinc analog in solution. *Spectrochim. Acta A* **2013**, *116*, 466-472.

7. Siggel, U.; bindig, U.; Endisch, C.; Komatsu, T.; Tsuchida, E.; Voigt, J.; Fuhrhop, J. -H. Photophysical and photochemical properties of porphyrin aggregates. *Ber. Bunsen-Ges. Phys. Chem.* **1996**, *12*, 2070.

8. Azenha, E. G.; Serra, A. C.; Pineiro, M.; Pereira, M. M.; Seixas de Melo, J.; Arnaut, L. G.; Formosinho, S. J.; Rocha Gonsalves, A. M. d. A. Heavy-atom effects on metalloporphyrins and polyhalogenated porphyrins. *Chem. Phys.* **2002**, *280*, 177-190.

9. Wang, C. L.; Chang, Y. C.; Lan, C. M.; Lo, C. F.; Diau, E. W. G.; Lin, C. Y. Enhanced light harvesting with π-conjugated cyclic aromatic hydrocarbons for porphyrin-sensitized solar cells. *Energy Eniviron. Sci.* **2011**, *4*, 1788-1795.

10. Kelly, K. L.; Coronado, E.; Zhao, L. L.; Schatz, G. C. The Optical Properties of Metal Nanoparticles: The Influence of Size, Shape, and Dielectric Environment. *J. Phys. Chem. B* **2003**, *107*, 668-677.

11. Willets, K. A.; Van Duyne, R. P. Localized Surface Plasmon Resonance Spectroscopy and Sensing. *Annu. Rev. Phys. Chem.* **2007**, *58*, 267-297.

12. E. Hao, and G. C. Schatz, Electromagnetic fields around silver nanoparticles and dimers. *J. Chem. Phys.* **2004**, *120*, 357.

13. Knauer, A.; Koehler, J. M. Explanation of the size dependent in-plane optical resonance of triangular silver nanoprisms. *Phys. Chem. Chem. Phys.* **2016**, *18*, 15943-15949.

14. Johnson, R. B.; Christy, R. W. Optical Constants of the Noble Metals. *Phys. Rev. B* **1972**, *6*(12), 4370.

15. Dong, X.; Ji, X.; Jing, J.; Li, M.; Li, J.; Yang, W. Synthesis of Triangular Silver Nanoprisms by Stepwose Reduction of Sodium Borohydride and Trisodium Citrate. *J. Phys. Chem. C* **2010**, *114*(5), 2070-2074.

16. Aherne, D.; Ledwith, D. M.; Gara, M.; Kelly J. M. Optical Properties and Growth Aspects of Silver Nanoprisms Produced by a Highly Reproducible and Rapid Synthesis at Room Temperature. *Adv. Funct. Mater.* **2008**, *18*, 2005-2016.

17. Haber, J.; Sokolov, K. Synthesis of Stable Citrate-Capped Silver Nanoprisms. *Langmuir* **2017**, *33*, 10525-10530.

18. Rastoriza-Sntos, I.; Liz-Marzan L. M. Synthesis of Silver Nanoprisms in DMF. *Nano Lett.* **2002**, *2*(8), 903-905.

19. Jin, R.; Cao, Y.; Mirkin, C. A.; Kelly, K. L., Schatz, G. C.; Zheng, J. G. Photoinduced conversion of silver nanospheres to nanoprisms. *Science* **2001**, *294*(5548), 1901-1903.

20.Jin, R.; Cao, Y. C.; Hao, E.; Metraux, G. S.; Schatz, G. C.; Mirkin, C. A. Controlling anisotropic nanoparticle growth through plasmon excitation. *Nature* **2003**, *425*, 487-490.

21. Wu, X.; Redmond, P. L.; Liu, H.; Chen, Y.; Steigerwald, M.; Brus, L. Photovoltange Mechanism for Room Light Conversion of Citrate Stabilized Silver Nanocrystal Seeds to Large Nanoprisms. *J. Am. Chem. Soc.* **2008**, *130*, 9500-9506.

22. Langile, M. R.; Personick, M. L.; Mirkin, C. A. Plasmon-Mediated Syntheses of Metallic Nanostructure. *Angew. Chem. Int. Ed.* **2013**, *52*, 13910-13940.

23. Xue, C.; Mirkin, C. A. pH-Switchable Silver Nanoprism Growth Pathways. *Angew. Chem. Int. Ed.* **2007**, *46*, 2036-2038.

24. Casas, J.; Venkataramasubramani, M.; Wang, Y.; Tang, L. Replacement of cetyltrimethylammoniumbromide bilayer on gold nanorod by alkanethiol crosslinker for enhanced plasmon resonance sensitivity. *Biosens. Bioelectron*. **2013**, *49*, 525-530.

25. Pelton, M. Modified spontaneous emission in nanophotonic structures. *Nature Photonics* **2015**, *9*, 427-435.

26. Lakowicz, J. R. Radiative Decay Engineering: Biophysical and Biomedical Applications. *Anal. Biochem.* **2001**, *298*, 1-24.

27. Zasedatelev, A. V.; Dubinina, T. V.; Krichevsky, D. M.; Krasovskii, V. I.; Gak, V. Y.; Pushkarev, V. E.; Tomilova, L. G.; Chistyakov, A. A. Plasmon-Induced Light Absorption of Phthalocyanine Layer in Hybrid Nanoparticles: Enhancement Factor and Effective Spectra. *J. Phys. Chem. C* **2016**, *120*, 1816−1823.

28. Zhang, Y.; Aslan, K.; Prevote, M. J. R.; Geddes, C. D. Metal-enhanced fluorescence: Surface plasmons can radiate a fluorophore's emission. *Appl. Phys. Lett.* **2007**, *90*,

053107.

29. Munechika, K.; Chen, Y.; Tillack, A. F.; Kulkarni, A. P.; Plante, I. J. L.; Munro, A. M.; Ginger, D. S. Spectral Control of Plasmonic Emission Enhancement from Quantum Dots near Single Silver Nanoprisms. *Nano Lett.* **2010**, *10*, 2598–2603.

30. Pan, S.; Rothberg, L. J. Enhancement of Platinum Octaethyl Porphyrin Phosphorescence near Nanostructured Silver Surface. *J. Am. Chem. Soc.* **2005**, *127*(16), 6087-6094.

31. Hugall, J. T.; Singh, A.; van Hulst, N. F. Plasmonic Cavity Coupling. *ACS Photonics* **2018**, *5*, 43−53.

32. Baranov, D. G.; Wersall, M.; Cuadra, J.; Antosiewicz, T. J.; Shegai, T. Novel Nanostructures and Materials for Strong Light-Matter Interactions. *ACS Photonics* **2018**, *5*, 24−42.

33. Dovzhenko, D. S.; Ryabchuk, S. V.; Rakovich, Y. P.; Nabiev, I. R. Light-matter interaction in the strong coupling regime: configurations, conditions, and applications. *Nanoscale* **2018**, *10*, 3589-3605.

34. Pelton, M.; Strom, S. D.; Leng, H. Strong coupling of emitters to single plasmonic nanoparticles: Exciton-induced transparency and Rabi splitting. *Nanoscale* **2019**, *11*, 14540-14552.

35. Garoff, S.; Weitz, D. A.; Gramila, T. J.; Hanson, C. D. Optical absorption resonances of dye-coated silver-island films. **1981**, *6*(5), 245-247.

36. Zengin, G.; Geshneidtner, T.; Verre, R.; Shao, L.; Antosiewicz, T. J.; Moth-Poulsen, K.; Kall, M.; Shegai, T. Evaluating Conditions for Strong Coupling between Nanoparticle Plasmons and Organic Dyes using Scattering and Absorption Spectroscopy. *J. Phys. Chem. C* **2016**, *120*(37), 20588-20596.

37. Antosiewicz, T. J.; Apell, S.P.; Shegai, T. Plasmon-exciton interactions in a core-shell geometry: from enhanced absorption to strong coupling. *ACS Photonics* **2014**, *1*(5), 454-463.

38. Balci, S.; Karademir, E.; Kocabas, C.; Aydinli, A. Absorption enhancement of molecules in the weak plasmon-exciton coupling regime. *Opt. lett.* **2014**, *39*(17), 4994-4997.

39. Wersall, M.; Cuadra, J.; Antosiewicz, T. J.; Balci, S.; Shegai, T. Observation of Mode Splitting in Photoluminescence of Individual Plasmonic Nanoparticles Strongly Coupled to Molecular Excitons. *Nano Lett.* **2017**, *17*(1), 551-558.

40. Zhao, W.; Wang, S.; Liu, B.; Verzhbitskiy, I.; Li, S.; Giustiniano, F.; Kozawa, D.; Loh, K. P.; Matsuda, K.; Okamoto, K.; Oulton, R. F.; Eda, G. Exciton-Plasmon Coupling and Electromagnetically Induced Transparency in Monolayer Semiconductors Hybridized

with Ag Nanoparticles. *Adv. Mater.* **2016**, *28*, 2709-2715.

41. Akiyama, t.; Nakada, M.; Terasaki, N.; Yamada, S. Photocurrent enhancement in a porphyrin-gold nanoparticle nanostructure assisted by localized plasmon excitation. *Chem. Commun.* **2006**, *4*, 395-397.

42. Sugawa, K.; Hirono, S.; Akiyama, T.; Yamada, S. Photocurrent enhancement tuned with plasmonic resonance in self-assembled monolayers fabricated on regularly arrayed gold nanostructures. *Photochem. Photobiol. Sci.* **2012**, *11*, 318-322.

43. Sugawa, K.: Uchida, K.; Takeshima, N.; Jin, S.; Tsunenari, N.; Takeda, H.; Kida, Y.; Akiyama, T.; Otsuki, J.; Takase K.; Yamada, S. Extraordinary enhancement of porphyrin photocurrent utilizing plasmonic silver arrays. *Nanoscale* **2016**, *8*, 15467-15472.

44. Sugawa, K.; Yamaguchi, D.; Tsunenari, N.; Uchida, K.; Tahara, H.; Takeda, H.; Tokuda, K.; Jin, S.; Kusaka, Y.; Fukuda, N.; Ushijima, H.; Akiyama, T.; Watanuki, Y.; Nishimiya, N.; Otsuki, J.; Yamada, S. Efficient Photocurrent Enhancement from Porphyrin Molecules on Plasmonic Copper Arrays: Beneficial Utilization of Copper Nanoanntenae on Plasmonic Photoelectric Conversion Systems *ACS Appl. Mater. Inter.* **2017**, *9*, 750-762.

45. Sugawa, K.; Takeshima, N.; Uchida, K.; Tahara, H.; Jin, S.; Tsunenari, N.; Akiyama, T.; Kusaka, Y.; Fukuda, N.; Ushijima, H.; Tsuchido, Y.; Hashimoto, T.; Hayashita, T.; Otsuki, J. Photocurrent Enhancement of Porphyrin Molecules over a Wide-Wavelength Region Based on Combined Use of Silver Nanoprisms with Different Aspect Ratios. *J. Mater. Chem. C* **2015**, *3*, 11439-11448.

46. Kawawaki, T.; Wang, H.; Kubo, T.; Saito, K.; Nakazaki, J.; Segawa, H.; Tatsuma, T. Efficiency Enhancement of PbS Quantum Dot/ZnO Nanowire Bulk-Heterojunction Solar Cells by Plasmonic Silver Nanocubes. *ACS Nano* **2015**, *9*, 4165-4172.

47. Kwon, M.-K.; Kim, J.-Y.; Kim, B.-H.; Park, I.-K.; Cho, C.-Y.; Byeon, C. C.; Park, S.-J. Surface-Plasmon-Enhanced Light-Emitting Diodes. *Adv. Mater.* **2008**, *20*, 1253 –1257.

48. Fu, Y.; Zhang, J.; Lakowicz, J. R. Plasmon-Enhanced Fluorescence from Single Fluorophores Emd-linked to Gold Nanords. *J. Am. Chem. Soc.* **2010**, *132*(16), 5540-5541.

49. Kinkhabwala, A.; Yu, Z.; Fan, S.; Avlasevich, Y.; Mullen, K.; Moerner, W. E. Large single-molecule fluorescence enhancements produced by a bowtie nanoantenna. *Nature Photonics* **2009**, *3*(11), 654-657.

50. Wang, Y.; Yan, Bing.; Chen, L. SERS Tags: Novel Optical Nanoprobes for Bioanalysis. *Chem. Rev.* **2013**, *113*, 1391-1428.

51. Taylor, A. B.; Zijlstra, P. Single-Molecule Plasmon Sensing: Current Status and Future Prospects. *ACS Sensor* **2017**, *2*, 1103-1122.

52. Munkbat, B.; Wersall, M.; Baranoc, D. G.; Antosiewicz, T. J.; Shegai, T. Suppression

of photo-oxidation of organic chromophores by strong coupling to plasmonic nanoantennas. *Sci. Adv.* **2018**, *4*, eaas9552.

53. Berghuis, M.; Halpin, A.; Le-Van, Q.; Ramezani, M.; Wang, S.; Murai, S.; Rivas, J. G. Enhanced Delayed Fluorescence in Tetracene Crystals by Strong Light-Matter Coupling. *Adv. Funct. Mater.* **2019**, *29*, 1901317.

Chapter 2

Optical Property of Phosphorescent Porphyrin

with Silver Nanoprisms

2-0. Summary

Emissive mode control of fluorescence and phosphorescence is an important research subject for the development of optical devices. In this chapter, we investigated the radiative decay process of the hybrids composed of phosphorescent palladium porphyrin derivative (Pd-porphyrin), in which the rate of intersystem crossing is nearly 1 and triangular silver nanoprisms (AgPRs). Significant fluorescence intensity was obtained from the hybrids, in which localized surface plasmon (LSP) wavelength of AgPRs was adjusted to fluorescence wavelength of Pd-porphyrin. From the fluorescence lifetime measurement, it was suggested that the radiative decay process of the excited singlet state of Pd-porphyrin was accelerated by LSP resonance and its modified process competed with ultrafast ISC process. Moreover, when we controlled a spatial distance between Pd-porphyrin and AgPRs, the opposite dependences of fluorescence and phosphorescence on the distance was observed. This result indicated that the distance in the order of nanometers between them is one of the important parameters to control emissive property of Pd-porphyrin. We demonstrated the succeeding in emissive mode control of Pd-porphyrin by precisely tuning the LSP wavelength. Results obtained in this chapter will contribute to the development of optical devices such as organic light emitting diodes (OLED), bioimaging, biosensing, and laser.

2-1. Introduction

The techniques controlling exciton dynamics in emitters are very important because of the contribution to bioimaging, biosensing, and performance improvement of advanced optical devices like organic light-emitting diodes. [1-4] In particular, the arbitrary adjustment between the fluorescence and the phosphorescence in relaxation processes is an important challenge for the development of intelligent emissive materials because different spectral regions within visible to near-infrared wavelengths are covered by these emissive modes owing to the difference in their emission energies. The selective control between the phosphorescence from the triplet excited state and the fluorescence from the singlet excited state of metalloporphyrins has been achieved by controlling the intramolecular singlet-triplet transition through the selection of the metal centre. [5,6] Also, recently, the emissive mode of molecular gold nanoclusters ([core + exo]-type $[Au_8]^{4+}$) could be controlled between fluorescence and phosphorescence by adjusting nanocluster aggregation state. [7] In addition, in some π-functional molecules, the singlet-triplet emissive switching was achieved by the formation of their helical self-assembly. [8,9] However, the development of an arbitrary control technique between the fluorescence and the phosphorescence is still challenging because the successful examples are few.

Recently, the nanophotonics-based radiative decay engineering techniques are being developed rapidly. In particular, the LSP resonance of metal nanoparticles has a powerful impact on the relaxation processes of photoexcited emitters by Purcell effect. [10-14] According to the radiating plasmon model, when the extinction band of LSP resonance of metal nanoparticles spectrally overlaps with the fluorescence band of fluorophores, the nonradiative energy transfer from the adjacent fluorophores to the LSP is induced, leading to the enhanced far-field radiation created by highly-efficient scattering of metal nanoparticles. [15-20] Likewise, the plasmon-coupled phosphorescence can be induced by the overlapping of the LSP resonance band with the phosphorescence band of phosphors. [21-23] However, the LSP resonance of metal nanoparticles could rarely change the intrinsic major relaxation pathway of emitters from phosphorescence to fluorescence radiation and *vice versa*. Exceptionally, it has recently been reported that the fluorescence of a platinum porphyrin derivative, in which the intersystem crossing rate (Φ_{ISC}) is close to 1 owing to the strong spin-orbit coupling by the presence of the heavy platinum atom, was substantially enhanced by the surface plasmon of nonmetallic graphene nanosheets. [24] The strong effect of graphene plasmon on the relaxation process of the photoexcited metalloporphyrin was suggested to be owing to the localization charges at the interface between graphene and platinum porphyrin faced on the graphene. [25-27]

We report in this study that the arbitrary control of emissive modes between

28

fluorescence and phosphorescence of a palladium porphyrin derivative, which intrinsically shows phosphorescence emission as a major relaxation process (Φ_{ISC}: ~1), is possible through the interaction with the LSP resonances of plasmonic metal nanoparticles. In particular, as we concluded here, the prominent generation of fluorescence, a manifestation of the dramatically changed intrinsic radiation property, was the result of effective competition of the nonradiative energy transfer from the singlet excited state of palladium porphyrin to the LSP of AgPRs against the ultrafast intramolecular intersystem crossing in the palladium porphyrin. Furthermore, the dependences of phosphorescence and fluorescence intensities on the distance between the AgPR surfaces and the palladium porphyrin exhibited interesting opposite trends. Consequently, it was demonstrated that the emissive property can be controlled by adjusting the distance as well as the control of LSP resonance wavelengths of AgPRs.

2-2. Experimental Section

Materials

Milli-Q-grade water (resistivity: 18.2 MΩ cm) was used to prepare all aqueous solutions. Toluene was purchased from Kishida Chemical (Japan). Sodium tetrahydroborate ($NaBH_4$), silver nitrate ($AgNO_3$), PEI (MW: ~10,000), and PMMA were purchased from Fujifilm Wako Pure Chemical (Japan). Trisodium citrate dihydrate, sodium hydroxide (NaOH), and hydrogen peroxide solution (H_2O_2, 30%) were purchased from Kanto Chemical (Japan). PSS (MW: ~70,000) and Pd-porphyrin were purchased from Sigma Aldrich (United States). All chemicals were used without further purification.

Measurements

Absorption and extinction spectra were recorded by a JASCO V-630 spectrophotometer. Emission spectra were measured by a JASCO FP-8600. Scanning electron microscopy (SEM), transmission electron microscopy (TEM), and atomic force microscopy (AFM) measurements were conducted using a Hitachi S-4500, a Hitachi HF-2000 and a Hitachi SPI-3800N-SPA400, respectively. The fluorescence decay profiles were measured with a time-resolved luminescence spectrometer based on a streak camera (Hamamatsu, C4334). The excitation wavelength was 400 nm (second harmonic of the output from a Ti:sapphire laser; Spectra-Physics, Tsunami). The repetition rate of the oscillator was reduced from 80 to 8 MHz with a pulse selector (Spectra-Physics, Model 3980). For phosphorescence lifetime measurements, a blue laser diode (402 nm) equipped with an optical chopper was used as a light source and phosphorescence was detected with a photomultiplier (Hamamatsu, R928) after being dispersed with a monochromator (JASCO, M50-T). Signals were processed with an oscilloscope and accumulated with a computer. Electromagnetic field enhancement contours of AgPRs were calculated by BEM within quasi-static (QS) approximation using MNPBEM17 program on MATLAB. [64] The employed dielectric function of silver was obtained from the report of Rakic *et al*. [65] All the measurements were performed under atmospheric conditions, except for the investigation of the optical property of the Pd-porphyrin in a toluene solution

Synthesis of AgPRs

Two kinds of AgPRs (SAgPRs and LAgPRs), which had different aspect ratios, were synthesized by a modified photochemical method described previously. [33-36] A freshly prepared aqueous solution containing $NaBH_4$ (0.2 mM, 1 mL) as a reductant and trisodium citrate (5 mM, 100 mL) as a stabilizer were added to an aqueous solution containing $AgNO_3$ (1 mM, 100 mL) in an ice bath, followed by stirring for 1 h to

synthesize Ag nanospheres (average diameter: ~10 nm). The pH of Ag colloidal aqueous solution was adjusted to 11.2 by the addition of an aqueous solution of NaOH (0.2 M) and then the solution was irradiated for 24 h with light from a light emitting diode (LED) with a center wavelength of 470 nm, resulting in the formation of SAgPRs. The LAgPRs were synthesized by the sequential irradiation of LED light with center wavelengths of 470 nm (the irradiation time: 2.0 h, 525 nm (0.5 h), and 590 nm (48 h).

Preparation of Hybrids of AgPRs and Pd-porphyrin

The glass substrates (1.5×2.0 cm^2) were immersed into a mixture solution of H_2O_2 (30 %) and NH_3 (28 %) (1/1 = v/v) at 100 ºC for 1 h to clean the surfaces, followed by washing with Milli-Q water. Then, the glass substrates were immersed into an aqueous solution of positively charged PEI (4.5 mg/mL) for 1 min, followed by washing thoroughly with Milli-Q water. The resultant PEI-modified glass substrates were immersed into the colloidal aqueous solution of AgPRs to deposit the AgPRs onto the glass surfaces (SAgPRs/glass and LAgPRs/glass) *via* the electrostatic interaction.

The hybrid thin layers consisting of the AgPRs and the Pd-porphyrin were prepared by spin-coating (3000 rpm, 30 sec) a toluene solution of PMMA (2 mg/mL) containing Pd-porphyrin (0.05 mM) as an emitter onto the AgPRs-deposited glass substrates (Pd-porphyrin/SAgPRs and Pd-porphyrin/LAgPRs). A reference sample without any AgPRs was prepared by spin-coating the Pd-porphyrin solution onto a bare glass substrate according to the manner as described above.

Investigation of Spatial Distance Dependence of Emission Properties

To investigate the dependence of the spatial distance between the AgPRs and the Pd-porphyrin on the emission properties, polyelectrolyte multilayers consisting of positively charged PEI and negatively charged PSS were inserted between them following an electrostatic layer-by-layer process. [58] First, the AgPRs/glass were immersed in an aqueous solution of PEI (0.1 wt%) for 1 s, followed by washing with Milli-Q water for 10 s. Next, the resultant PEI-modified AgPRs/glass were immersed into an aqueous solution of PSS (0.2 wt%) for 1 s, followed by washing with Milli-Q water for 10 s. After the arbitrary sequential immersion processes into the polyelectrolyte solutions, the PMMA solution containing Pd-porphyrin was spin-coated (3000 rpm, 30 s) onto the multilayers-modified AgPRs/glass (Pd-porphyrin/[PSS-PEI(*Y*)]/SAgPRs(0.25) and Pd-porphyrin/[PSS-PEI(*Y*)]/LAgPRs(0.25)). The insertion of multilayers ensures precisely-controlled spatial distance between the AgPRs and the Pd-porphyrin layer by controlling the numbers of deposition cycles.

2-3. Results and Discussion

2-3-1. Optical and Structural Properties of Pd-porphyrin and AgPRs

The absorption and the emission spectra of a toluene solution (50 μM) of 2,3,7,8,12,13,17,18-octaethyl-21H,23H-porphine palladium (II) (Pd-porphyrin, molecular structure: **Figure 2-1 (a)**) used as an emitter in this study are shown in **Figure 2-1 (b)**. The Pd-porphyrin solution showed characteristic absorption bands consisting of the Soret band at 394 nm and the Q-bands at 513 and 546 nm, which were selected as the excitation bands for the investigation of the emissive property of the Pd-porphyrin in the absence or presence of AgPRs. The emission spectrum shows a prominent phosphorescence emission band at 667 nm assigned to the radiative decay from the triplet excited state to the singlet ground state concomitant with a very small fluorescence bands at 550-610 nm, which are assigned to the radiative decay from the singlet excited state to the singlet ground state. [28-30] These emissive properties originate from the heavy atom effects by the palladium atom situated at the center of the porphyrin skeleton, resulting in the ultrafast and efficient transition from the singlet excited state to the triplet excited state (Φ_{ISC}: ~1). [31] Consequently, the quantum yields of fluorescence (Φ_{fluo}) and phosphorescence (Φ_{phos}) of Pd-porphyrin are generally < 0.1 % and 10-30 %, respectively. [28-30]
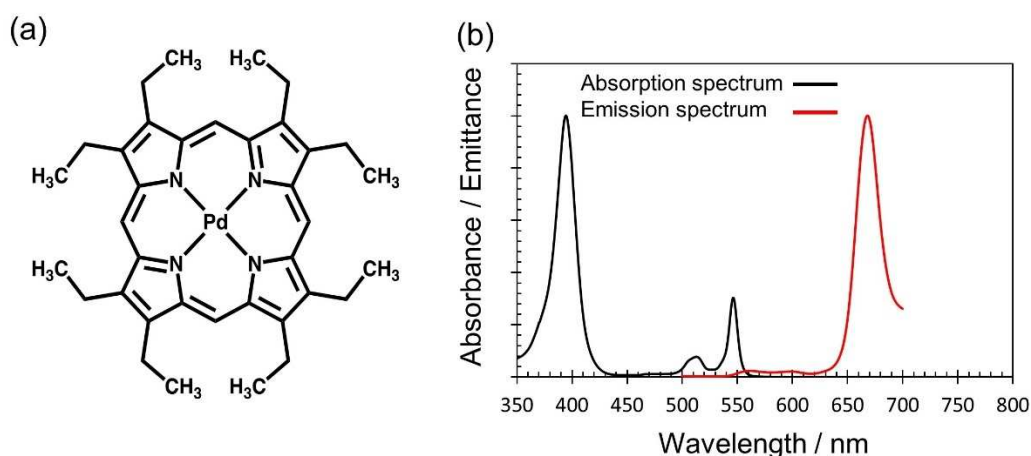

Figure 2-1. Optical properties of the Pd-porphyrin and the AgPRs. **(a)** Molecular structure of Pd-porphyrin. **(b)** Absorption and emission spectra (λ_{ex} = 391 nm) of the toluene solution of Pd-porphyrin (50 μM).

In this study, AgPRs were used as an LSP-responsive metal nanoparticles because of their LSP resonance-induced strong local electromagnetic fields (*vide infra*) and the tunability of LSP resonance wavelengths through the adjustment of their aspect ratio (the

ratio of edge length to thickness) over a wide range from visible to near-infrared region. [32-35] The two kinds of AgPRs with different aspect ratios were synthesized using a modified photochemical method reported previously by us (the detailed procedures are described in Experimental Section): SAgPRs (a smaller aspect ratio) and LAgPRs (a larger aspect ratio). [32-35]

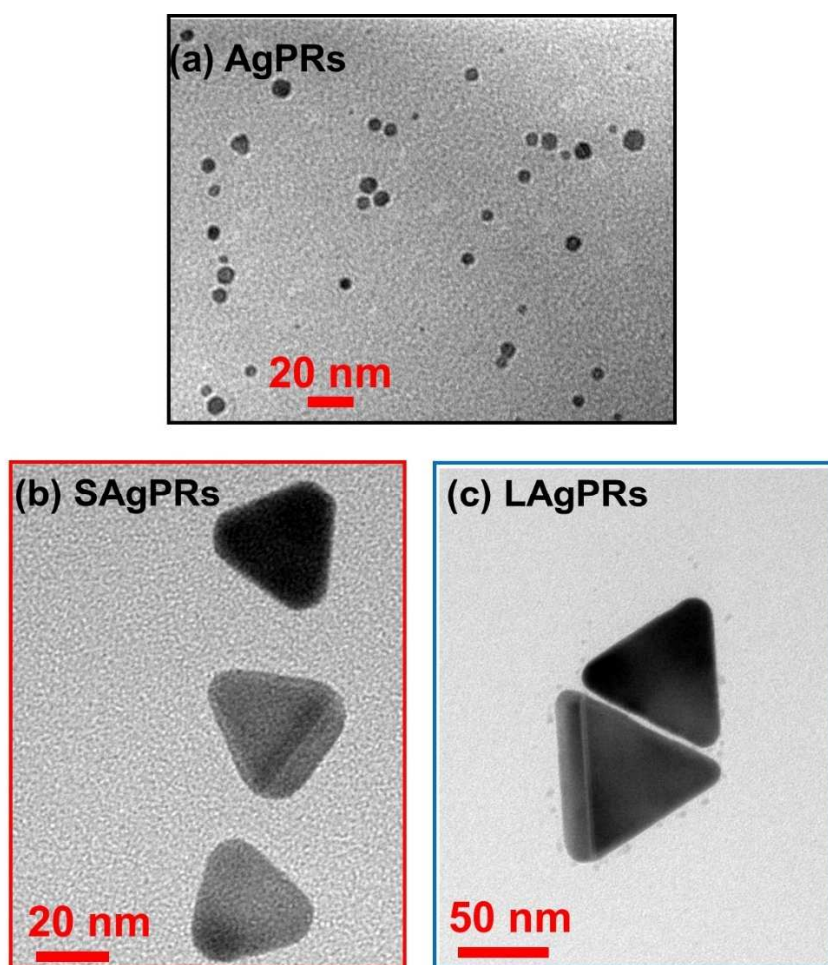The transmission electron microscopy (TEM) images of AgNPs, SAgPRs and LAgPRs are shown in **Figure 2-2 (a, b, and c)**.

Figure 2-2. TEM images of **(a)** AgNPs (as a seed), **(b)** SAgPRs and **(c)** LAgPRs.

The diameter of AgNPs is ~10 nm and the edge lengths of SAgPRs and LAgPRs are found to be 27 ± 2 nm and 51 ± 5 nm, respectively. We reported previously that the thicknesses of AgPRs, which were generated by our synthetic method, were almost the same as 10 nm regardless of their edge lengths. [36] Therefore, the difference in the generating wavelengths of the LSP resonance bands of SAgPRs and LAgPRs is attributed to the difference in their aspect ratios (SAgPRs: 2.7, LAgPRs: 5.1). Normalized extinction

spectra for the colloidal aqueous solutions of Ag nanospheres (used as a seed), SAgPRs, and LAgPRs are shown in **Figure 2-3**.
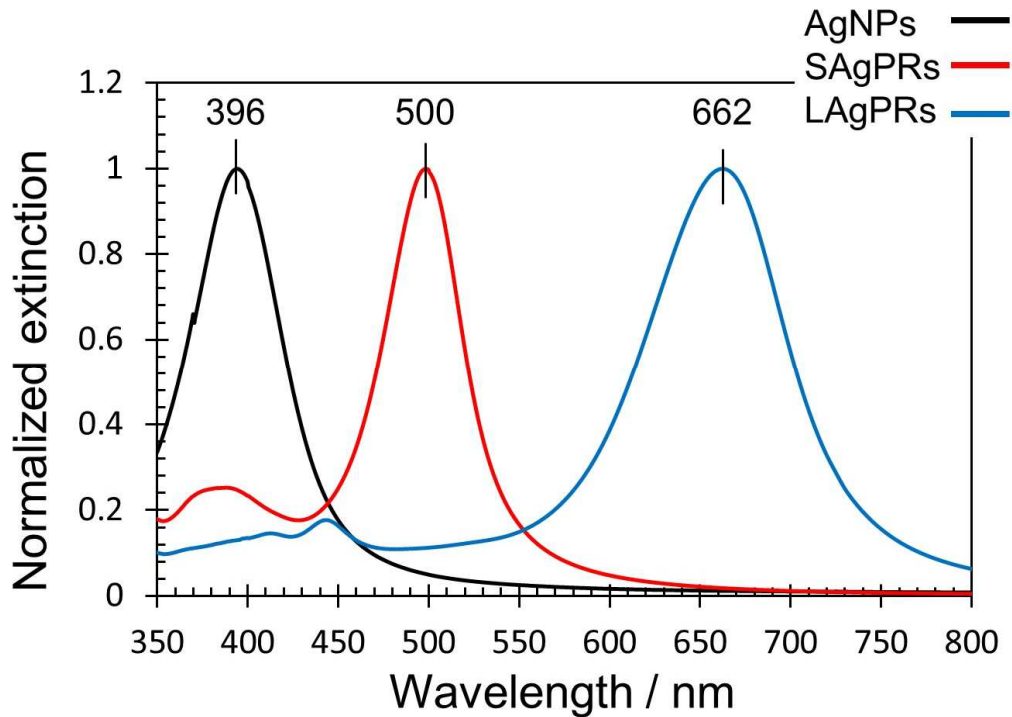

Figure 2-3. Normalized extinction spectra of colloidal aqueous solutions of Ag nanospheres, SAgPRs, and LAgPRs.

While the colloidal aqueous solution of Ag nanospheres shows a maximum extinction wavelength (λ_{max}) at 396 nm, which is originated from the LSP resonance of the dipole mode, the λ_{max} are observed at 500 nm and 662 nm from the colloidal aqueous solutions of SAgPRs and LAgPRs, respectively. These bands originate from the LSP resonances of their in-plane dipole mode. [33-36]

2-3-2. Effect of Wavelengths and Intensity of LSP Resonance on the Emissive Mode

We found radical changes in the emissive properties of phosphorescent Pd-porphyrin by constructing the hybridized substrates composed of AgPRs covered with the poly(methyl methacrylate) (PMMA) layers containing Pd-porphyrin. The fabrication scheme is shown in **Figure 2-4**.
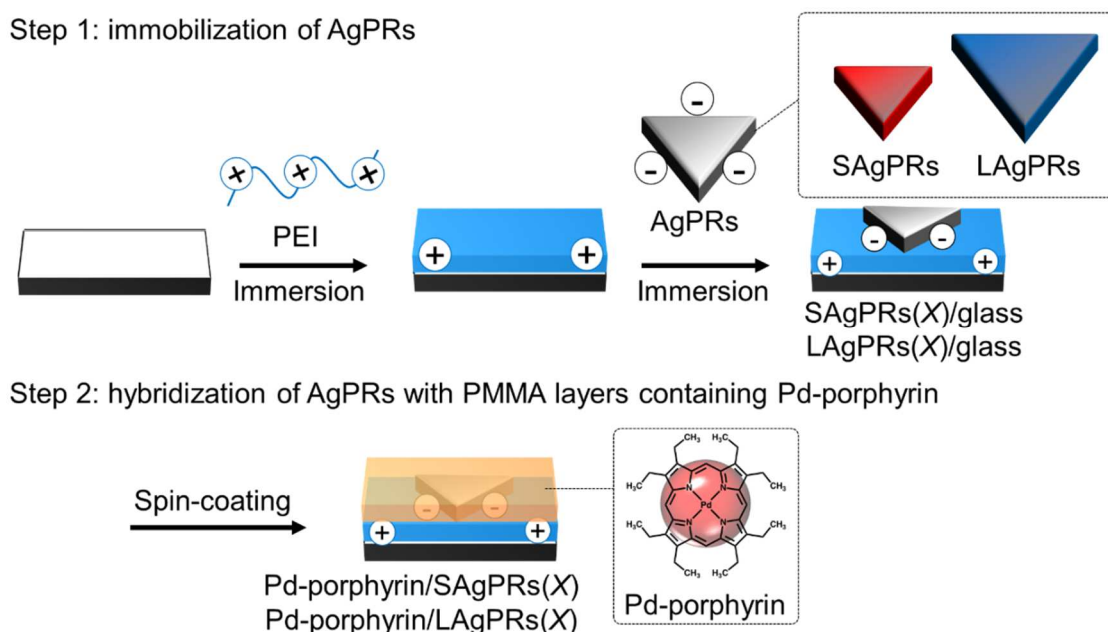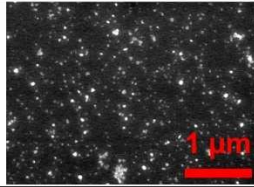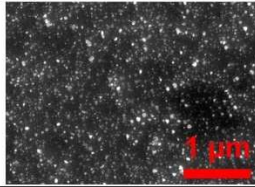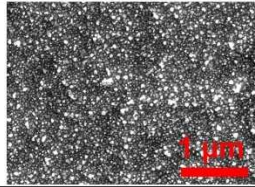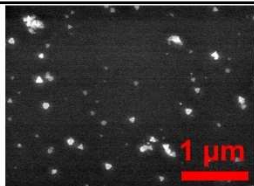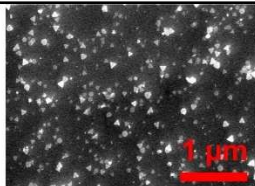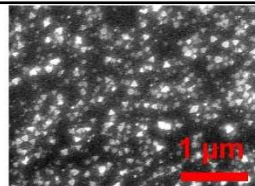

Figure 2-4. Schematic showing for the fabrication of hybrids of the AgPRs and the PMMA layers containing Pd-porphyrin.

First, SAgPRs and LAgPRs were respectively immobilized onto the surfaces of glass substrates (SAgPRs/glass and LAgPRs/glass) by the electrostatic adsorption between the glass surfaces modified with positively-charged polyethyleneimine (PEI) and AgPRs (Step 1 in **Figure 2-4**). AgPRs have negatively-charged surfaces because of being protected with citrate. SAgPRs/glass and LAgPRs/glass having the main LSP resonance bands with maximum extinction intensities of ~0.07, ~0.15, and ~0.25 were fabricated by controlling the immersion time of the PEI-covered glass substrates into the colloidal aqueous solutions of AgPRs (SAgPRs(X)/glass and LAgPRs(X)/glass, X: the maximum extinction intensity of the main LSP resonance bands of only the S(L)AgPRs on the PEI-covered glass substrates). The scanning electron microscopy (SEM) images of SAgPRs(X)/glass and LAgPRs(X)/glass are shown in **Figure 2-5 (a)**, as well as the surface coverages estimated from these images. For both AgPRs, as shown in **Figure 2-5 (b)**, the linear relationship between the maximum extinction intensities of LSP

resonance bands and the coverages of AgPRs is found.

(a)

(b)

Figure 2-5. Morphological characterization and optical properties and of AgPRs(X)/glass and Pd-porphyrin/AgPRs(X). **(a)** SEM images of SAgPRs(X)/glass and LAgPRs(X)/glass and coverages of SAgPRs and LAgPRs on glass substrates. **(b)** Plots of the coverage of SAgPRs and LAgPRs against maximum extinction intensity of SAgPRs(X)/glass and LAgPRs(X)/glass.

The extinction spectra of SAgPRs(X)/glass and LAgPRs(X)/glass are shown in **Figure 2-6(a,b)**, respectively.

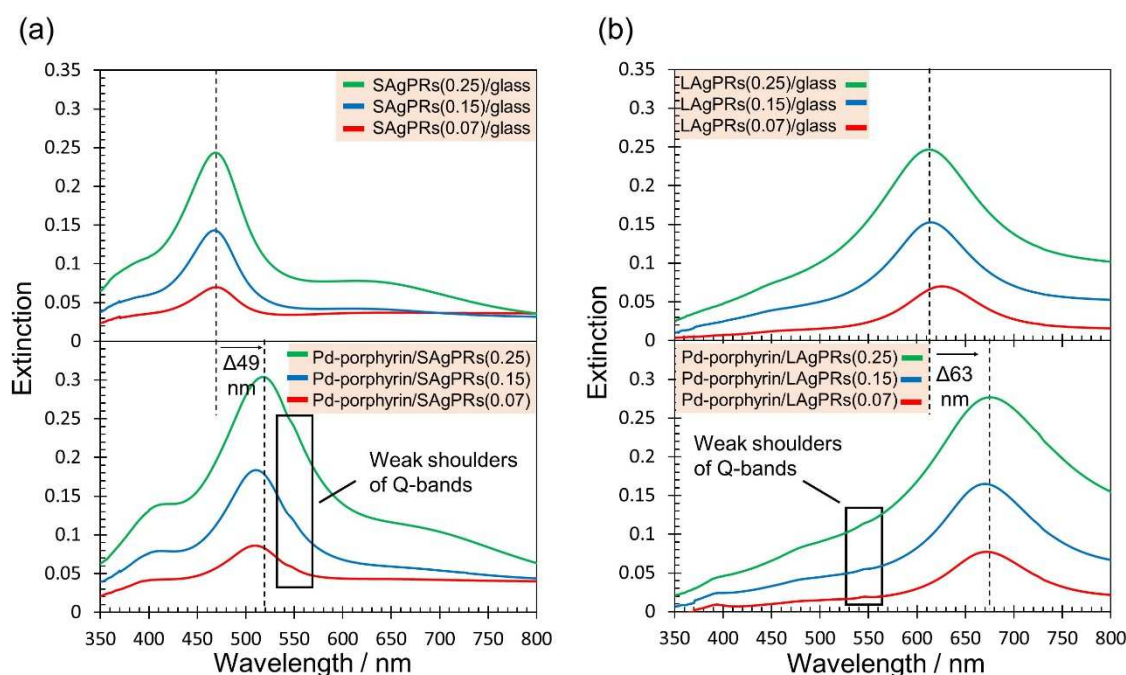**Figure 2-6.** Extinction spectra of **(a)** SAgPRs(*X*)/glass and **(b)** Pd-porphyrin/SAgPRs(*X*), *X* (0.07, 0.15, and 0.25) denotes the maximum extinction intensity of the LSP resonance bands of SAgPRs on glass substrates.

The λ_{max} of LSP resonance bands for both of SAgPRs(*X*)/glass (469 nm) and LAgPRs(*X*)/glass (612 nm) were blue-shifted by ~30 nm and ~50 nm, respectively, as compared with those dispersed in the colloidal aqueous solutions (**Figure 2-3**). After spreading the PMMA thin layers containing Pd-porphyrin over the AgPRs-immobilized glass substrates (Step 2 in **Figure 2-4**), the moderate red-shifts of λ_{max} (SAgPRs: 49 nm, LAgPRs: 63 nm) were observed (**Figure 2-6**). The blue shifts of LSP resonance band of SAgPRs and LAgPRs from aqueous phase onto the glass substrates are attributed to the change in surrounding refractive index. Although the bottom of silver nanoprisms is attached onto the surface of PEI of which the refractive index (1.53) is higher than water (1.33), the other four faces are exposed to air (1.00). Since the local electromagnetic fields are generated at the side faces exposed to air, it is reasonable to consider that the blue shifts were owing to the reduction of their surrounding refractive index. [66-68] Also, the LSP resonance bands of Pd-porphyrin/SAgPRs(*X*) and Pd-porphyrin/LAgPRs(*X*), shown in **Figure 2-6 respectively,** were moderately red-shifted (SAgPRs: 49 nm, LAgPRs: 63 nm) because of the increase in the refractive index around AgPRs by covering them with the PMMA layers (refractive index: 1.49). [69] While the LSP resonance band of SAgPRs (λ_{max} = 518 nm) overlaps with the absorption band (Q-bands: 510 and 546 nm) and the

fluorescence band (550-610 nm), that of LAgPRs (λ_{max} = 675 nm) overlaps well with the phosphorescence band (667 nm). The weak shoulders, which are attributed to the Q-bands of Pd-porphyrin, are observed around 546 nm on the extinction spectra for both Pd-porphyrin/SAgPRs(*X*) and Pd-porphyrin/LAgPRs(*X*), indicating the hybridization of AgPRs and Pd-porphyrin layers. To estimate the thickness of PMMA layers, we measured the thickness of Pd-porphyrin-containing PMMA layers on glass substrates (a reference sample, Pd-porphyrin/glass) prepared in a manner similar to the fabrication of Pd-porphyrin/SAgPRs(*X*) and Pd-porphyrin/LAgPRs(*X*) using an atomic force microscope (AFM). As shown in **Figure 2-7**, the layer is relatively uniform and the thickness was estimated to be 6.7 ± 0.1 nm.
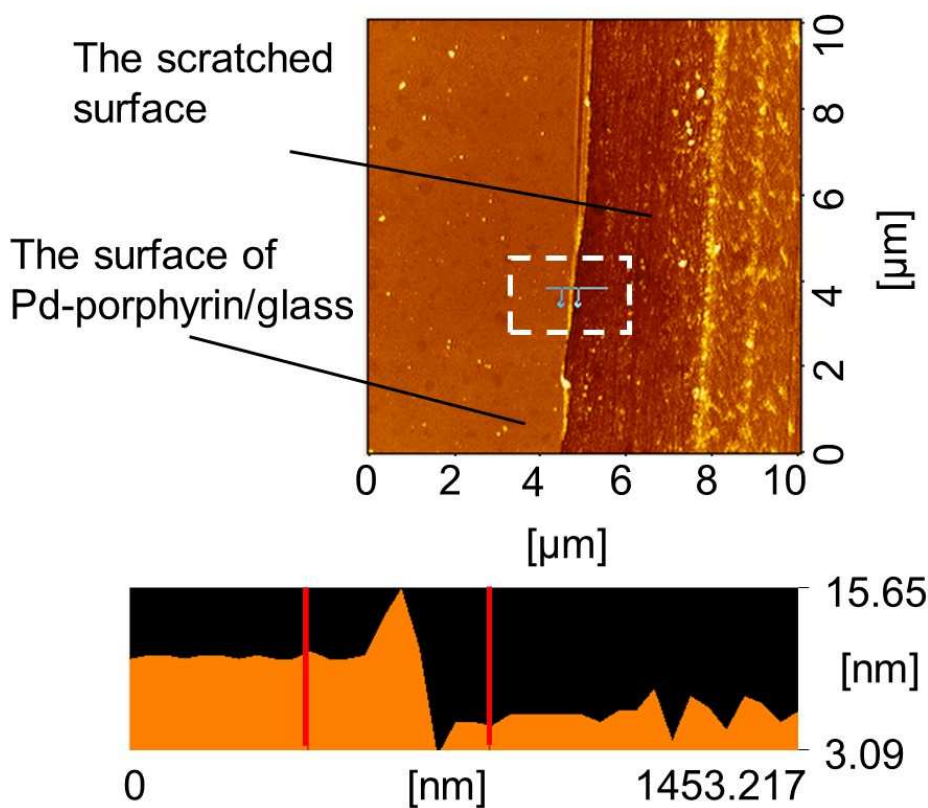
Figure 2-7. AFM image of Pd-porphyrin/glass. To estimate the thickness of PMMA layer, the probe needle was scanned over the layer surfaces scratched by a sharp tweezer. The thickness of PMMA layers on glass substrate are estimated to be 6.7± 0.1 nm.

This thickness is thin enough for the Pd-porphyrin molecules contained in the layers to lie in the strong local electromagnetic fields of the LSP resonance of AgPRs which extend over some dozen nanometers (see **Figure 2-10**).

The emission spectra (excitation wavelength: λ_{ex} = 510 nm corresponding to the Q-bands of Pd-porphyrin) of Pd-porphyrin/SAgPRs(X) and Pd-porphyrin/LAgPRs(X) are shown in **Figures 2-8 (a) and (b)**, respectively.
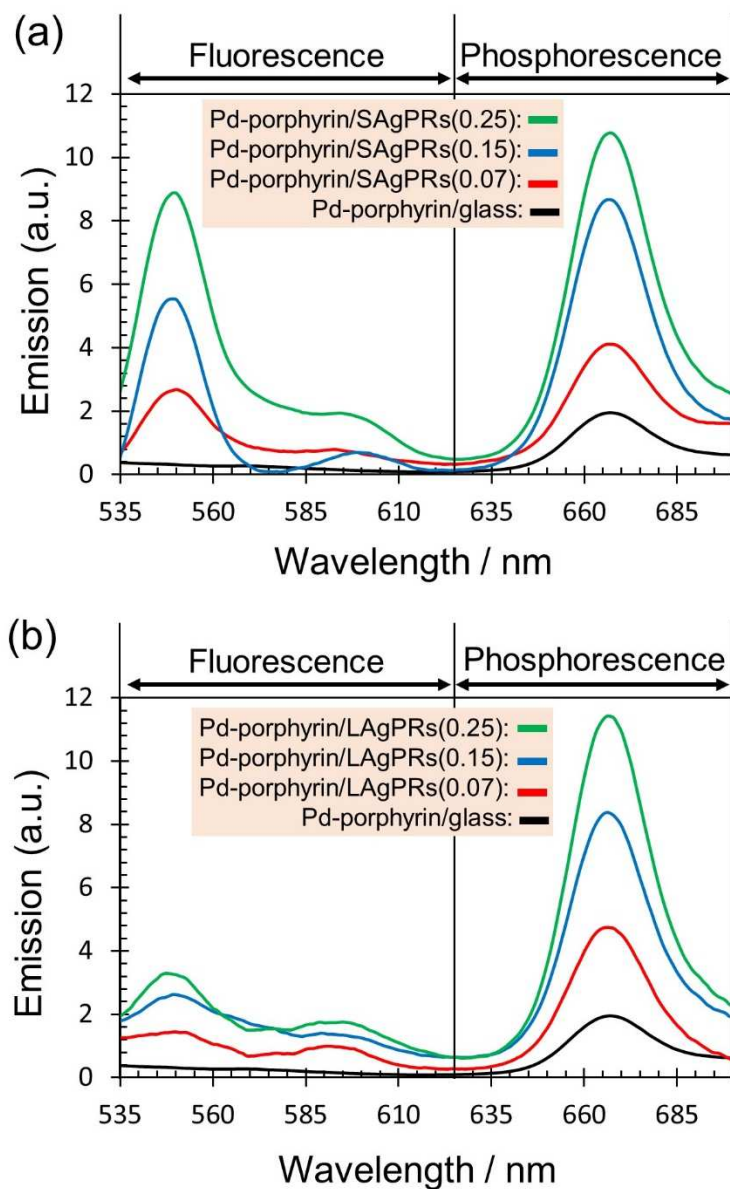
Figure 2-8. Emission properties of Pd-porphyrin with and without AgPRs. The emission spectra (λ_{ex} = 510 nm) of **(a)** Pd-porphyrin/SAgPRs(X) and **(b)** Pd-porphyrin/LAgPRs(X) (X: 0.07, 0.15, and 0.25). Both figures contain the emission spectrum of Pd-porphyrin/glass as a reference.

In the emission spectrum of Pd-porphyrin/glass, only a prominent phosphorescence band centered at 667 nm was observed and the fluorescence radiation was not observed. In

contrast, we noted that new prominent emission bands at 540-610 nm concomitant with the enhanced phosphorescence band appeared by hybridizing the Pd-porphyrin layers with SAgPRs and LAgPRs. While prominent emission was observed, the enhancement of the fluorescence emission originated by escaping Pd atom from the center of porphyrin skeleton may be possible. Thus, we measured the emission spectra of the free base octaethyl porphyrin (OEP) since the molecular structure of the OEP was analogous to the Pd-porphyrin except for the absence of the Pd metal in the center of the porphyrin skeleton (**Figure 2-9**). The OEP in PMMA was fabricated in a similar manner for the preparation of the Pd-porphyrin hybrids.
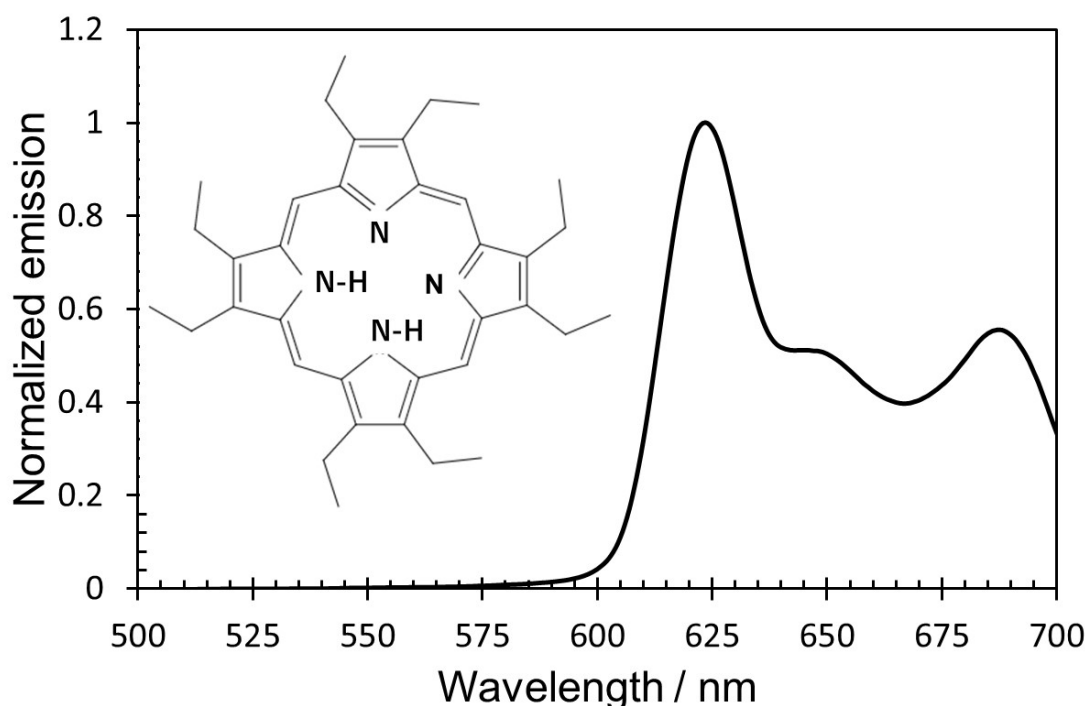
Figure 2-9. Emission spectrum of free base octaethyl porphyrin (OEP) in PMMA deposited on glass substrate. Inset shows molecular structure of OEP.

Fluorescence bands of OEP molecules were observed above 600 nm. This emission bands of OEP are far from fluorescence wavelength of Pd-porphyrin in this study, thus, the possibility aforementioned can be eliminated.

It has frequently been reported that the original emissive modes of emitters can be enhanced by the strong local electromagnetic fields of plasmonic metal nanoparticles. The newly generated emission at the shorter wavelengths may be assigned to the fluorescence radiation because the wavelengths are similar to those of the quite weak

fluorescence bands observed in the Pd-porphyrin solution (**Figure 2-1 (b)**). We suggest that the generation of fluorescence radiation is induced by selectively enhancing the relaxation pathway from the singlet excited state to the singlet ground state by the LSP resonances of AgPRs because a reasonable correlation between the LSP resonance properties of AgPRs and the radiation properties and changes in the lifetime of fluorescence and phosphorescence was obtained (*vide infra*). We found that the intensities of fluorescence and phosphorescence gradually increased upon increasing the LSP resonance bands of in-plane dipole modes (*i.e.* increasing the coverage of AgPRs) for both SAgPRs and LAgPRs. In addition, the intensity of fluorescence induced by the SAgPRs, the LSP resonance band of which overlaps well with the photoexcitation and fluorescence wavelengths of Pd-porphyrin (**Figure 2-8 (a)**), was significantly stronger than that induced by the LAgPRs, the LSP resonance band of which overlaps less with both of them (**Figure 2-8 (b)**). These results suggest that the control of emissive modes of phosphorescent Pd-porphyrin between fluorescence and phosphorescence was successfully achieved by controlling the generating wavelengths and the intensity of the LSP resonance band of AgPRs. The generation mechanism(s) of the characteristic emissive properties were investigated as described below.

2-3-3. Effect of LSP Resonance on Relaxation Pathway

To investigate the effects of the LSP resonance on the relaxation pathway from the photoexcited state of Pd-porphyrin, the λ_{ex} used for the emission measurements was changed to 391 nm (corresponding to the Soret band of Pd-porphyrin) from 510 nm used in the previous section. Since the λ_{ex} is spectrally far from the main LSP resonance bands of both SAgPRs and LAgPRs, the LSP resonances may not affect the excitation process but mainly affect the pathways of the singlet excited state to the singlet ground state and the triplet excited state to the singlet ground state in the relaxation process, respectively. [15-20] As shown in **Figure 2-10**, from the results of calculation of local electromagnetic field intensity by boundary element method (BEM), the maximum electromagnetic fields ($|E_{max}/E_0|^2$) of SAgPRs and LAgPRs, which are surrounded by the PMMA, were found to be significantly weaker at 391 nm than at 550 nm (the center wavelength of fluorescence band) and at 667 nm (the center wavelength of phosphorescence band). Also, while the $|E_{max}/E_0|^2$ at 550 nm for SAgPRs is significantly stronger than that for LAgPRs, the opposite is the case at 667 nm. These calculated values strongly support the above assumption.
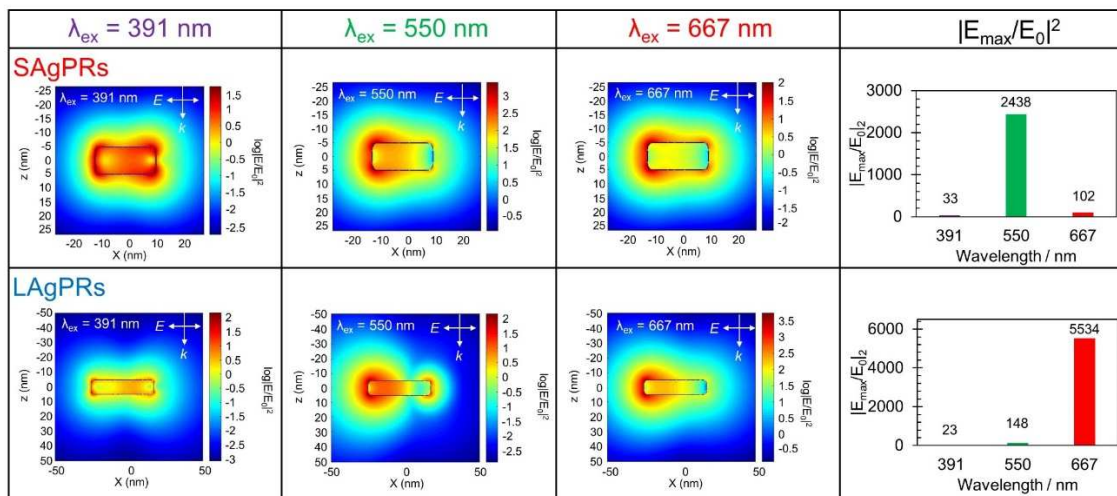

Figure 2-10. Electromagnetic field calculation of AgPRs Electromagnetic field intensities calculated by BEM of SAgPR and LAgPR at 391 nm, 550 nm, and 667 nm (surrounding refractive index: 1.49). Summary of maximum field intensities at each wavelength of SAgPRs and LAgPRs.

As shown in **Figure 2-11 (a,b)**, the fluorescence as well as the phosphorescence were largely enhanced by inserting the AgPRs between the glass substrates and the Pd-porphyrin layers, as compared with the reference substrate (Pd-porphyrin/glass). The fluorescence from Pd-porphyrin/glass was slightly observable because the molar absorption coefficient of Pd-porphyrin at the Soret band (1.3×10^5 M^{-1}cm^{-1} in toluene solution) is more than ten times larger than that at the Q-bands (1.1×10^4 M^{-1}cm^{-1}) used in the previous section.
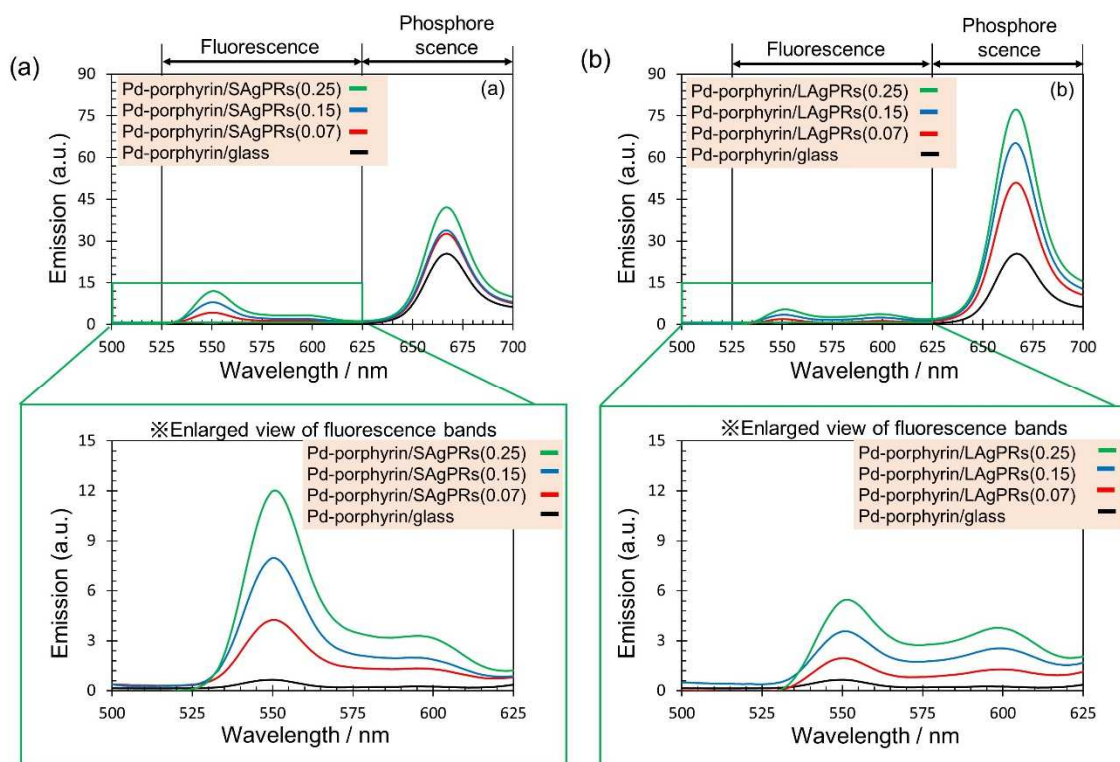

Figure 2-11. Emission properties of Pd-porphyrin with and without AgPRs. The emission spectra (λ_{ex} = 391 nm) of (**a**) Pd-porphyrin/SAgPRs and (**b**) Pd-porphyrin/LAgPRs(X) (X: 0.07, 0.15, and 0.25). (X) (X: 0.07, 0.15, and 0.25).

The enhancement factors (EFs) of the fluorescence and the phosphorescence intensities from Pd-porphyrin/SAgPRs(X) and Pd-porphyrin/LAgPRs(X) with respect to that from Pd-porphyrin/glass are plotted against the maximum extinction intensity of the respective LSP resonance bands (**Figure 2-12**). The EFs for both the fluorescence and the phosphorescence increase linearly with an increase in the extinction intensity of LSP resonance bands. These results clearly indicate that these emission enhancements can be attributed to the effect of strong local electromagnetic fields by the LSP resonance of AgPRs because the number of Pd-porphyrin molecules, which are placed within the

strong local electromagnetic fields increases linearly with the coverage of AgPRs. For Pd-porphyrin/SAgPRs(X), the EFs of the fluorescence and the phosphorescence achieved are 18.2 ± 1.3 and 1.70 ± 0.02 at the highest extinction intensity ($X = 0.25$), respectively, while for Pd-porphyrin/LAgPRs(X), those achieved are 8.20 ± 0.48 and 3.10 ± 0.13 at the same extinction intensity, respectively.
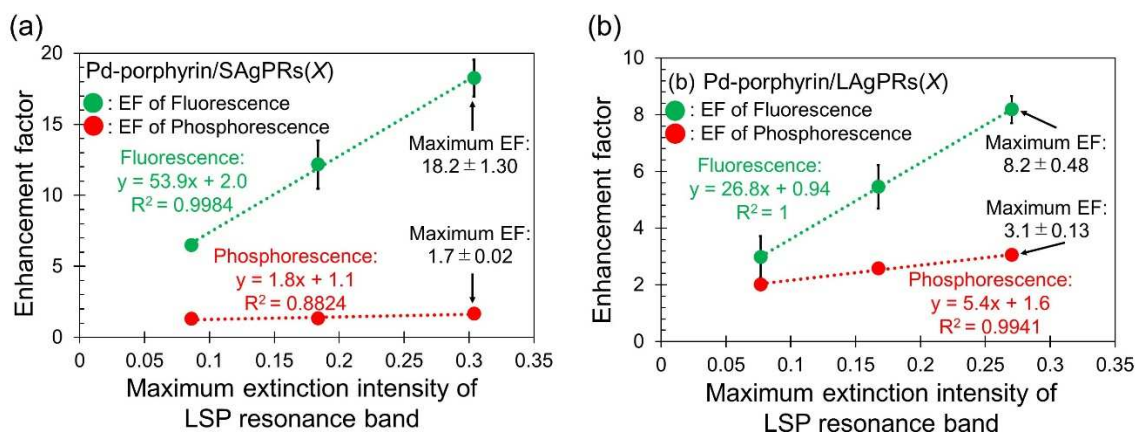

Figure 2-12. Plots of EFs of fluorescence at 550 nm and phosphorescence at 667 nm against the extinction intensities of the LSP resonance bands of (**a**) Pd-porphyrin/SAgPRs(X) and (**b**) Pd-porphyrin/LAgPRs(X).

Furthermore, the slope of the EF plot for the fluorescence of Pd-porphyrin/SAgPRs(X) (53.9) is larger than that of the Pd-porphyrin/LAgPRs(X) (26.8), while the slope for the phosphorescence of Pd-porphyrin/SAgPRs(X) (1.76) is smaller than that of Pd-porphyrin/LAgPRs(X) (5.36). These results indicate that the fluorescence and phosphorescence was selectively enhanced by adjusting the wavelengths of the LSP resonance band.

According to the radiating plasmon model, the nonradiative energy transfer from the singlet excited state of Pd-porphyrin to the LSP of SAgPRs is induced, followed by radiation mirroring the spectral properties of the excited state of the molecule. [15-20] Consequently, the apparent fluorescence was significantly enhanced. Although the above-mentioned explanation seems reasonable, the fluorescence lifetime of Pd-porphyrin is significantly shorter (*vide infra*) than those of typical fluorophores (2-20 ns) which have frequently been used for plasmonic metal-enhanced fluorescence. [15-20] This is because the relaxation process from the singlet excited state is dominated by the ultrafast intersystem crossing to the triplet state. Therefore, to further clarify the mechanism of significant fluorescence enhancement, the effect of LSP on the short-lived singlet excited

state of Pd-porphyrin was investigated in more detail.

We measured the lifetimes of phosphorescence from the Pd-porphyrin/LAgPRs(0.25), and the Pd-porphyrin/glass (**Figure 2-13**).
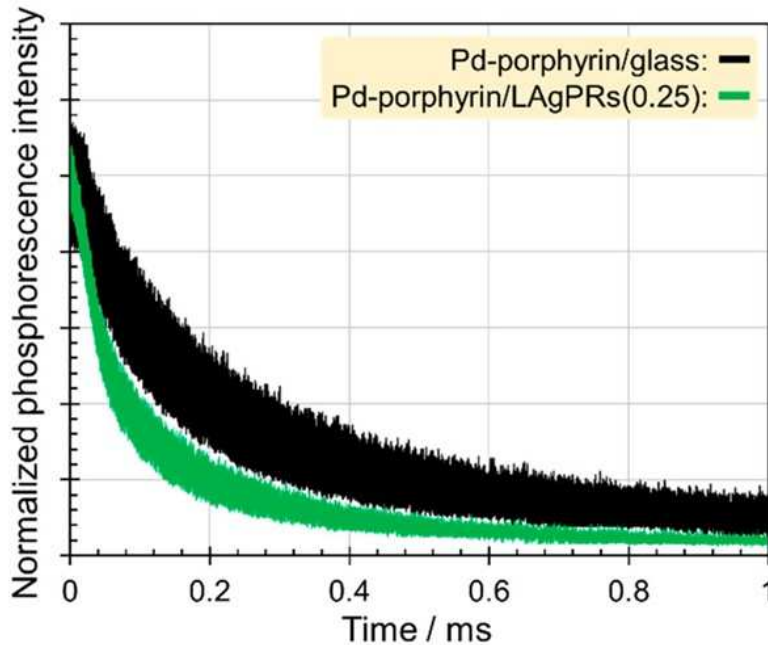

Figure 2-13. Emission lifetime measurements of phosphorescence obtained from Pd-porphyrin/glass and Pd-porphyrin/LAgPRs(0.25) (λ_{ex} = 402 nm).

This result suggests that the process of radiation through the nonradiative energy transfer from the triplet excited state to the LSP of LAgPRs became dominant (schematic showing in **(b) in Figure 2-14**) over the original relaxation process from the triplet excited state to the singlet ground state (that in **(a) in Figure 2-14**). Consequently, the original energy diagram of Pd-porphyrin/glass described in **(a) in Figure 2-14** is modified as described in **(b) in Figure 2-14** by the effect of LSP of LAgPRs. The $k_{singlet,rad}$, $k_{singlet,nonrad}$ and k_{ISC} indicate the radiative decay rate, nonradiative decay rate, and intersystem crossing rate from the singlet excited state to the triplet excited state, respectively. The $k_{triplet,rad}$ and $k_{triplet,nonrad}$ are radiative decay rate and nonradiative decay rate, respectively, from the triplet excited state. The Purcell effect indicates the enhancement of spontaneous emission rates by modifying the photonic environment by the LSP resonance. The F_{rad} is the partial Purcell factor that leads to the enhancement of the radiative decay rate and the F_{nonrad} is the remaining Purcell factor corresponding to the nonradiative quenching effect due to the metal.
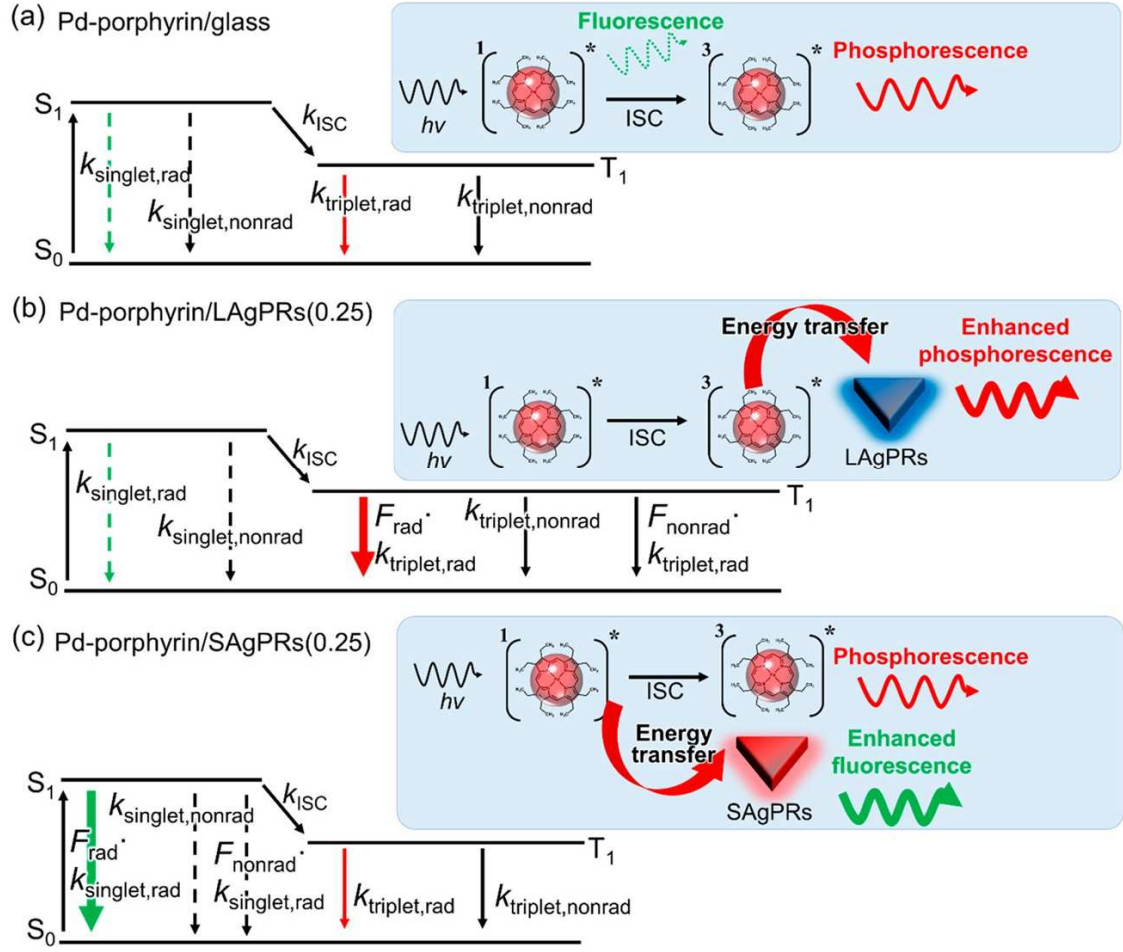
Figure 2-14. (a) Typical schematic energy diagram of free Pd-porphyrin (Pd-porphyrin/glass) and modified schematic energy diagrams of the Pd-porphyrin near **(b)** LAgPRs (Pd-porphyrin/LAgPRs(0.25)) and **(c)** SAgPRs (Pd-porphyrin/SAgPRs(0.25)). The emission enhancement mechanisms according to the radiating plasmon model are also described within blue region.

Along with this, the original Φ_{phos} (equation (1)) is changed to the $\Phi_{\text{phos,LAgPR}}$ (equation (2)) by the presence of LAgPRs. [37]

$$\Phi_{\text{phos}} = \frac{k_{\text{triplet,rad}}}{k_{\text{triplet,rad}} + k_{\text{triplet,nonrad}}} \quad (1)$$

$$\Phi_{\text{phos,LAgPR}} = \frac{F_{\text{rad}} \cdot k_{\text{triplet,rad}}}{F_{\text{rad}} \cdot k_{\text{triplet,rad}} + F_{\text{nonrad}} \cdot k_{\text{triplet,rad}} + k_{\text{triplet,nonrad}}} \quad (2)$$

For equation (2), it is assumed that the intrinsic nonradiative decay rate does not change

with the insertion of AgPRs. The energy transfer rate to LSP can be in orders similar to or much larger than fluorescence decay rates $(2\text{-}20\text{ ns})^{-1}$, considering that, in general, fluorescence is effectively enhanced through energy transfer to the LSP in the radiating plasmon model, it is not surprising that the energy transfer from the triplet state (lifetime: 55 μs) overwhelms the phosphorescence process in the present system. On the other hand, the enhancement of phosphorescence radiation process may be more complex. As shown in **Figure 2-15**, a steep gradient of the highly-confined electromagnetic fields can be generated at the spatial region within *ca.* 1.5 nm, which corresponds to the lateral size of Pd-porphyrin (1.2 nm), around AgPR surfaces.
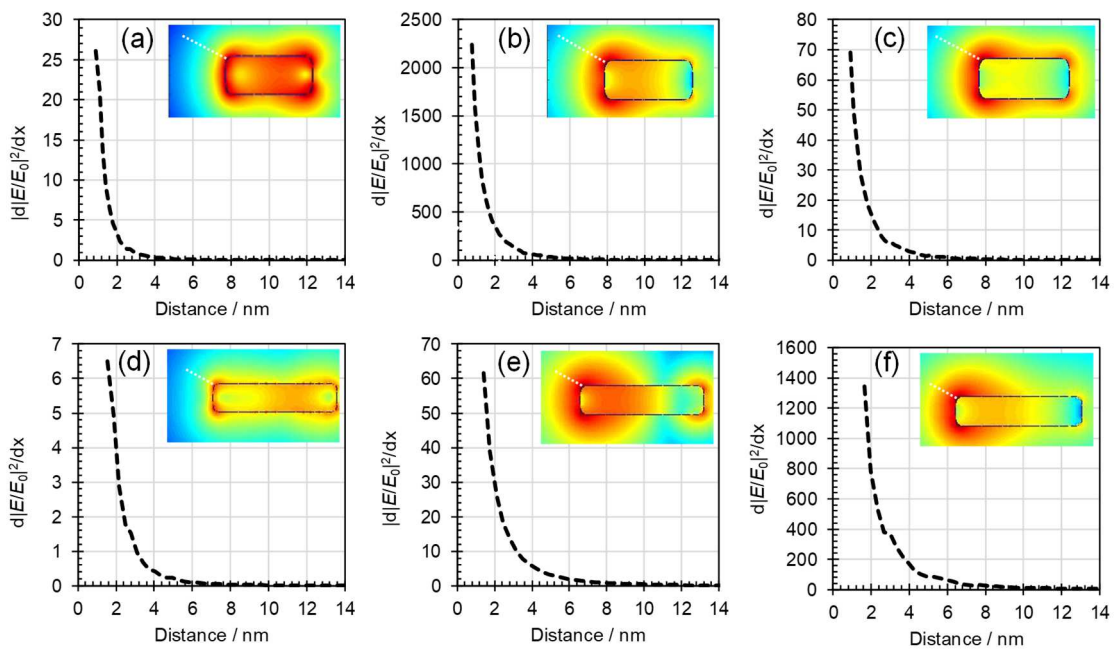
Figure 2-15. Gradient of electromagnetic field around SAgPRs and LAgPRs obtained from the cross-section along the white dot line at the inset figure in Figure 2-9; (a) 391 nm, (b) 550 nm, and (c) 667 nm for SAgPR and (d) 391 nm, (e) 550 nm, and (f) 667 nm for LAgPR.

Therefore, in addition to the Purcell effect, which is commonly applicable for the pure dipolar transitions, the steep gradient in highly-confined electromagnetic fields generated around AgPRs (**Figure 2-10**) may also partly contribute to the phosphorescence enhancement for a small number of Pd-Porphyrin close to AgPRs because the phosphorescence process involves transitions between states of different spin multiplicities. [38-42]

Next, we measured the fluorescence decay in the presence and absence of SAgPRs (**Figure 2-16**). The fluorescence decay curve of Pd-porphyrin/glass as the reference can

be well-fitted by using a convolution method with the monoexponential decay with a time constant of 15 ps, indicating that the average fluorescence lifetime of Pd-porphyrin in PMMA layers without the SAgPRs was 15 ps.
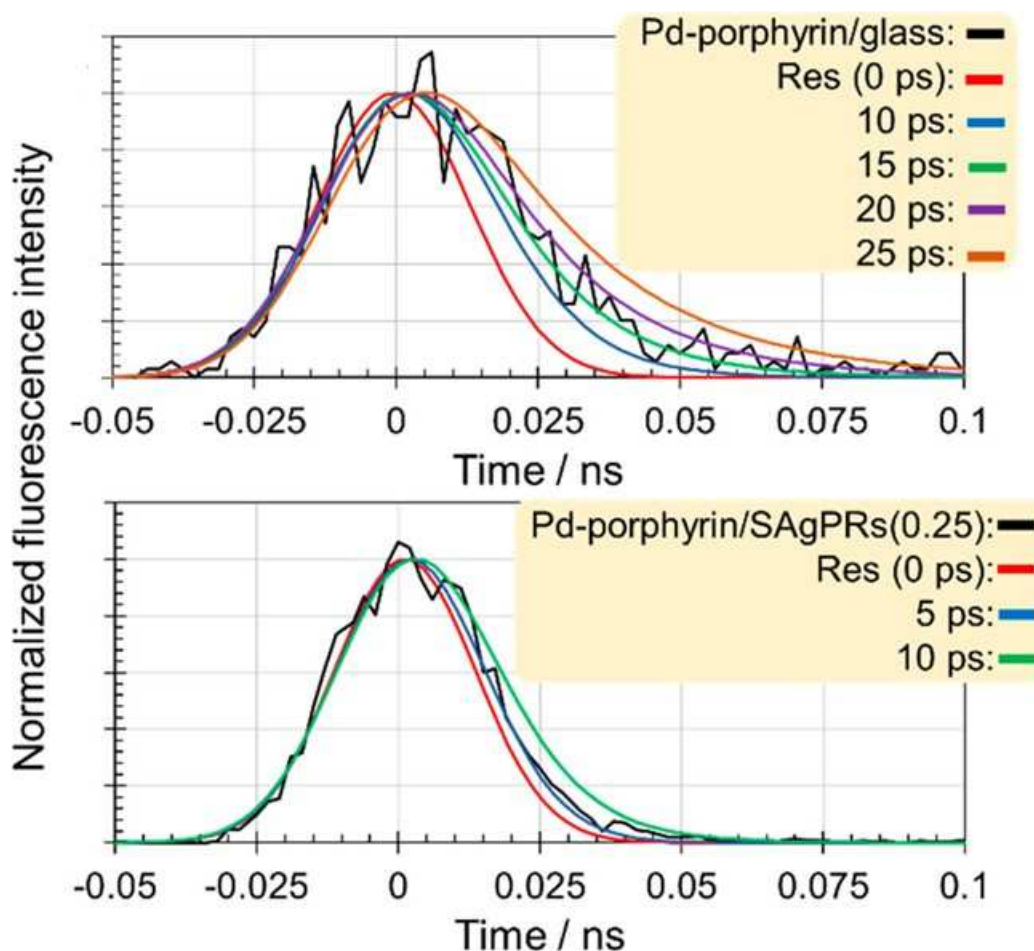

Figure 2-16. Emission lifetime measurements of fluorescence obtained from Pd-porphyrin/glass and Pd-porphyrin/SAgPRs(0.25) (λ_{ex} = 402 nm).

The fluorescence decay curve obtained from the Pd-porphyrin/SAgPRs(0.25) was similar to the monoexponential decay with a time constant of 5 ps, indicating that the average lifetime was estimated to be 5 ps. Therefore, it is clear that the fluorescence lifetime of Pd-porphyrin/SAgPRs(0.25) was significantly shorter than that of Pd-porphyrin/glass. Since the rate of Φ_{ISC} is almost 1, the k_{ISC} is much larger than the $k_{singlet,rad}$ and the $k_{singlet,nonrad}$ in the original energy diagram (**(a) in Figure 2-14**). Furthermore, the intersystem crossing, which is a dipole-forbidden spin-flip-required process, may be accelerated by the steep gradient of electromagnetic fields around AgPRs for a small fraction of Pd-porphyrin molecules closest to AgPRs (**Figure 2-15**). [38-42] Nevertheless,

the further-shortened fluorescence lifetime and the significant fluorescence enhancement, which are induced by the effect of LSP of SAgPRs spectrally overlapping with the fluorescence band of Pd-porphyrin, suggest that the $k_{singlet,rad}$ was modified by the Purcell effect ($F_{rad} \cdot k_{singlet,rad}$). It is reasonable that the Φ_{fluo} (equation (3)) was modified into equation (4) for $\Phi_{fluo,SAgPR}$ by the effect of LSP.

$$\Phi_{fluo} = \frac{k_{singlet,rad}}{k_{singlet,rad} + k_{singlet,nonrad} + k_{ISC}} \quad (3)$$

$$\Phi_{fluo,SAgPR} = \frac{F_{rad} \cdot k_{singlet,rad}}{F_{rad} \cdot k_{singlet,rad} + F_{nonrad} \cdot k_{singlet,rad} + k_{singlet,nonrad} + k_{ISC}} \quad (4)$$

Recently, the giant emission enhancement from emitters (*e.g.* organic fluorophores, quantum dots, and light-harvesting complexes) has been achieved by positioning them in the region of nanogaps between metal nanoparticle dimers and metal nanoparticle/metal films and in the regions adjacent to anisotropic metal nanoparticles. Along with these enhancements, the emission lifetimes have been reported to be significantly reduced from the original lifetimes (280 ps-10 ns) to < 10-35 ps. [43-48] In the present case, the original quite short lifetime owing to the intramolecular ultrafast intersystem crossing was further shortened to 5 ps by the LSP resonance effect. In terms of the radiating plasmon model, the $F_{rad} \cdot k_{singlet,rad}$ (2×10^{11} s^{-1}) became to be comparable to the k_{ISC} (~ 10^{11} s^{-1} in solution), [49] the insertion of pathway of fluorescence radiation through the nonradiative energy transfer from the singlet excited state to the LSP of SAgPRs into the relaxation process of singlet excited Pd-porphyrin was possible regardless of the ultrafast intersystem crossing process owing to the strong spin-orbit coupling by the presence of heavy palladium atom and maybe the steep gradients of electromagnetic fields (**(c) in Figure 2-14**).

Besides, when *platinum* octaethylporphyrin (Pt-porphyrin), whose heavy atom effect is stronger than that of Pd-porphyrin was hybridized with the SAgPRs in the same manner as employed in this study, the fluorescence was hardly observed (**Figure 2-17**). These results imply that the insertion of the nonradiative energy transfer process to the LSP of SAgPRs to the rapid intramolecular intersystem crossing from the singlet excited state is possible for the Pd-porphyrin, but is impossible for Pt-porphyrin which has a larger intersystem crossing rate (k_{ISC}: ~ 10^{12} s^{-1} in solution). [50,51]
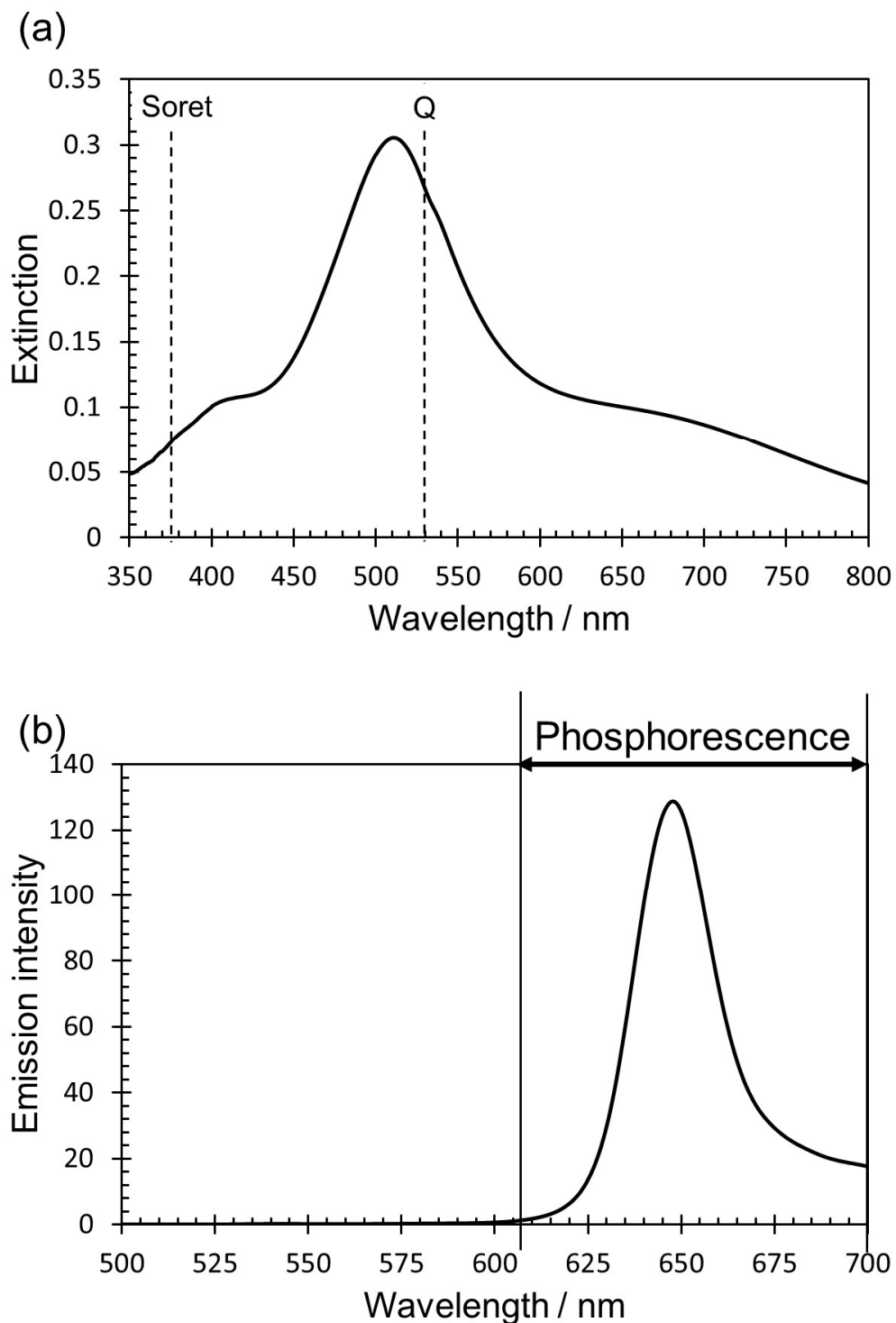
Figure 2-17. Optical properties of hybrids of Pt-porphyrin and SAgPRs. **(a)** Extinction spectrum of Pt-porphyrin/SAgPRs(0.25). **(b)** Emission spectrum of Pt-porphyrin/SAgPRs(0.25) (λ_{ex} = 381 nm corresponding to the Soret band of Pt-porphyrin). The prominent emission band around 650 nm was ascribed to the phosphorescence radiation.

50

2-3-4. Effect of Distance between Pd-porphyrin and AgPRs on Emissive Mode

Although the emission is enhanced by approximately positioning emitters near the plasmonic metal nanoparticles, when the metal nanoparticles are too close (less than *ca.* 5 nm), the emission is rather quenched by the metal nanoparticles owing to the energy transfer and/or exciton recombination. [52-54] On the other hand, the emitter positioned outside the nanospace of local electromagnetic fields cannot benefit from the enhancement effects. Thus, the spatial arrangement of the emitter from the metal nanoparticles must be precisely optimized to achieve the maximum emission enhancement. [55-57] To investigate the distance dependences for both the fluorescence and phosphorescence enhancement in the hybrids of Pd-porphyrin and AgPRs, the polyelectrolyte multilayers composed of negatively charged polystyrene sulfonate (PSS) and positively charged PEI were inserted between the PMMA layers containing Pd-porphyrin and the SAgPRs(0.25)/glass and LAgPRs(0.25)/glass (denoted as Pd-porphyrin/[PSS-PEI(Y)]/SAgPRs and Pd-porphyrin/[PSS-PEI(Y)]/LAgPRs, Y denoting the deposition number of the PSS-PEI bilayers). [58] The polyelectrolyte multilayer composed of the cationic polymer and the anionic polymer is frequently used as spacers to control the distance between emitters and plasmonic materials, because that can be easily fabricated by a layer-by-layer technique and the thickness of them can be precisely tuned on the order of the nanometer scale. [55-57] In addition, since aqueous solutions of PSS and PEI were transparent, it was expected that the formation of the PSS-PEI bilayers did not affect the optical property of Pd-porphyrin. The thickness of one bilayer of PSS and PEI was estimated by the AFM measurement for the [PSS-PEI(Y)]/glass substrate (Y = 10 and 20). (**Figure 2-18**).
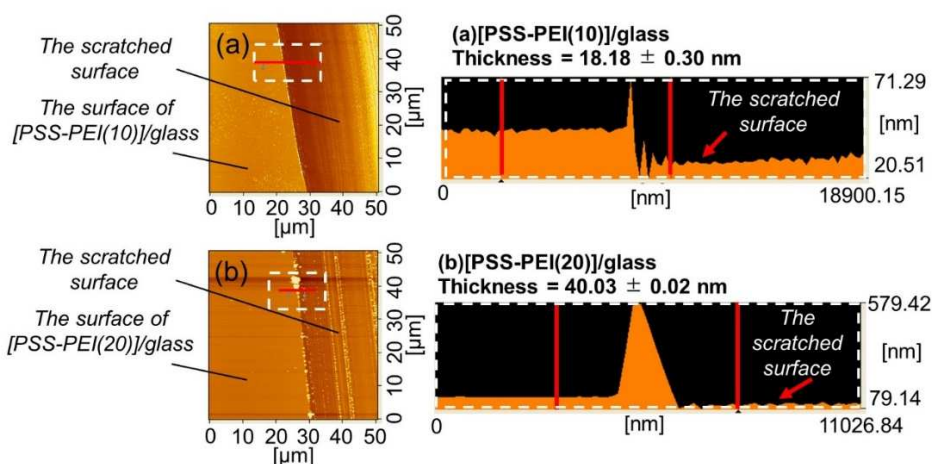

Figure 2-18. AFM images obtained from **(a)** [PSS-PEI(10)]/glass and **(b)** [PSS-PEI(20)]/glass for the estimation of the thickness of PSS-PEI bilayers.

The probe needle was scanned over the layer surfaces scratched by a sharp tweezer. The thickness of [PSS-PEI(10)]/glass and of [PSS-PEI(20)]/glass are estimated to be 18.2 ± 0.3 nm and 40.0 ± 0.0 nm, respectively. Therefore, the thickness of one bilayer was estimated to be *ca.* 1.9 nm.

Normalized extinction spectra for the [PSS-PEI(Y)]/SAgPRs(0.25) and [PSS-PEI(Y)]/LAgPRs(0.25) (Y = 0 - 5) are shown in **Figure 2-19,** respectively.
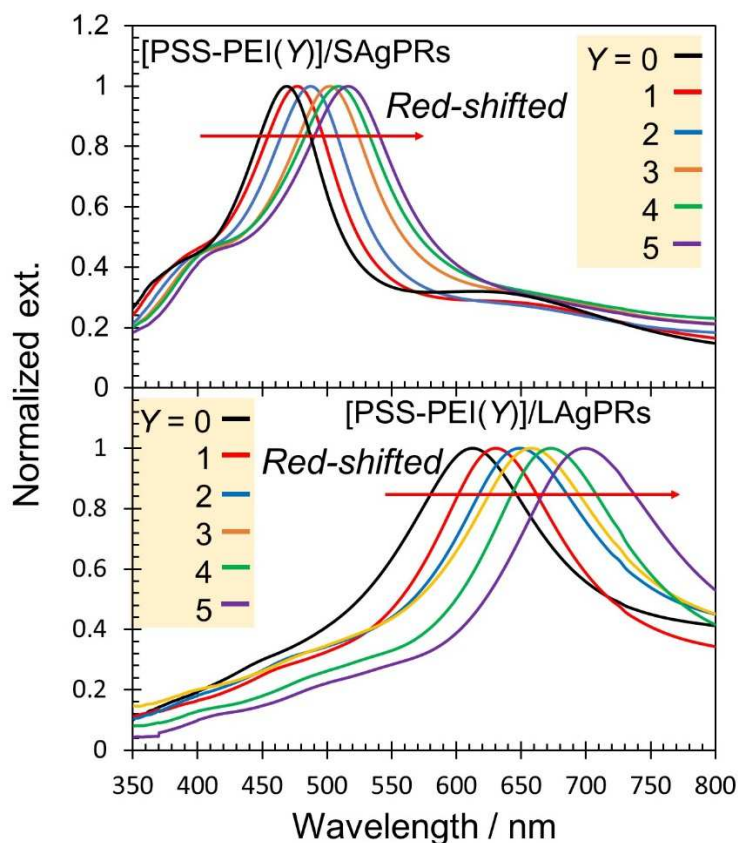
Figure 2-19. Change in optical properties with the deposition cycles of PSS-PEI bilayers inserted between the Pd-porphyrin layers and the AgPRs. Normalized extinction spectra of [PSS-PEI(Y)]/SAgPRs and [PSS-PEI(Y)]/LAgPRs (Y denotes the deposition number of the PSS-PEI bilayers (0 - 5)).

The main LSP resonance bands of SAgPRs and LAgPRs are red-shifted linearly with the increase in the deposition number of the PSS/PEI bilayer (**Figure 2-20**). These results indicate that the thickness of the polyelectrolyte layer of which the refractive index (*ca.* >1.5) is higher than that of air uniformly increases around the AgPRs with an increase in the deposition number. [59] The slope of [PSS-PEI(Y)]/SAgPRs(0.25) (9.9) in **Figure 2-20** is lower than that of [PSS-PEI(Y)]/LAgPRs(0.25) (15.7).
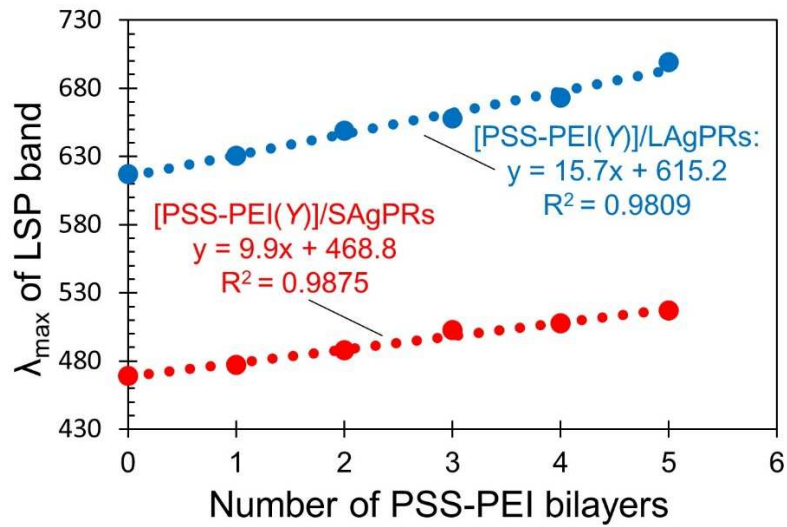
Figure 2-20. The plots of LSP peak wavelengths against the number of PSS-PEI bilayers.

This would be attributed to the difference in the response sensitivity of SAgPRs and LAgPRs because the AgPRs with a higher aspect ratio exhibit a higher response sensitivity against the change in the surrounding refractive index. [60] The distance (d) between the AgPRs and Pd-porphyrin in Pd-porphyrin/[PSS-PEI(0)]/SAgPRs(LAgPRs)(0.25) without PSS-PEI bilayer is the shortest and is estimated to be ~1 nm because the AgPRs are protected with citrate. [61,62] It should be noted that the LSP resonance bands of AgPRs after the modification of the PMMA layers containing Pd-porphyrin are not very different with or without the PSS/PEI bilayers (**Figure 2-21**).
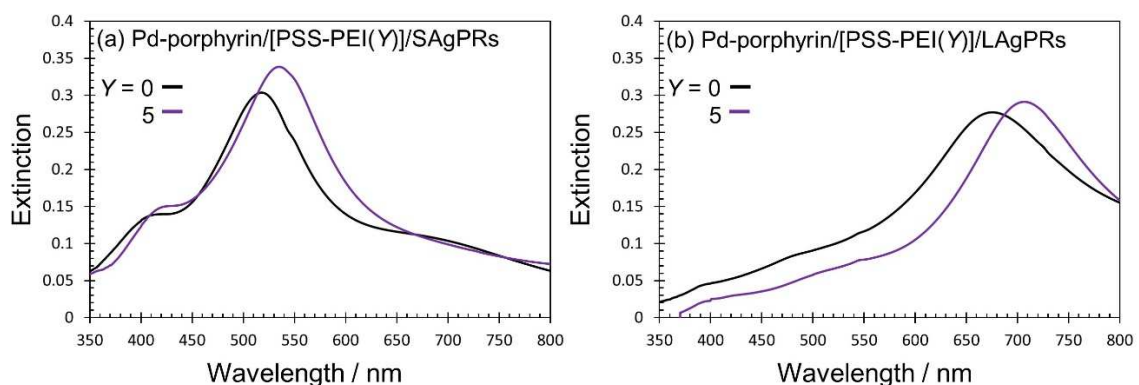
Figure 2-21. Extinction spectra of **(a)** Pd-porphyrin/[PSS-PEI(*Y*)]/SAgPRs and **(b)** Pd-porphyrin/[PSS-PEI(*Y*)]/LAgPRs (*Y* = 0 and 5). The difference in λ_{max} with and without the [PSS-PEI(5)] layers are estimated to be 24 and 31 nm for the Pd-porphyrin/[PSS-PEI(*Y*)]/SAgPRs and Pd-porphyrin/[PSS-PEI(*Y*)]/LAgPRs.

53

Therefore, it is confirmed that the degree of spectral overlap between the LSP resonance bands and the emission (fluorescence and phosphorescence) bands are not largely affected by the insertion of PSS/PEI bilayers.

The emission spectra of Pd-porphyrin/[PSS-PEI(Y)]/SAgPRs(0.25) and Pd-porphyrin/[PSS-PEI(Y)]/LAgPRs(0.25) are shown in **Figure 2-22 (a) and (b),** respectively.
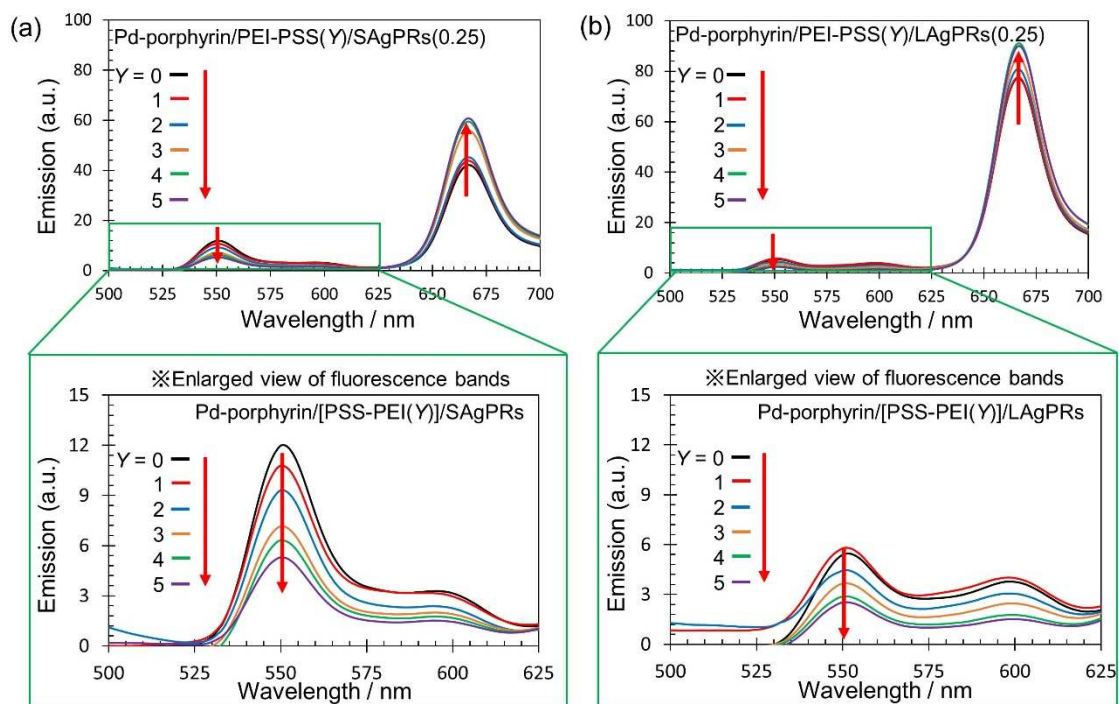

Figure 2-22. Change in emission properties with the deposition cycles of PSS-PEI bilayers inserted between the Pd-porphyrin layers and the AgPRs. Emission spectra (λ_{ex} = 391 nm) of Pd-porphyrin/[PSS-PEI(Y)]/ **(a)** SAgPRs(0.25) and **(b)** Pd-porphyrin/[PSS-PEI(Y)]/LAgPRs, respectively (Y: 0 - 5).

Also, the EFs of fluorescence at 550 nm and phosphorescence at 667 nm, which were calculated by comparing with those of the Pd-porphyrin/glass, are plotted in **Figure 2-23 (a,b) and Figure 2-24 (a,b)**, respectively. Interestingly, the distance dependences of the EFs for fluorescence and phosphorescence signals showed an opposite tendency: while the phosphorescence of Pd-porphyrin became stronger with increasing distance, the fluorescence became weaker. The significant enhancement of radiative decay rate from the triplet excited state of Pd-porphyrin would be expected at the closest distance owing to the strong local electromagnetic fields of AgPRs and perhaps the steep gradient of local electromagnetic fields. Therefore, the smallest EFs at the closest distance suggest that the

quenching effect owing to the AgPRs became dominant. [55-57, 63] In contrast, the fluorescence from the singlet excited state at the closest distance is not greatly affected by the quenching effect in the present system.
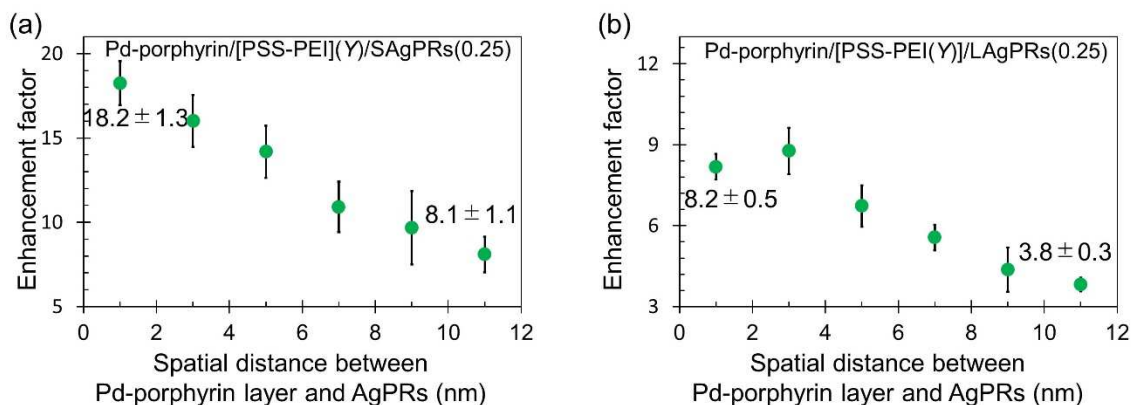
Figure 2-23. Plots of EFs of fluorescence intensity at 550 nm of **(a)** Pd-porphyrin/[PSS-PEI(*Y*)]/SAgPRs(0.25) and **(b)** Pd-porphyrin/[PSS-PEI(*Y*)]/LAgPRs(0.25) against the spatial distance between Pd-porphyrin layer and AgPRs.
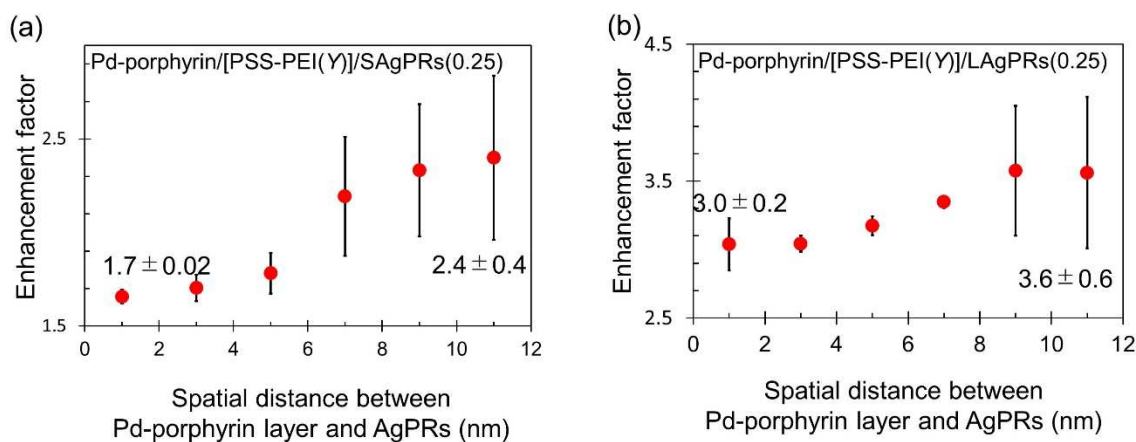
Figure 2-24. Plots of EFs of phosphorescence intensity at 667 nm of **(a)** Pd-porphyrin/[PSS-PEI(*Y*)]/SAgPRs(0.25) and **(b)** Pd-porphyrin/[PSS-PEI(*Y*)]/LAgPRs(0.25) against the spatial distance between Pd-porphyrin layer and AgPRs.

The unusual effect would be due to the quite fast intersystem crossing of Pd-porphyrin. As the k_{ISC} is very fast, the EF of fluorescence is described in equation (5) because equations (3) and (4) are reduced to $\Phi_{fluo} \sim k_{singlet,rad}/k_{ISC}$ and $\Phi_{fluo,SAgPR} \sim F_{rad} \cdot k_{singlet,rad}/k_{ISC}$, respectively.

$$\frac{\Phi_{\text{fluo,SAgPR}}}{\Phi_{\text{fluo}}} = F_{\text{rad}} \quad (5)$$

Equation (5) indicates that the F_{nonrad} term disappears and hence the fluorescence is less susceptible to the quenching. As a result, it is found that while the closest distance is suitable for the selective enhancement of fluorescence, the intermediate separation distance (above *ca.* 10 nm) is suitable for the selective enhancement of phosphorescence regardless of the aspect ratio of AgPRs. While the fluorescence radiation from phosphorescent molecule triggered by surface plasmon resonance of plasmonic metal nanoparticles was achieved, a related effect was reported for graphene plasmon of nonmetallic graphene. [24] It was advocated that the fluorescence radiation using graphene plasmon is attributed to the localization charges at the interface between graphene and Pt-porphyrin faced on the graphene. Indeed, the prominent fluorescence was observed only by a directly-adsorbed, well-ordered, and closely-packed single layer of Pt-porphyrin onto the surface of graphene layers. On the other hand, in this study, the fluorescence enhancement factor of > 5 was maintained for phosphorescent Pd-porphyrin even though the Pd-porphyrin molecules and SAgPRs was separated by > 10 nm. These results suggest that the fluorescence radiation was induced by positioning the Pd-porphyrin within the spatial region of strong local electromagnetic fields on the SAgPRs. We observed that the LSP resonance of metal nanoparticles significantly modified the emission dynamics of Pd-porphyrin, but not that of Pt-porphyrin, while the emission dynamics of Pt-porphyrin were significantly modified by the graphene plasmon. We need to further investigate the difference in the impact on emission dynamics. Unlike the graphene plasmon, the fluorescence radiation of phosphorescent molecule using metal nanoparticles will be useful for the easy preparation (*e.g.*, spin-coating) of intelligent emissive materials, the development of sensitive fluorescence-based biosensors, and so on.

2-4. Conclusion

We have succeeded in controlling the emissive modes between fluorescence and phosphorescence from intrinsically phosphorescent Pd-porphyrin by controlling the extinction intensity and the wavelengths of LSP resonance of AgPRs. It was found that the plasmon-induced emissive mode control is achieved by the insertion of nonradiative energy transfer process from the singlet excited state to the LSP of AgPRs into the original relaxation processes including the ultrafast intramolecular intersystem crossing process. The distance dependence between Pd-porphyrin and the AgPRs of these emissive modes showed an interesting opposite trend. Namely, the distance can be one of the parameters for the emissive mode control of Pd-porphyrin.

2-5. References

1. Cui, L.-S.; Ruan, S.-B.; Bencheikh, F.; Nagata, R.; Zhang, L.; Inada, K.; Nakanotani, H.; Liao, L.-S.; Adachi, C. Long-lived Efficient Delayed Fluorescence Organic Light-Emitting Diodes Using *n*-Type Hosts. *Nat. Commun.* **2017**, *8*, 1-8.

2. Okabe, K.; Inada, N.; Gota, C.; Harada, Y.; Funatsu, T.; Uchiyama, S. Intracellular Temperature Mapping with a Fluorescent Polymeric Thermometer and Fluorescence Lifetime Imaging Microscopy. *Nat. Commun.* **2012**, *3*, 1714/1-1714/9.

3. Anwar, S.; Ding, H.; Xu, M.; Hu, X.; Li, Z.; Wang, J.; Liu, L.; Jiang, L.; Wang, D.; Dong, C.; Yan, M.; Wang, Q.; Bi, H. Recent Advances in Synthesis, Optical Properties, and Biomedical Applications of Carbon Dots. *ACS Appl. Bio Mater.* **2019**, *2*, 2317-2338.

4. Li, J.; Wang, B.; Zhang, H.; Yu, J. Carbon Dots-in-Matrix Boosting Intriguing Luminescence Properties and Applications. *Small*, **2019**, *15*, e1805504.

5. Harriman, A. Luminescence of Porphyrins and Metalloporphyrins. Part 1.—Zinc (II), Nickel (II) and Manganese (II) Porphyrins. *J. Chem. Soc., Faraday Trans. 1* **1980**, *76*, 1978−1985.

6. Harriman, A. Luminescence of Porphyrins and Metalloporphyrins. Part 3.—Heavy-Atom Effects. *J. Chem. Soc., Faraday Trans. 2* **1981**, *77*, 1281−1291.

7. Sugiuchi, M.; Maeba, J.; Okubo, N.; Iwamura, M.; Nozaki, K.; Konishi, K. Aggregation-Induced Fluorescence-to-Phosphorescence Switching of Molecular Gold Clusters. *J. Am. Chem. Soc.* **2017**, *139*, 17731−17734.

8. Liu, G.; Zhao, Y. Switching between Phosphorescence and Fluorescence Controlled by Chiral Self-Assembly. *Adv. Sci.* **2017**, *4*, 1700021/1−1700021/4.

9. Wu, H.; Zhou, Y.; Yin, L.; Hang, C.; Li, X.; Ågren, H.; Yi, T.; Zhang, Q.; Zhu, L. Helical Self-Assembly-Induced Singlet−Triplet Emissive Switching in a Mechanically Sensitive System. *J. Am. Chem. Soc.* **2017**, *139*, 785−791.

10. Purcell, E. M. Spontaneous Emission Probabilities at Radio Frequencies. *Phys. Rev.* **1946**, *69*, 681.

11. Tam, F.; Goodrich, G. P.; Johnson, B. R.; Halas, N. J. Plasmonic Enhancement of Molecular Fluorescence. *Nano Lett.* **2007**, *7*, 496-501.

12. Srinivasan, V.; Ramamurthy, S. S. Purcell Factor: A Tunable Metric for Plasmon-Coupled Fluorescence Emission Enhancements in Cermet Nanocavities. *J. Phys. Chem. C* **2016**, *120*, 2908-2913.

13. Akselrod, G. M.; Ming, T.; Argyropoulos, C.; Hoang, T. B.; Lin, Y.; Ling, X.; Smith, D. R.; Kong, J.; Mikkelsen, M. H. Leveraging Nanocavity Harmonics for Control of Optical Processes in 2D Semiconductors. *Nano Lett.* **2015**, *15*, 3578-3584.

14. Krasnok, A. E.; Slobozhanyuk, A. P.; Simovski, C. R.; Tretyakov, S. A.; Poddubny, A.

N.; Miroshnichenko, A. E.; Kivshar, Y. S.; Belov, P. A. An Antenna Model for the Purcell Effect. *Sci. Rep.* **2015**, *5*, 12956/1− 12956/16.

15. Lakowicz, Joseph R. Radiative Decay Engineering: Biophysical and Biomedical Applications. *Anal. Biochem.* **2001**, *298*, 1-24.

16. Aslan, K.; Gryczynski, I.; Malicka, J.; Matveeva, E.; Lakowicz, J. R.; Geddes, C. D. Metal-Enhanced Fluorescence: an Emerging Tool in Biotechnology. *Curr. Opin. Biotechnol.* **2005**, *16*, 55-62.

17. Lakowicz, J. R.; Ray, K.; Chowdhury, M.; Szmacinski, H.; Fu, Y.; Zhang, J.; Nowaczyk, K. Plasmon-Controlled Fluorescence: a New Paradigm in Fluorescence Spectroscopy. *Analyst* **2008**, *133*, 1308-1346.

18. Ming, T.; Chen, H.; Jiang, R.; Li, Q.; Wang, J. Plasmon-Controlled Fluorescence: Beyond the Intensity Enhancement. *J. Phys. Chem. Lett.* **2012**, *3*, 191-202.

19. Ming, T.; Zhao, L.; Chen, H.; Woo, K. C.; Wang, J.; Lin, H.-Q. Experimental Evidence of Plasmophores: Plasmon-Directed Polarized Emission from Gold Nanorod-Fluorophore Hybrid Nanostructures. *Nano Lett.* **2011**, *11*, 2296-2303.

20. Ming, T.; Zhao, L.; Yang, Z.; Chen, H.; Sun, L.; Wang, J.; Yan, C. Strong Polarization Dependence of Plasmon-Enhanced Fluorescence on Single Gold Nanorods. *Nano Lett.* **2009**, *9*, 3896-3903.

21. Pan, S.; Rothberg, L. J. Enhancement of Platinum Octaethyl Porphyrin Phosphorescence near Nanotextured Silver Surfaces. *J. Am. Chem. Soc.* **2005**, *127*, 6087-6094.

22. Previte, M. J. R.; Aslan, K.; Zhang, Y.; Geddes, C. D. Metal-Enhanced Surface Plasmon-Coupled Phosphorescence. *J. Phys. Chem. C* **2007**, *111*, 6051-6059.

23. Gill, R.; Tian, L.; van Amerongen, H.; Subramaniam, V. Emission Enhancement and Lifetime Modification of Phosphorescence on Silver Nanoparticle Aggregates. *Phys. Chem. Chem. Phys.* **2013**, *15*, 15734-15739.

24. Kim, B.-H.; Kim, D. C.; Jang, M.; Baek, J.; Park, D.; Kang, I.; Park, Y. C.; Ahn, S.; Cho, Y.-H.; Kim, J.; Jeon, S. Extraordinary Strong Fluorescence Evolution in Phosphor on Graphene. *Adv. Mater.* **2016**, *28*, 1657-1662.

25. Grigorenko, A. N.; Polini, M.; Novoselov, K. S. Graphene plasmonics. *Nat. Photonics* **2012**, *6*, 749-758.

26. Hlawacek, G.; Khokhar, F. S.; van Gastel, R.; Poelsema, B.; Teichert, C. Smooth Growth of Organic Semiconductor Films on Graphene for High-Efficiency Electronics. *Nano Lett.* **2011**, *11*, 333-337.

27. Chen, J.; Badioli, M.; Alonso-Gonzalez, P.; Thongrattanasiri, S.; Huth, F.; Osmond, J.; Spasenovic, M.; Centeno, A.; Pesquera, A.; Godignon, P.; Zurutuza Elorza, A.; Camara,

N.; Garcia de Abajo, F. J.; Hillenbrand, R.; Koppens, F. H. L. Optical Nano-Imaging of Gate-Tunable Graphene Plasmons. *Nature* **2012**, *487*, 77-81.

28. Losev, A. P.; Aghion, J. Absorbance and Emission Properties of Palladium Octaethylporphyrin and Palladium Tetrahexylporphyrin in Solution and in Phospholipid Membranes. *J. Photochem. Photobiol. B* **1990**, *7*, 181-187.

29. Sagun, E. I.; Zen'kevich, E. I.; Knyukshto, V. N.; Tikhomirov, S. A.; Shul'ga, A. M. Picosecond Dynamics of Photoinduced Electron Transfer Involving Singlet and Triplet States in Nitroporphyrin Molecules. *Opt. Spectrosc.* **2004**, *96*, 359-372.

30. Bolze, F.; Gros, C. P.; Harvey, P. D.; Guilard, R. Luminescence Properties of a Cofacial Dipalladium Porphyrin Dimer under Argon and in the Presence of Dioxygen. *J. Porphyrins and Phthalocyanines* **2001**, *5*, 560-574.

31. Knyukshto, V. N.; Shul'ga, A. M.; Sagun, E. I.; Zen'kevich, E. I. Spectral Manifestations of Nonplanarity Effects in Pd Complexes of Porphyrins. *Opt. Spectrosc.* **2002**, *92*, 53-62.

32. Kelly, K. L.; Coronado, E.; Zhao, L. L.; Schatz, G. C. The Optical Properties of Metal Nanoparticles: The Influence of Size, Shape, and Dielectric Environment. *J. Phys. Chem. B* **2003**, *107*, 668-677.

33. Jin, R.; Cao, Y. C.; Hao, E.; Metraux, G. S.; Schatz, G. C.; Mirkin, C. A. Controlling Anisotropic Nanoparticle Growth Through Plasmon Excitation. *Nature* **2003**, *425*, 487-490.

34. Jin, R.; Cao, Y.; Mirkin, C. A.; Kelly, K. L.; Schatz, G. C.; Zheng, J. G. Photoinduced Conversion of Silver Nanospheres to Nanoprisms. *Science* **2001**, *294*, 1901-1903.

35. Xue, C.; Mirkin, C. A. pH-Switchable Silver Nanoprism Growth Pathways. *Angew. Chem., Int. Ed.* **2007**, *46*, 2036-2038.

36. Sugawa, K.; Takeshima, N.; Uchida, K.; Tahara, H.; Jin, S.; Tsunenari, N.; Akiyama, T.; Kusaka, Y.; Fukuda, N.; Ushijima, H.; Tsuchido, Y.; Hashimoto, T.; Hayashita, T.; Otsuki, J. Photocurrent Enhancement of Porphyrin Molecules over a Wide-Wavelength Region Based on Combined Use of Silver Nanoprisms with Different Aspect Ratios. *J. Mater. Chem. C* **2015**, *3*, 11439-11448.

37. Zhao, W.; Wang, S.; Liu, B.; Verzhbitskiy, I.; Li, S.; Giustiniano, F.; Kozawa, D.; Loh, K. P.; Matsuda, K.; Okamoto, K.; Oulton, R. F.; Eda, G. Exciton-Plasmon Coupling and Electromagnetically Induced Transparency in Monolayer Semiconductors Hybridized with Ag Nanoparticles. *Adv. Mater.* **2016**, *28*, 2709-2715.

38. Connell, T. U.; Earl, S. K.; Ng, C.; Roberts, A.; Davis, T. J.; White, J. M.; Polyzos, A.; Gómez, D. E. Luminescence of a Transition Metal Complex Inside a Metamaterial Nanocavity. *Small*, **2017**, *13*, 1700692.

39. Yang, N.; Tang, Y.; Cohen, A. E. Spectroscopy in Sculpted Fields. *Nano Today*, **2009**, *4*, 269-279.

40. Duan, S.; Rinkevicius, Z.; Tian, G.; Luo, Y. Optomagnetic Effect Induced by Magnetized Nanocavity Plasmon. *J. Am. Chem. Soc.*, **2019**, *141*, 13795-13798.

41. Roth, D. J.; Ginzburg, P.; Hirvonen, L. M.; Levitt, J. A.; Nasir, M. E.; Suhling, K.; Richards, D.; Podolskiy, V. A.; Zayats, A. V. Singlet–Triplet Transition Rate Enhancement inside Hyperbolic Metamaterials. *Laser Photonics Rev.* **2019**, *13*, 1900101.

42. Rivera, N.; Kaminer, I.; Zhen, B.; Joannopoulos, J. D.; Soljačić, M. Shrinking Light to Allow Forbidden Transitions on the Atomic Scale. *Science*, **2016**, *353*, 263-269.

43. Kinkhabwala, A.; Yu, Z.; Fan, S.; Avlasevich, Y.; Muellen, K.; Moerner, W. E. Large Single-Molecule Fluorescence Enhancements Produced by a Bowtie Nanoantenna. *Nat. Photonics* **2009**, *3*, 654-657.

44. Busson, M. P.; Rolly, B.; Stout, B.; Bonod, N.; Bidault S. Accelerated Single Photon Emission from Dye Molecule-Driven Nanoantennas Assembled on DNA. *Nat. Commun.* **2012**, *3*, 962/1-962/6.

45. Wientjes, E.; Renger, J.; Curto, A. G.; Cogdell, R.; van Hulst, N. F. Strong Antenna-Enhanced Fluorescence of a Single Light-Harvesting Complex Shows Photon Antibunching. *Nat. Commun.* **2014**, *5*, 4236/1−4236/7.

46. Hoang, T. B.; Akselrod, G. M.; Argyropoulos, C.; Huang, J.; Smith, D. R.; Mikkelsen, M. H. Ultrafast Spontaneous Emission Source Using Plasmonic Nanoantennas. *Nat. Commun.* **2015**, *6*, 7788.

47. Bidault, S.; Devilez, A.; Maillard, V.; Lermusiaux, L.; Guigner, J.-M.; Bonod, N.; Wenger, J. Picosecond Lifetimes with High Quantum Yields from Single-Photon-Emitting Colloidal Nanostructures at Room Temperature. *ACS Nano* **2016**, *10*, 4806-4815.

48. Hoang, T. B.; Akselrod, G. M.; Mikkelsen, M. H. Ultrafast Room-Temperature Single Photon Emission from Quantum Dots Coupled to Plasmonic Nanocavities. *Nano Lett.* **2016**, *16*, 270-275.

49. Filatov, M. A.; Etzold, F.; Gehrig, D.; Laquai, F.; Busko, D.; Landfester, K.; Baluschevade, S. Interplay between Singlet and Triplet Excited States in a Conformationally Locked Donor–Acceptor Dyad. *Dalton Trans.* **2015**, *44*, 19207-19217.

50. Hinke, J. A.; Pundsack, T. J; Luhman, W. A.; Holmes R. J.; Blank, D. A. Communication: Trapping Upconverted Energy in Neat Platinum Porphyrin Films *via* an Unexpected Fusion Mechanism. *J. Chem. Phys.* **2013**, *139*, 101102/1−101102/4.

51. Roberts, S. T.; Schlenker C. W.; Barlier, V.; McAnally, R. E.; Zhang, Y.; Mastron, J. N.; Thompson, M. E.; Bradforth, S. E. Observation of Triplet Exciton Formation in a Platinum-Sensitized Organic Photovoltaic Device. *J. Phys. Chem. Lett.* **2011**, *2*, 48-54.

52. Kulakovich, O.; Strekal, N.; Yaroshevich, A.; Maskevich, S.; Gaponenko, S.; Nabiev, I.; Woggon, U.; Artemyev, M. Enhanced Luminescence of CdSe Quantum Dots on Gold Colloids. *Nano Lett.* **2002**, *2*, 1449-1452.

53. Li, M.; Cushing, S. K.; Wang, Q.; Shi, X.; Hornak, L. A.; Hong, Z.; Wu, N. Size-Dependent Energy Transfer between CdSe/ZnS Quantum Dots and Gold Nanoparticles. *J. Phys. Chem. Lett.* **2011**, *2*, 2125-2129.

54. Anger, P.; Bharadwaj, P.; Novotny, L. Enhancement and Quenching of Single-Molecule Fluorescence. *Phys. Rev. Lett.* **2006**, *96*, 113002/1-113002/4.

55. Ray, K.; Badugu, R.; Lakowicz, J. R. Polyelectrolyte Layer-by-Layer Assembly to Control the Distance between Fluorophores and Plasmonic Nanostructures. *Chem. Mater.* **2007**, *19*, 5902-5909.

56. Cheng, D.; Xu, Q.-H. Separation Distance Dependent Fluorescence Enhancement of Fluorescein Isothiocyanate by Silver Nanoparticles. *Chem. Commun.* **2007**, 248-250.

57. Nooney, R. I.; Stranik, O.; McDonagh, C.; MacCraith, B. D. Optimization of Plasmonic Enhancement of Fluorescence on Plastic Substrates. *Langmuir* **2008**, *24*, 11261-11267.

58. Hagen, D. A.; Foster, B.; Stevens, B.; Grunlan, J. C. Shift-Time Polyelectrolyte Multilayer Assembly: Fast Film Growth and High Gas Barrier with Fewer Layers by Adjusting Deposition Time. *ACS Macro Lett.* **2014**, *3*, 663-666.

59. Wang, D.; Zhang, J.; He, Y.; Li, W.; Li, S.; Fu, X.; Tian, M.; Zhou, Y.; Yao, Z. Large Area, Highly Transparent, and Mechanically Stable Adhesive Films with Tunable Refractive Indices. *Macromol. Chem. Phys.* **2018**, *219*, 8, 1700608/1−1700608/9.

60. Charles, D. E.; Aherne, D.; Gara, M.; Ledwith, D. M.; Gun'ko, Y. K.; Kelly, J. M.; Blau, W. J.; Brennan-Fournet, M. E. Versatile Solution Phase Triangular Silver Nanoplates for Highly Sensitive Plasmon Resonance Sensing. *ACS Nano* **2010**, *4*, 55-64.

61. Stobiecka, M.; Coopersmith, K.; Hepel, M. Resonance Elastic Light Scattering (RELS) Spectroscopy of Fast Non-Langmuirian Ligand-Exchange in Glutathione-Induced Gold Nanoparticle Assembly. *J. Colloid Interface Sci.* **2010**, *350*, 168-177.

62. Monti, S.; Barcaro, G.; Sementa, L.; Carravetta, V.; Agren, H. Characterization of the Adsorption Dynamics of Trisodium Citrate on Gold in Water Solution. *RSC Adv.* **2017**, *7*, 49655-49663.

63. Jin, S.; Sugawa, K.; Takeshima, N.; Tahara, H.; Igari, S.; Yoshinari, S.; Kurihara, Y.; Watanabe, S.; Enoki, M.; Sato, K.; Inoue, W.; Tokuda, K.; Akiyama, T.; Katoh, R.; Takase, K.; Ozawa, H.; Okazaki, T.; Watanabe, T.; Otsuki, J. Precise Control of Localized Surface Plasmon Wavelengths Is Needed for Effective Enhancement of Triplet-Triplet Annihilation-Based Upconversion Emission. *ACS Photonics* **2018**, *5*, 5025-5037.

64. Waxenegger, J.; Trügler, A.; Hohenester, U. Plasmonics Simulations with the MNPBEM Toolbox: Consideration of Substrates and Layer Structures. *Comput. Phys. Commun.* **2015**, *193*, 138−150.

65. Rakic, A. D.; Djurisic, A. B.; Elazar, J. M.; Majewski, M. L. Optical Properties of Metallic Films for Vertical-Cavity Optoelectronic Devices. *Appl. Opt.* **1998**, *37*, 5271−5283.

66. Underwood, S.; Mulvaney, P. Effect of the Solution Refractive Index on the Color of Gold Colloids. *Langmui*r **1994**, *10*, 3427-3430.

67. Anker, J. N.; Hall, W. P.; Lyandres, O.; Shah, N. C.; Zhao, J.; Van Duyne, R. P. Biosensing with Plasmonic Nanosensors. *Nat. Mater.* **2008**, *7*, 442-453.

68. Mahmoud, M. A.; Tabor, C. E.; El-Sayed, M. A. Surface-Enhanced Raman Scattering Enhancement by Aggregated Silver Nanocube Monolayers Assembled by the Langmuir-Blodgett Technique at Different Surface Pressures. *J. Phys. Chem. C* **2009**, *113*, 5493−5501.

69. Beadie, G.; Brindza, M.; Flynn, R. A.; Rosenberg, A.; Shirk, J. S. Refractive Index Measurements of Poly(Methyl Methacrylate) (PMMA) from 0.4-1.6 μm. *Appl. Opt.* **2015**, *54*, F139-F143.

Chapter 3

Optical Property of Tetraphenyl Porphyrin

with Silver Nanoprisms

3-0. Summary

Absorption enhancement over wide wavelength region is beneficial for the light-driven electrochemical devices, such as solar cells and photocatalysts. Tetraphenyl porphyrin (TPP), which is one of porphyrin derivatives, has four absorption peaks from 500 to 700 nm (Q-bands), thus, one could be expected to act as a light harvester in broadband wavelength regions. However, the low molecular absorption coefficient of the Q-bands hinders the utilization of TPP for the development of the optoelectronic devices. In this chapter, we investigated the photoexcitation process of the hybrids composed of tetraphenyl porphyrin (TPP) and AgPRs with precisely-tuned LSP wavelength. Spectral dips were observed on the extinction spectra of the hybrids in which LSP wavelength well-overlapped with Q-bands. By measuring the absorption and scattering spectra of the hybrids, it was suggested that the absorption enhancement was induced based on plasmon-exciton coupling. Furthermore, we succeeded in the absorption enhancement in whole Q-bands of the hybrids comprised of TPP and three types of AgPRs having different aspect ratios. Therefore, we demonstrated the usefulness of the combined use of AgPRs with different aspect ratios, which paves the way to enhance absorption efficiency of the photofunctional materials over wide-wavelength region. Results in this chapter have a great potential for the development of the high-performance light-driven devices.

3-1. Introduction

Controlling light-matter interaction is one of the intensively researched topics in the photochemical science. [1] The utilization of metal nanoparticles has been recognized as a way to strengthen the light-matter interaction because they generate strong electromagnetic fields at the nanoscale dimension upon excitation of the localized surface plasmon (LSP) resonance. In particular, the interaction between LSP and exciton of photofunctional molecules is attracting much attention because of the occurrence of various beneficial optical phenomena including a huge emission enhancement, [2] suppression of photochemical quenching, [3] plasmonic resonance energy transfer, [4] enhanced water splitting, [5] and so on. Antosiewicz et al. classified the interactions between metal nanoparticles and photofunctional molecules into three regimes according to the strength of interaction: (1) the enhanced absorption regime, (2) the induced transparency regime, and (3) the strong coupling regime. [6] The strong coupling leads to the splitting of state in which the LSP and molecular exciton states are mixed, which is manifested in the splitting of the extinction peak at the wavelength of the molecular resonance peak. On the other hand, in the enhanced absorption regime, the absorption and scattering components of the LSP are damped whereas the molecular absorption is increased by the energy transfer from the LSP to the molecule. The enhanced molecular absorption cancels the damped absorption component of LSP resonance but the uncompensated damped scattering component remains as a dip in the extinction spectrum. The induced transparency regime refers to an intermediate case between the absorption enhancement regime and the strong coupling regime. Among these, the absorption enhancement is quite important for the development of highly efficient solar devices. [7-11] Particularly, absorption enhancement over a wide range of wavelength is essential to utilize the wide solar spectrum. However, the multiwavelength generation of enhanced absorption through the interaction between the LSP and the exciton has never been demonstrated. The generation of spectral dips at multiple wavelengths was reported, which was achieved by using plasmonic metal nanoparticles in combination with two different dye molecules, but this phenomenon was attributed to the Rabi oscillation in the strong coupling case and did not lead to absorption enhancement. [12] In another report on the plasmon-exciton coupling at multiple wavelengths using a combination of cyanine dye molecules exhibiting two absorption bands and metal nanorods, [13] the absorption enhancement was not identified.

In this study, we have succeeded in enhancing light absorption at multiple wavelengths over a visible region through the interaction between the exciton of dye molecules and the LSP resonances of three different kinds of plasmonic metal nanoparticles. The

achievement was made possible by developing a precise tuning technique of LSP wavelength of triangular silver nanoprisms (AgPRs). Furthermore, the enhancement factors of absorption were quantitatively evaluated utilizing the fluorescence enhancement, which occurred as a result of the interaction of exciton of dye molecules with the LSP resonance.

3-2. Experimental Section

Materials

Milli-Q-grade water (resistivity: 18.2 MΩ cm) was used for the preparation of all aqueous solutions. Toluene was purchased from Kishida Chemical (Japan). 5,10,15,20-Tetraphenyl-21H,23H-porphyrin (TPP), sodium tetrahydroborate ($NaBH_4$), silver nitrate ($AgNO_3$), and polyethyleneimine (PEI) (MW: ~10,000) were purchased from Fujifilm Wako Pure Chemical (Japan). Trisodium citrate dihydrate, sodium hydroxide (NaOH), ammonium solution (NH_3, 28%), and hydrogen peroxide solution (H_2O_2, 30%) were purchased from Kanto Chemical (Japan). All chemicals were used without further purification.

Measurements

Transmission electron microscopy (TEM) and atomic force microscopy (AFM, tapping mode) were carried out using a Hitachi HF-2000 microscope and a Hitachi SPI-3800N-SPA400 microscope, respectively. The extinction spectra of sample substrates were measured by a normal transmittance setup using a JASCO V-770 spectrometer. The absorption and scattering spectra were measured by the setup consisting of the spectrometer (JASCO V-770) equipped with an integrating sphere according to a previous report. [14] Fluorescence excitation spectra of sample substrates were measured by a JASCO FP-8600 fluorescence spectrophotometer. The calculation for the extinction spectra of AgPRs was conducted using the boundary element method (BEM) with retarded electromagnetic fields for full Maxwell equation. [15] To produce the random orientation of the AgPRs in solution phase, the transmission spectra were averaged over all allowed combinations of the incident light polarization (E_x, E_y, E_z) and the incident light propagation orientation (k_x, k_y, k_z) (geometry models: **Figure 3-1**). The dielectric function of silver was taken from the previous report by Rakic et al. [16] All the measurements were performed under atmospheric conditions.
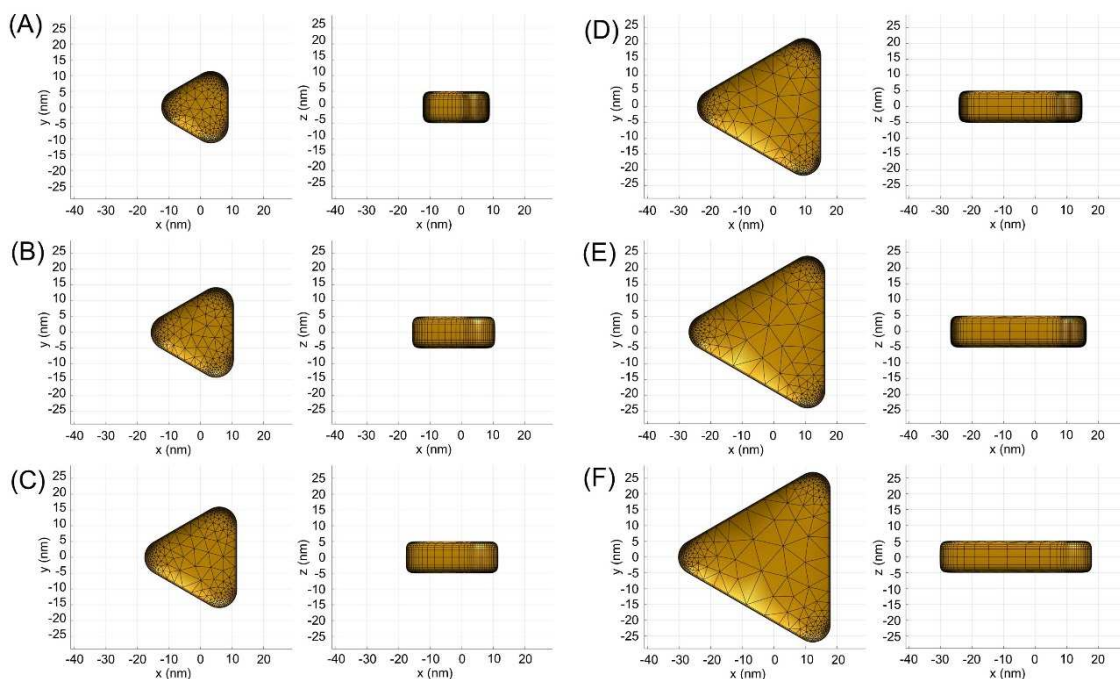
Figure 3-1. Geometric models of AgPRs with various LSP resonance wavelengths. (A) AgPRs-500, (B) AgPRs-540, (C) AgPRs-560, (D) AgPRs-625, (E) AgPRs-645 and (F) AgPRs-675.

Synthesis of AgPRs with different resonance wavelengths

The AgPRs with precisely-tuned resonance wavelengths of the in-plane dipole mode (500, 540, 560, 625, 645, and 675 nm) were synthesized by the light-mediated method developed by us. An aqueous solution (100 mL) containing trisodium citrate (5 mM) as a protective agent and $NaBH_4$ (0.2 mM) as a reducing agent was injected into an aqueous solution (100 mL) of $AgNO_3$ (1 mM) in an ice bath under stirring. The mixture was further stirred for 1 h, leading to the formation of Ag nanospheres with an average diameter of 11 nm. After an aqueous solution of NaOH (0.2 M, 100 µL) was injected into the colloidal aqueous solution of Ag nanospheres (10 mL) to adjust the pH to 11.2, LED (light emitting diode) light was irradiated, which led to the formation of AgPRs. Specifically, the resonance wavelength of in-plane dipole mode of AgPRs was precisely adjusted by sequential irradiation of LED light with different wavelengths of 470 ± 5 nm (5,800 mcd, 3×3 arrays), 525 ± 5 nm (18,000 mcd, 3×3 arrays), and 590 ± 5 nm (50,000 mcd, 3×3 arrays) for predetermined periods of time as summarized in **Table 1**, whereas the irradiation setup is shown in **Figure 3-2**. The obtained AgPRs are designated as AgPRs-*X*, in which *X* indicates the resonance wavelength.
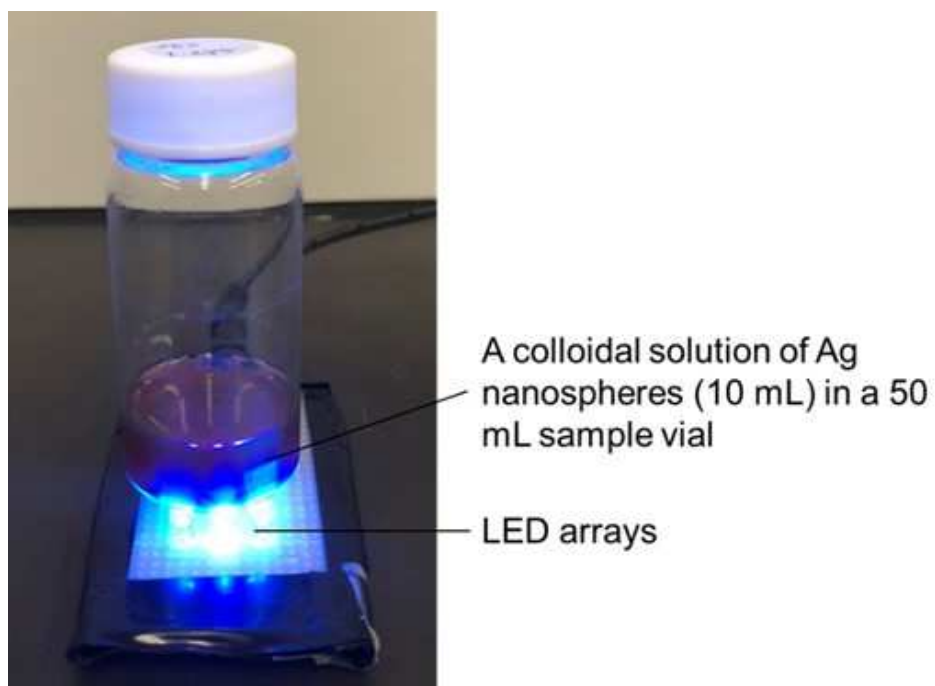
69

A colloidal solution of Ag nanospheres (10 mL) in a 50 mL sample vial

LED arrays

Figure 3-2. A Setup for the irradiation of LED light to a colloidal aqueous solution of Ag nanospheres.

Table 1. Synthetic conditions for AgPRs with various resonance wavelengths.

1: Irradiation period of 470 nm / h	2: Irradiation period of 525 nm / h	3: Irradiation period of 590 nm / h	Resonance wavelength[a] of AgPRs / nm
24	0	0	500 ± 2.0
4	20	0	540 ± 1.2
2	22	0	560 ± 0.6
0	6	42	625 ± 3.5
0	3	45	645 ± 5.0
0	2	46	675 ± 1.7

a) mean values and standard deviations

Preparation of hybrids of TPP and AgPRs

To clean the surface, a glass substrate (1.5×2.0 cm^2) was immersed into a mixed aqueous solution of 30% H_2O_2 and 28% NH_3 (1/1 = V/V) at 100 ºC for 3 h, followed by washing with Milli-Q water. The cleaned substrate was kept in Milli-Q water until use. The substrate was modified with positively-charged PEI by immersing it into an aqueous solution of PEI (4.2 mg/mL) for 1 min, followed by washing with Milli-Q water. The positively-charged substrate was then immersed in the colloidal solution to electrostatically immobilize AgPRs, which were negatively-charged owing to the citric acid sheath. The immersion was continued until the extinction intensity of the main LSP resonance band (in-plane dipole mode) reached 0.2; thus obtained substrate is referred to as AgPRs-X/glass. The extinction intensity of the LSP of AgPRs on the glass plate was set to be 0.2 to avoid the LSP coupling between adjacent AgPRs observed for more denser samples [17]. For the preparation of a glass plate on which three AgPRs (LSP resonance wavelengths of 500, 560, and 645 nm) were immobilized (AgPRs-ternary/glass), the positively-charged glass plate was immersed sequentially into respective colloidal aqueous solutions of AgPRs until each extinction intensity of the main LSP resonance reached 0.1. A toluene solution of TPP (1.5 mM) was spin-coated (3000 rpm, 30 s) on AgPRs-X/glass and AgPRs-ternary/glass, affording the hybrids of TPP and AgPRs (TPP/AgPRs-X and TPP/AgPRs-ternary). TPP was also deposited on a bare glass substrate as a reference by spin-coating the TPP solution onto the PEI-modified glass substrate (TPP/glass).

3-3. Results and Discussion

3-3-1. Optical Properties of TPP

In this study, a porphyrin derivative, TPP (molecular structure: **Figure 3-3 (a)**, absorption and emission spectra in toluene solution: **Figure 3-3 (b)**) was employed as a photofunctional molecule.
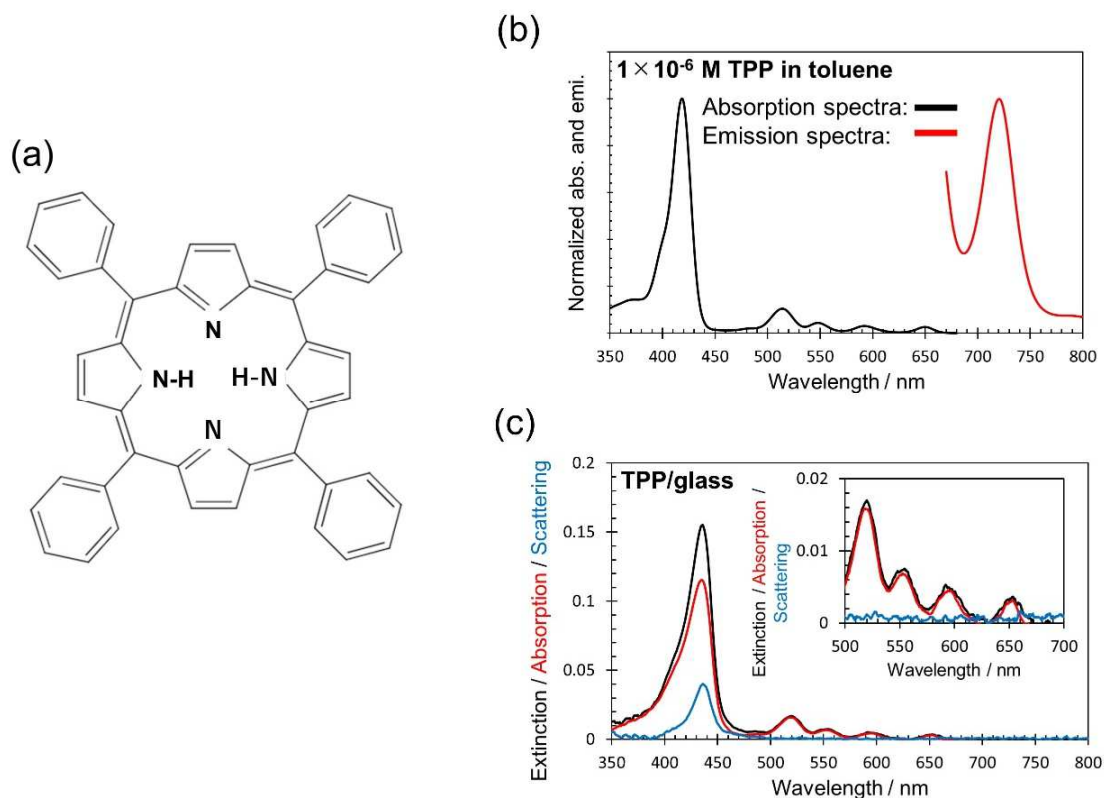

Figure 3-3. (a) Molecular structure of TPP. **(b)** Normalized absorption and emission spectra in toluene solution of TPP (1×10^{-6} M). **(c)** Extinction (black line), absorption (red line), and scattering (blue line) spectra of TPP/glass. Inset shows magnification of Q-bands.

Porphyrins, synthetic analogues of natural chlorophylls, are frequently used as light harvester owing to their wide absorption in the visible region. [18] However, the absorption coefficients of four absorption peaks in 500 – 700 nm region are relatively low (Q-bands, absorption coefficient: $\sim 10^4$ M^{-1} cm^{-1}) whereas the absorption around 420 nm is quite strong (Soret band, absorption coefficient: $> 10^5$ M^{-1} cm^{-1}). Therefore, we set out an attempt to enhance the absorption of Q-bands by means of the LSP of metal nanoparticles. **Figure 3-3 (c)** shows the extinction, absorption and scattering spectra of TPP/glass. An extinction peak of the Soret band at 435 nm and four extinction peaks of the Q-bands, located at 519, 552, 596 and 653 nm were observed. [19] Compared to the peak

wavelengths of Q-bands in a toluene solution of TPP (514, 548, 591, and 649 nm, **Figure 3-3 (b)**), those of the TPP/glass were slightly red-shifted. Also, the extinction at the Soret band was accompanied by a prominent scattering component. These results suggest that the TPP molecules densely aggregated on the glass substrate because the scattering cross section of molecular aggregates is proportional to the square of the volume of the aggregates and the red-shift can be attributed to the π-π interaction of TPP. [20] To investigate the morphology of the molecular aggregates, the AFM measurement was conducted for TPP/glass. As shown in **Figure 3-4**, the glass surface was scattered with the molecular aggregates having a height of 7 ± 2 nm and a diameter of 108 ± 29 nm.
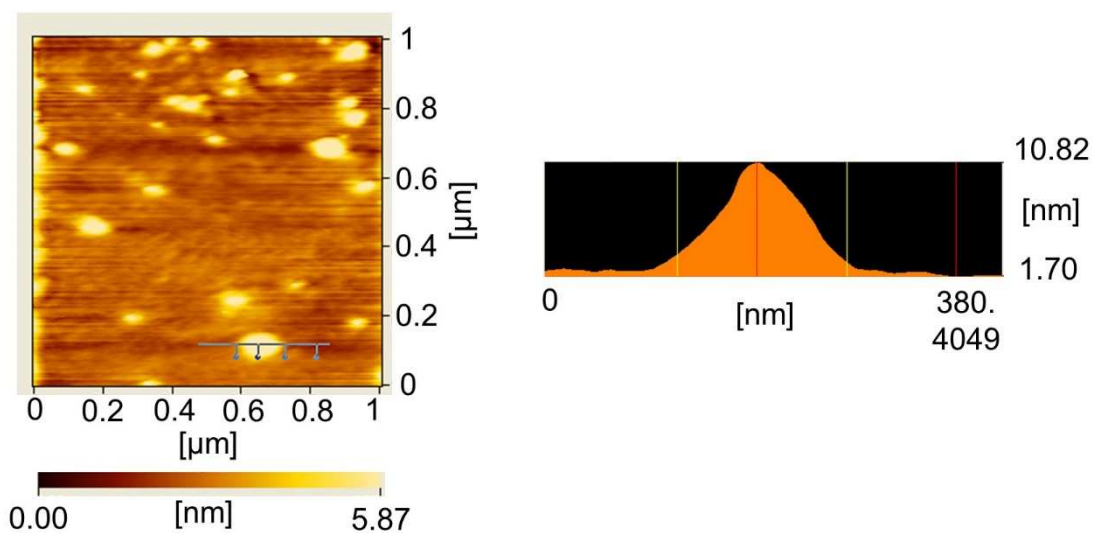

Figure 3-4. AFM image of the surface of TPP/glass.

3-3-2. Optical Properties and Morphologies of AgPRs

A large-scale, reproducible synthesis of plasmonic metal nanoparticles which generate strong LSP resonance at precisely tuned wavelengths is highly desired for a large-scale applications. Absorption enhancement of the Q-bands of porphyrins spread over a macroscopic substrate is a model case for such applications, which we will describe in this work. A satisfactory technique of metal nanoparticle preparation that meets the demand has been rarely reported. [21,22]

We have succeeded in synthesizing AgPRs which can generate strong local electromagnetic fields at precisely-tuned LSP resonance wavelengths in sufficient amount. [17,23] The wavelength region in which the LSP resonance occurs matches the Q-band region of porphyrins. Our method is based on the light-mediated method, which was originally developed by Mirkin's research group. [24,25] In the preparation, the AgPRs are synthesized by the irradiation of light to citrate-stabilized Ag nanospheres with a diameter below 10 nm. Hot electrons and holes are formed during the decay of the LSP resonance upon light irradiation. While the hot holes are transferred to citric acid adsorbed on the Ag surfaces, the hot electrons reduce silver ions, resulting in the formation of AgPRs. Although the LSP resonance wavelength was controlled by choosing the excitation light wavelength to a certain degree, the precise tuning has never been achieved by a single excitation wavelength as used in the previous reports. [25-27] In this study, we have succeeded in preparing AgPRs exhibiting the LSP resonance wavelengths with an unprecedented precision. This was achieved by tuning the sequence, wavelengths, and duration of irradiation (see experimental section and **Table 1**) in the process of converting the Ag nanospheres into AgPRs. For example, irradiation of 470 nm light alone produced AgPRs exhibiting the LSP resonance at 500 nm. Irradiation of 470 nm light followed by 525 nm light (keeping the total irradiation time unchanged) produced AgPRs with a red-shifted LSP resonance. During the first irradiation process of the 470 nm light, small AgPRs were formed by oriented attachment-like two-dimensional coalescence of Ag nanospheres. In the second 525 nm light irradiation, the AgPRs grew in an Ostwald ripening process to a specific size at the consumption of the remaining Ag nanospheres. Thus, obtained AgPRs (photo images: **Figure 3-5 (a)**) generated LSP resonance at exact wavelengths of 500, 540, 560, 625, 645, and 675 nm with small standard deviations (0.6 – 5 nm, see **Table 1**) under our specific conditions. The extinction spectra and of respective colloidal aqueous solutions of AgPRs with different resonance wavelengths, which were prepared 5 times, are shown in **Figure 3-5 (b)**, which clearly indicates that our synthetic method has a remarkable reproducibility in generating LSP resonances at exact wavelengths.
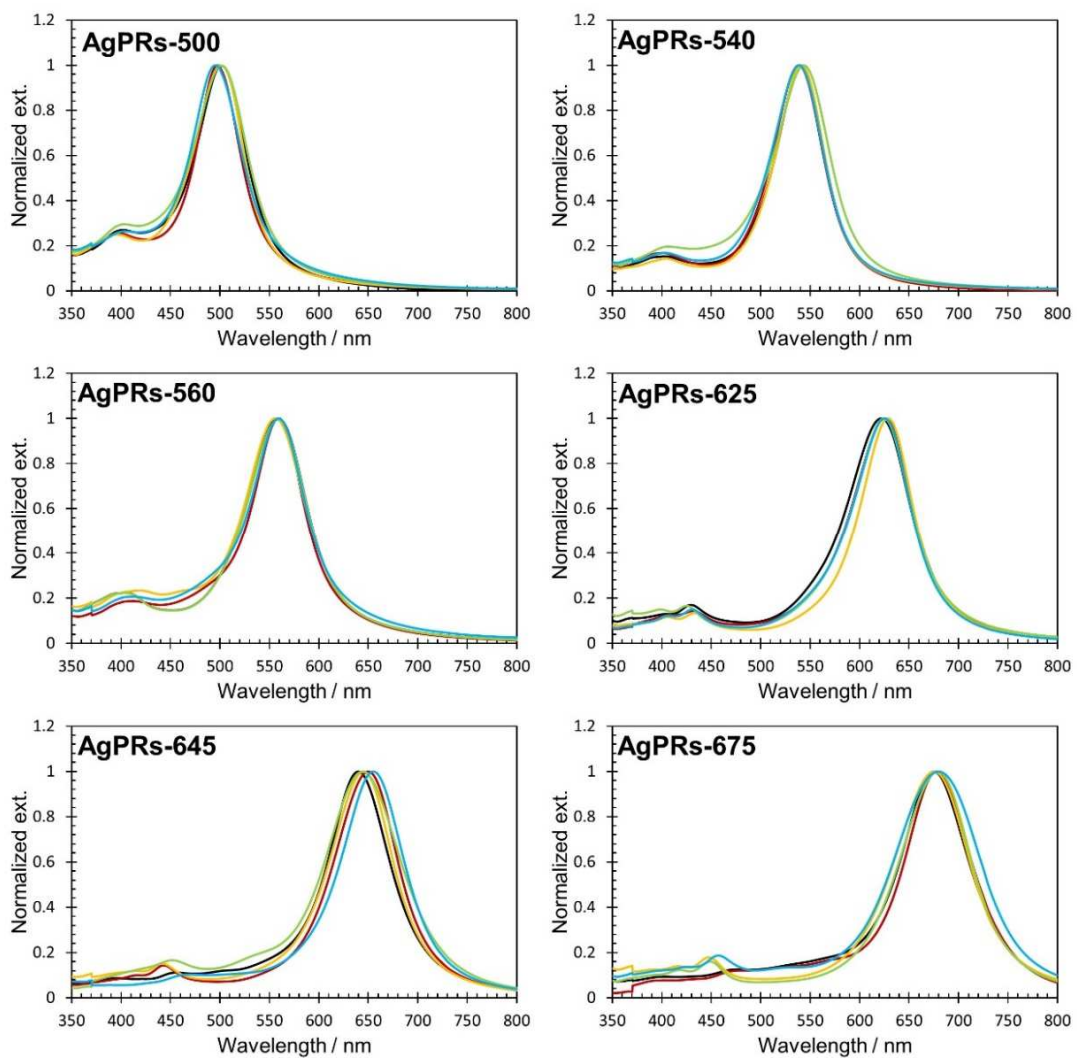
Figure 3-5. (a) Photo image of synthesized AgPRs. **(b)** Extinction spectra for colloidal aqueous solutions of AgPRs each synthesized five times.

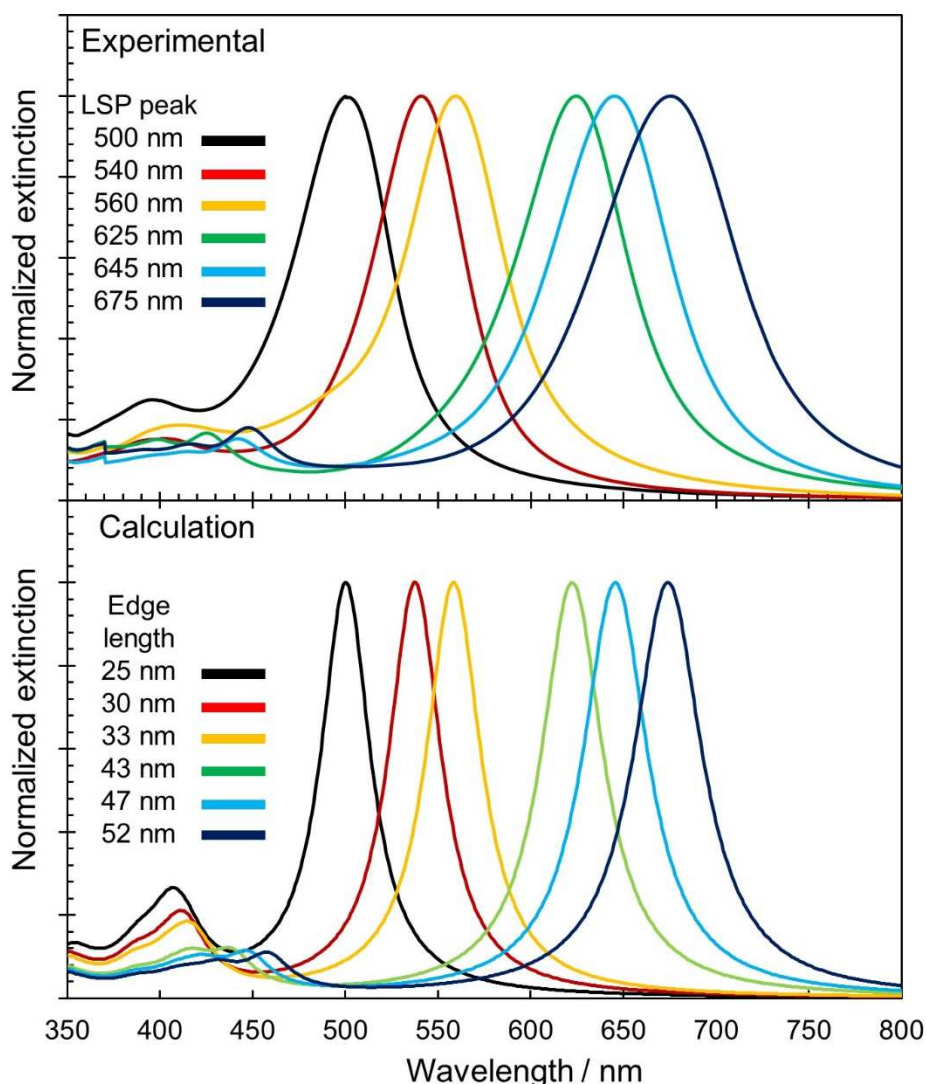Normalized extinction spectra are shown in **Figure 3-6**.

Figure 3-6. Normalized extinction spectra of colloidal aqueous solutions of AgPRs with different LSP peak wavelengths, and normalized extinction spectra calculated by BEM.

All the AgPRs showed a prominent resonance band within 500 – 700 nm. It was found by comparing the LSP wavelengths and the TEM images, which are shown in **Figure 3-7**, that the resonance band was red-shifted with increasing the edge length (AgPRs-500: 25 ± 3 nm, AgPRs-540: 30 ± 4 nm, AgPRs-560: 33 ± 5 nm, AgPRs-625: 44 ± 9 nm, AgPRs-645: 47 ± 10 nm, and AgPRs-675: 52 ± 7 nm). Since the thicknesses of AgPRs which are synthesized by the photochemical method are almost constant at *ca.* 10 nm regardless of their edge lengths, [28] the difference in the resonance wavelengths can be attributed to the difference in the aspect ratio (the ratio of edge length to thickness). [29]
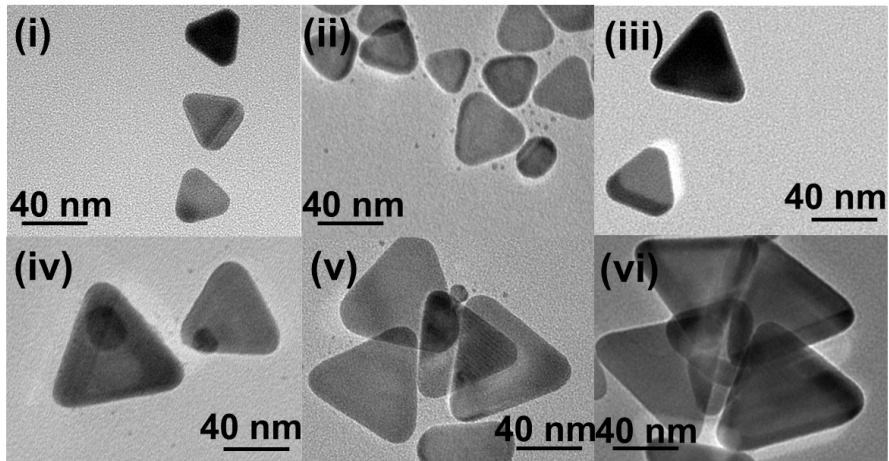
Figure 3-7. TEM images of various AgPRs (i-vi) synthesized by the modified photochemical methods.

To prove the correlation between the LSP wavelength and its aspect ratio, we calculated the extinction spectra using the BEM for AgPRs having the experimentally-obtained edge lengths and a fixed thickness of 10 nm which were surrounded by aqueous phase (refractive index: 1.333) (**Figure 3-6)**. The calculated resonance wavelengths agreed very well with the experimentally-obtained wavelengths (**Figure 3-8**), which indicated that the accurate control of resonance band of AgPRs was achieved by precisely-controlling the aspect ratio. The experimental extinction spectra of AgPRs were somewhat broader than the calculated ones. This may be partly because there was a distribution in the aspect ratios, albeit narrow, in the prepared AgPRs and partly because the solvent molecules (water) caused the chemical interface damping, [30] both of which were not included in the calculations.
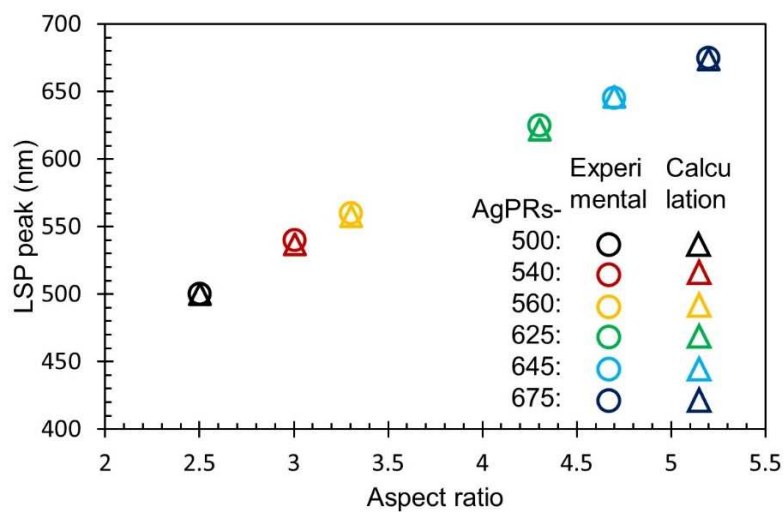

Figure 3-8. Plots of LSP peaks of AgPRs against their aspect ratios.

3-3-3. Effect of Interaction Between LSP of AgPRs and Exciton of TPP

To evaluate the interaction between the LSP of AgPRs and the exciton of TPP in TPP/AgPRs-*X*, the extinction spectra were measured for TPP/glass (as a reference), AgPRs/glass, and TPP/AgPRs-*X* (**Figure 3-9**).
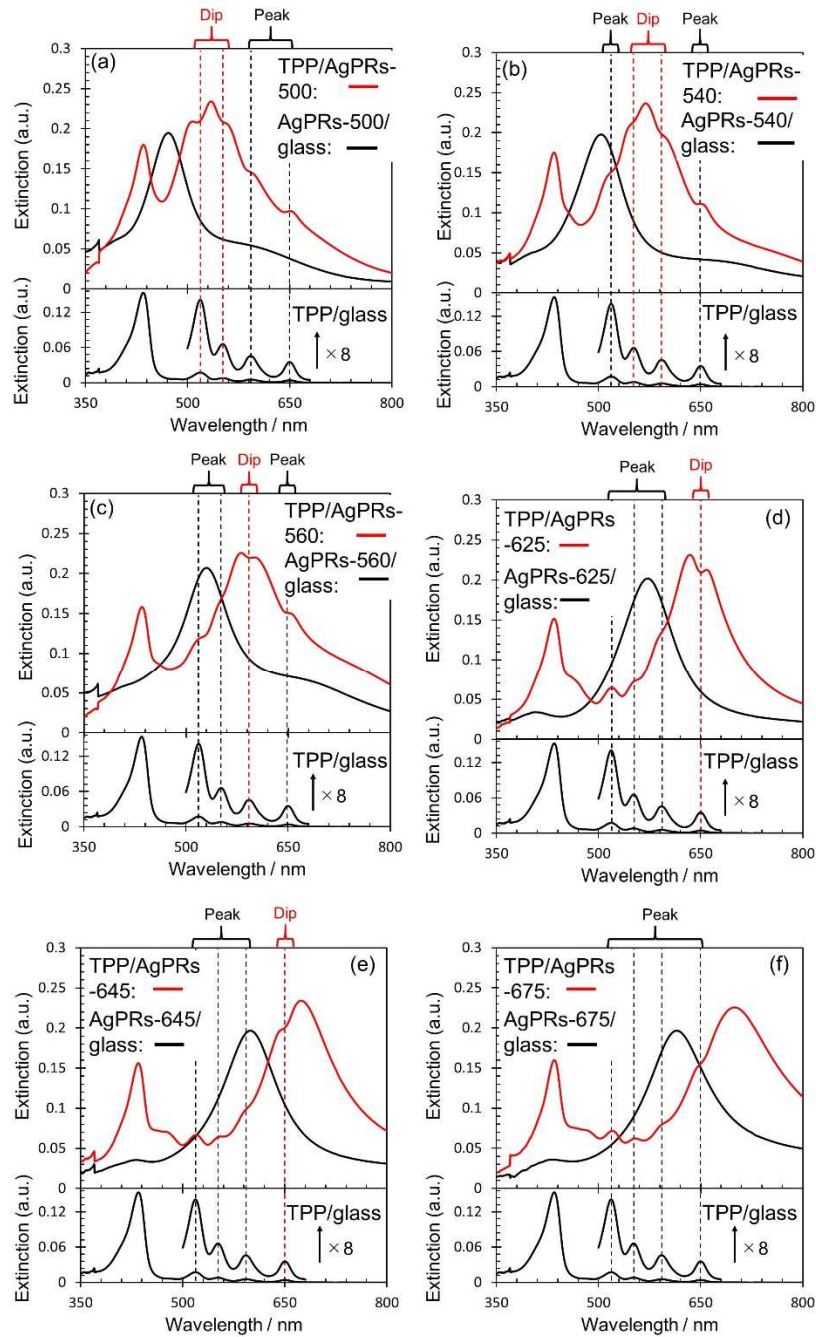

Figure 3-9. Extinction spectra. Dashed lines on the spectra represent absorption peak wavelengths of Q-bands of TPP/glass. (a) AgPRs-500/glass. (b) AgPRs-540/glass. (c) AgPRs-560/glass. (d) AgPRs-625/glass. (e) AgPRs-645/glass. (f) AgPRs-675/glass.

78

The dashed lines in **Figure 3-9** indicate the peak wavelengths of Q-bands observed on TPP/glass. The resonance wavelengths of the in-plane dipole mode for all AgPRs/glass were blue-shifted by several tens of nanometers, as compared with those for the corresponding AgPRs dispersed in an aqueous phase (**Figure 3-6**). These shifts are attributed to a change in the refractive index surrounding the AgPRs from the aqueous phase to air (refractive index: 1.000). [31-33] After spin-coating the TPP solution onto AgPRs-*X*/glass, the Soret band was observed at 436 nm. In addition, the LSP resonance bands were red-shifted, resulting in the LSP band within 500-700 nm for all AgPRs. These results suggest that the AgPRs were covered with TPP aggregates because the refractive index (approximately 1.6) of TPP is larger than that of air. [18] Note that prominent peaks or dips were observed at the wavelengths of the Q-band peaks on the LSP resonance band for all TPP/AgPRs-*X*. For example, in the case of TPP/AgPRs-500, while spectral dips were observed at 515 and 552 nm where the LSP resonance was strongly excited, peaks were observed at 595 and 654 nm in the edge region of the LSP resonance band. The latter positions are in the peripheral region of the LSP band where the electromagnetic field around the AgPRs is weak. Therefore, the coupling between the LSP resonance and the TPP exciton is weak, resulting in the overall spectrum resembling the sum of individual spectra. On the other hand, only peaks were observed for TPP/AgPRs-675 because the Q-bands overlap only with the peripheral region of the LSP band (**(f) in Figure 3-9**), suggesting inefficient interaction between the LSP and the exciton. [34] We emphasize based on these data that the strong interaction between the LSP and exciton, which is manifested by the appearance of dips, is efficiently induced only at a narrow wavelength region where the LSP resonance is strongly excited. Therefore, the combined use of multiple AgPRs with the LSP resonance at multiple wavelengths over the Q-band region is required.

In the case classified as the absorption enhancement, which represents a weak coupling case, light absorption attributed to the exciton generation increases whereas the extinction of LSP at the same wavelength decreases. As a result, the total absorption component changes little because the absorption enhancement to generate excitons is canceled out by the absorption decrease in the LSP band. On the other hand, the net scattering component decreases, resulting in a dip in the total extinction spectrum. [6] In the case of the strong coupling, prominent dips are observed similarly in both absorption and scattering spectra because two hybrid states separated in energy are formed in place of independent eigenstates. The IT refers an intermediate case between the absorption enhancement and the strong coupling. [6, 35, 36] To further clarify the strength of interaction between the LSP and the exciton in our hybrids, the absorption and scattering spectra of

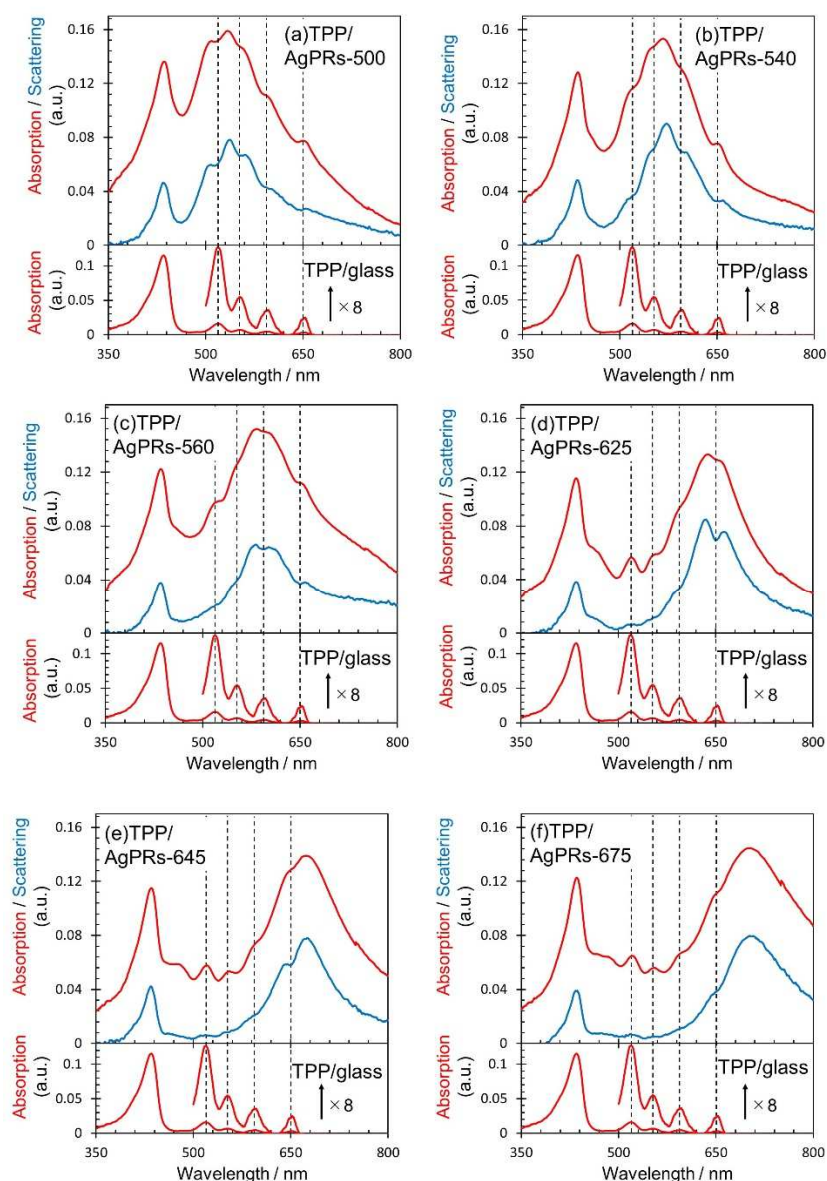TPP/AgPRs-*X* were measured (**Figure 3-10 (a-f)**). [6, 37, 38]

Figure 3-10. Absorption (red line) and scattering (blue line) spectra. Dashed lines on the spectra represent absorption peak wavelengths of Q-bands of TPP/glass. (a) TPP/AgPRs-500. (b) TPP/AgPRs-540. (c) TPP/AgPRs-560. (d) TPP/AgPRs-625. (e) TPP/AgPRs-645. (f)TPP/AgPRs-675.

Although prominent dips were observed in the region where the LSP was strongly excited in the scattering spectra for all TPP/AgPRs-*X* except for TPP/AgPRs-675, the dips were less prominent in the corresponding absorption-spectra. These observations suggested that our hybrids TPP/AgPRs-500, 540, 560, 625, and 645 were in the regime of absorption enhancement with respect to the coupling strength.

3-3-4. Effect of Enhanced Absorption Over Whole Q-bands

Although we have succeeded in achieving the absorption enhancement at the region where the LSP resonance is strongly excited, absorption enhancement over a wider range covering the whole Q-bands may be beneficial in terms of solar light utilization. To achieve this, we hybridized TPP and AgPRs-ternary/glass (denoted as TPP/AgPRs-ternary). The extinction spectrum of AgPRs-ternary/glass is shown in **Figure 3-11**.
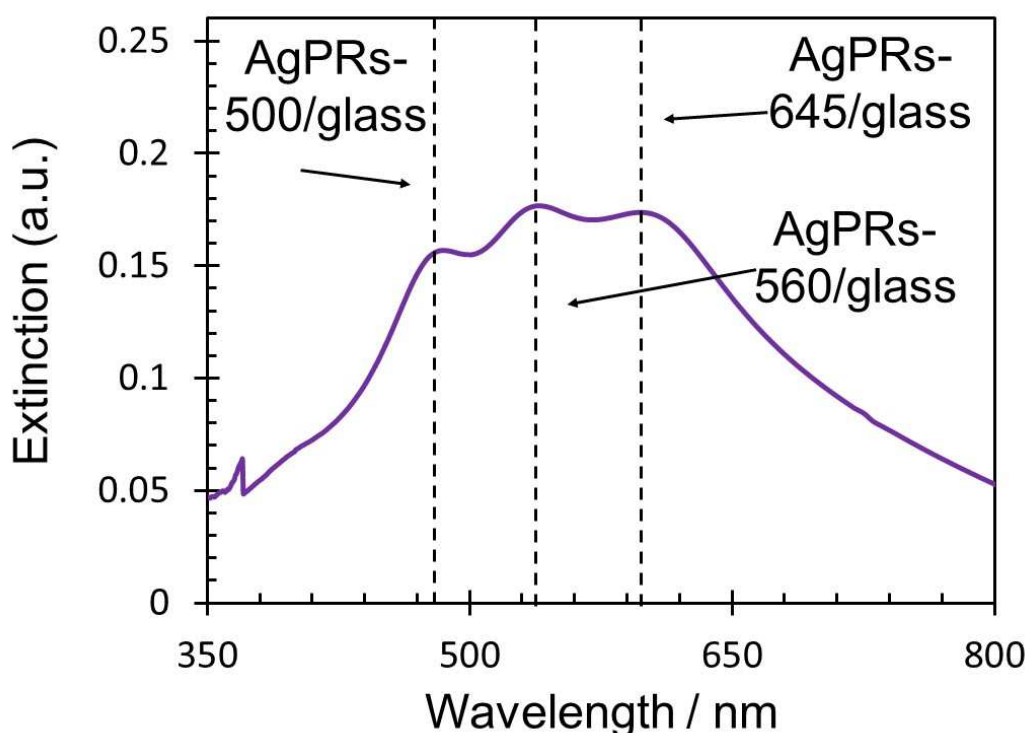

Figure 3-11. Extinction spectra of AgPRs-ternary/glass. Dashed lines represent LSP peaks of AgPRs-500/glass, AgPRs-560/glass, and AgPRs-645/glass.

Three distinct bands were observed at 485, 540, and 598 nm, which were assigned to the LSP resonance bands of AgPRs-500, 560, and 645, respectively. The extinction spectrum of TPP/AgPRs-ternary, which is shown in **Figure 3-12 (a)**, exhibited four dips at the wavelengths corresponding to the Q-band peaks. Furthermore, as shown in **Figure 3-12 (b)**, while the prominent four dips were observed at the Q-band wavelengths in the scattering spectrum, these dips did not appear in the absorption spectrum. These results suggested that the strength of interaction between the LSPs of AgPRs-500, 560, and 645 and the excitons generated in the whole Q-band wavelengths was in the enhanced absorption regime.
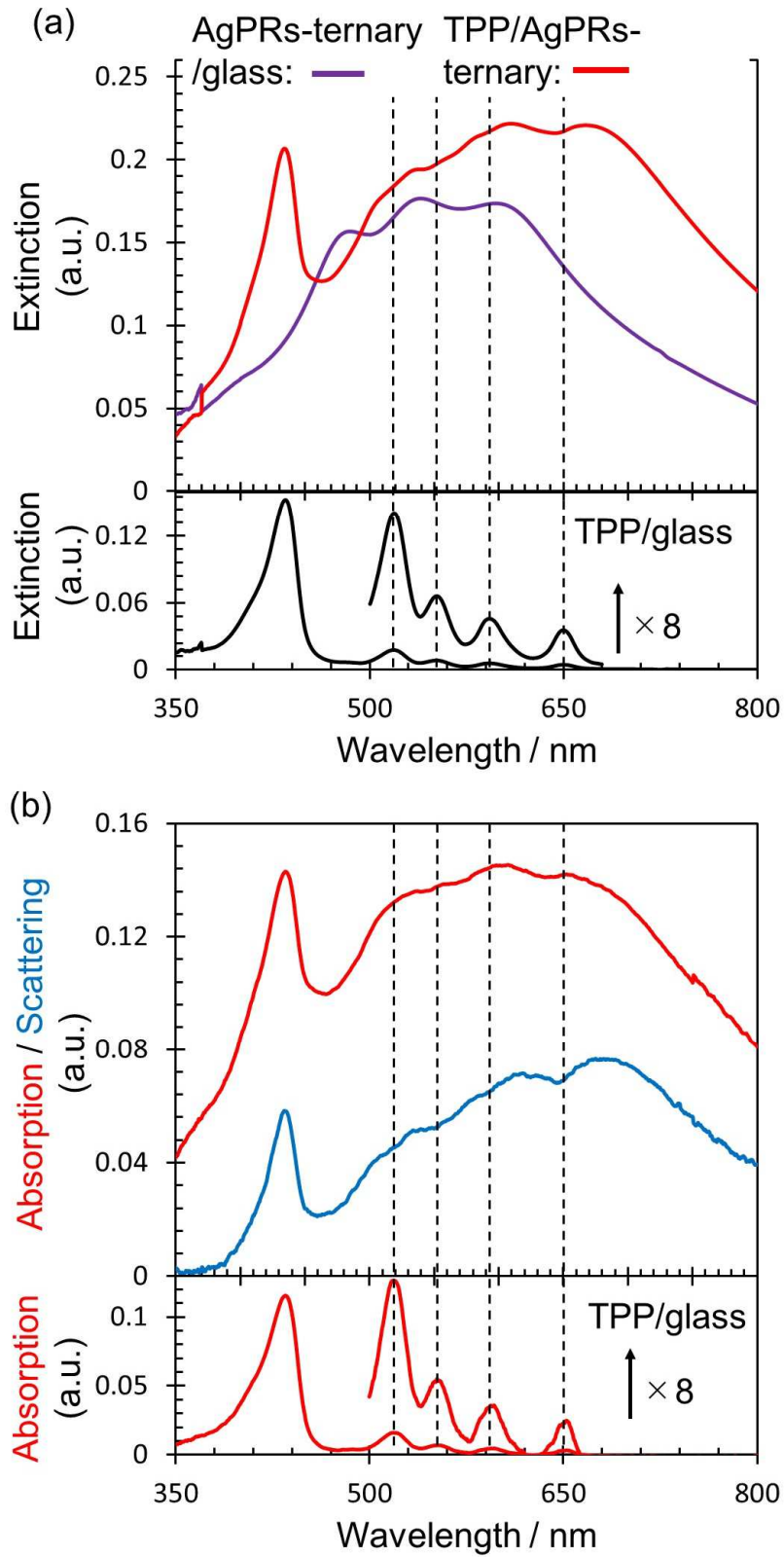
Figure 3-12. Optical property of AgPRs-ternary/glass, TPP/AgPRs-ternary, and TPP/glass. **(a)** Extinction spectra. **(b)** Absorption and scattering spectra.

82

3-3-5. Effect of Absorption Enhancement on Photodynamics of TPP

To quantitatively investigate the effect of the absorption enhancement on the photodynamics of TPP, the fluorescence excitation spectra of TPP/AgPRs-500, 560, 645, and ternary (λ_{em} = 720 nm) were measured (**Figure 3-13**).
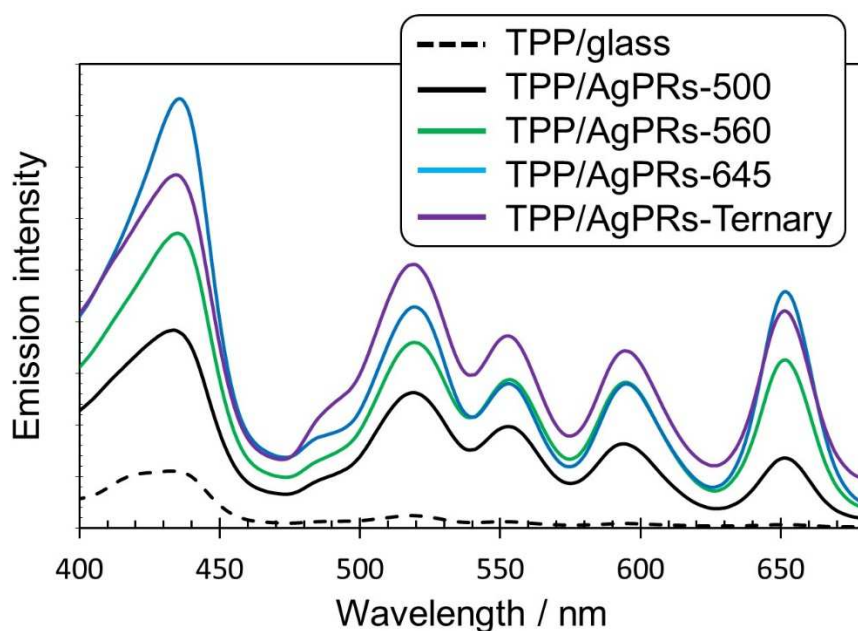

Figure 3-13. Fluorescence excitation spectra of TPP/AgPRs-500, TPP/AgPRs-560, TPP/AgPRs-645, and TPP-ternary (λ_{em} = 720) as measured.

The fluorescence radiation was significantly enhanced by excitation in the region of both the Soret and Q-bands, as compared to that of TPP/glass. The fluorescence enhancement factors at the Q-band peaks were in the range of 11-71 (**Figure 3-14**). The fluorescence enhancement owing to the LSP resonance can be attributed to two mechanisms: the photoexcitation enhancement (*i.e.* absorption enhancement), which is induced when the LSP resonance band overlaps with the photoexcitation wavelength, and the acceleration in radiative decay rate, which is induced when the LSP resonance band overlaps with the fluorescence wavelength. The fluorescence enhancement for the Q-bands excitation could be induced by both of these mechanisms because the photoexcitation and fluorescence wavelengths overlap with the LSP resonance bands of TPP/AgPRs-500, 560, 645, and ternary. On the other hand, the fluorescence was also enhanced by 2.9-6.4 times for the Soret band excitation (**(e) in Figure 3-14**). It is likely that the enhancement is solely attributed to the acceleration in the radiative decay rate because the excitation wavelength is separated far from the main LSP resonance bands of AgPRs.
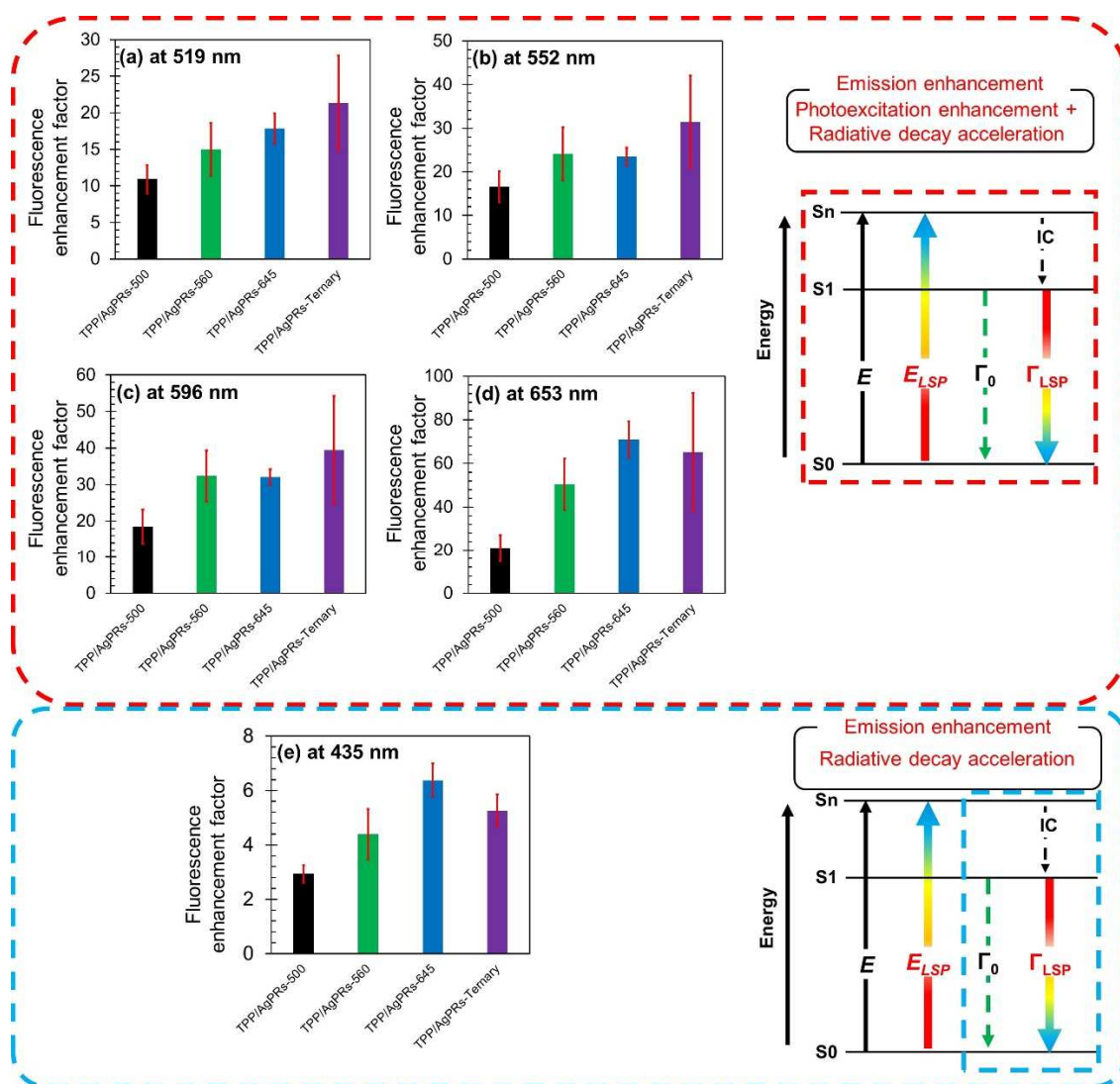
Figure 3-14. Absorption enhancement at **(a)** 519 nm, **(b)** 552 nm, **(c)** 596 nm, **(d)** 653 nm (Q-band wavelengths), and **(e)** average absorption enhancement factors of TPP/AgPRs-500, TPP/AgPRs-560, TPP/AgPRs-645, and TPP/AgPRs-ternary. The red lines indicate the standard deviations for the measurements repeated three times.

Thus, the fluorescence enhancement factors were calculated using the fluorescence excitation spectra normalized at the Soret band (435 nm, **Figure 3-15**), which can be attributed to the net absorption enhancement. The average enhancement factors for the Q-bands are shown in **(e) in Figure 3-16**, obtained by averaging enhancement factors for respective Q-band peaks (**(a-d) in Figure 3-16**). Consequently, TPP/AgPRs-ternary, which showed the absorption enhancement uniformly at all the Q-band peaks resulting in the enhancement factor of 7.4 (**(e) in Figure 3-16**). This result indicated that the absorption enhancement based on plasmon-exciton coupling was achieved over the broad

wavelength region by combined use of AgPRs with different aspect ratios, which points to the usefulness of our precise tuning technique of LSP wavelengths. Randomly distributed polydisperse AgPRs would also enhance a wide range of absorption but many molecules would be placed out of resonance with AgPRs. Combining AgPRs of which the LSP resonance wavelength is precisely tuned to the molecular absorption peak positions would be the most efficient strategy in harvesting a spectrum of light. Thus, our precise tuning technique is promising for the development of high-performance solar devices.
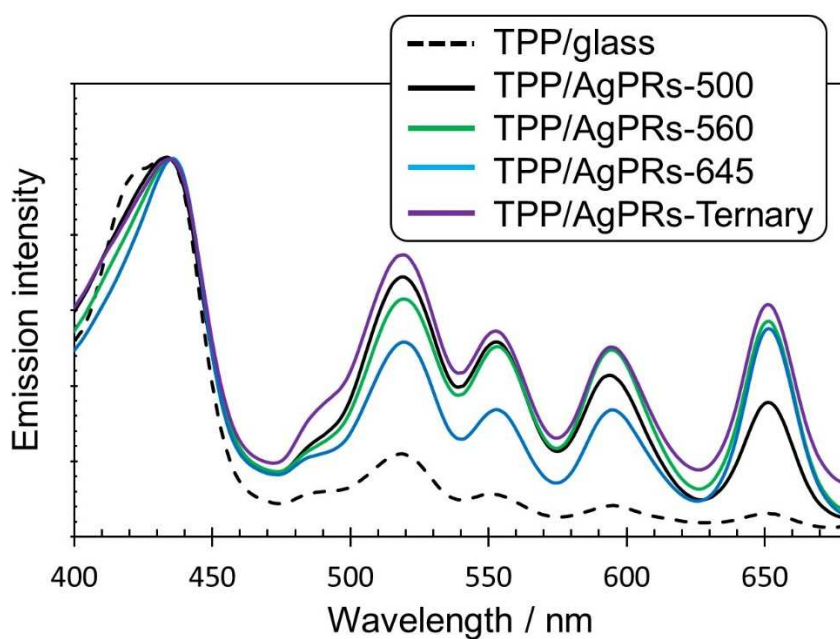

Figure 3-15. Normalized fluorescence excitation spectra (λ_{em} = 720 nm).
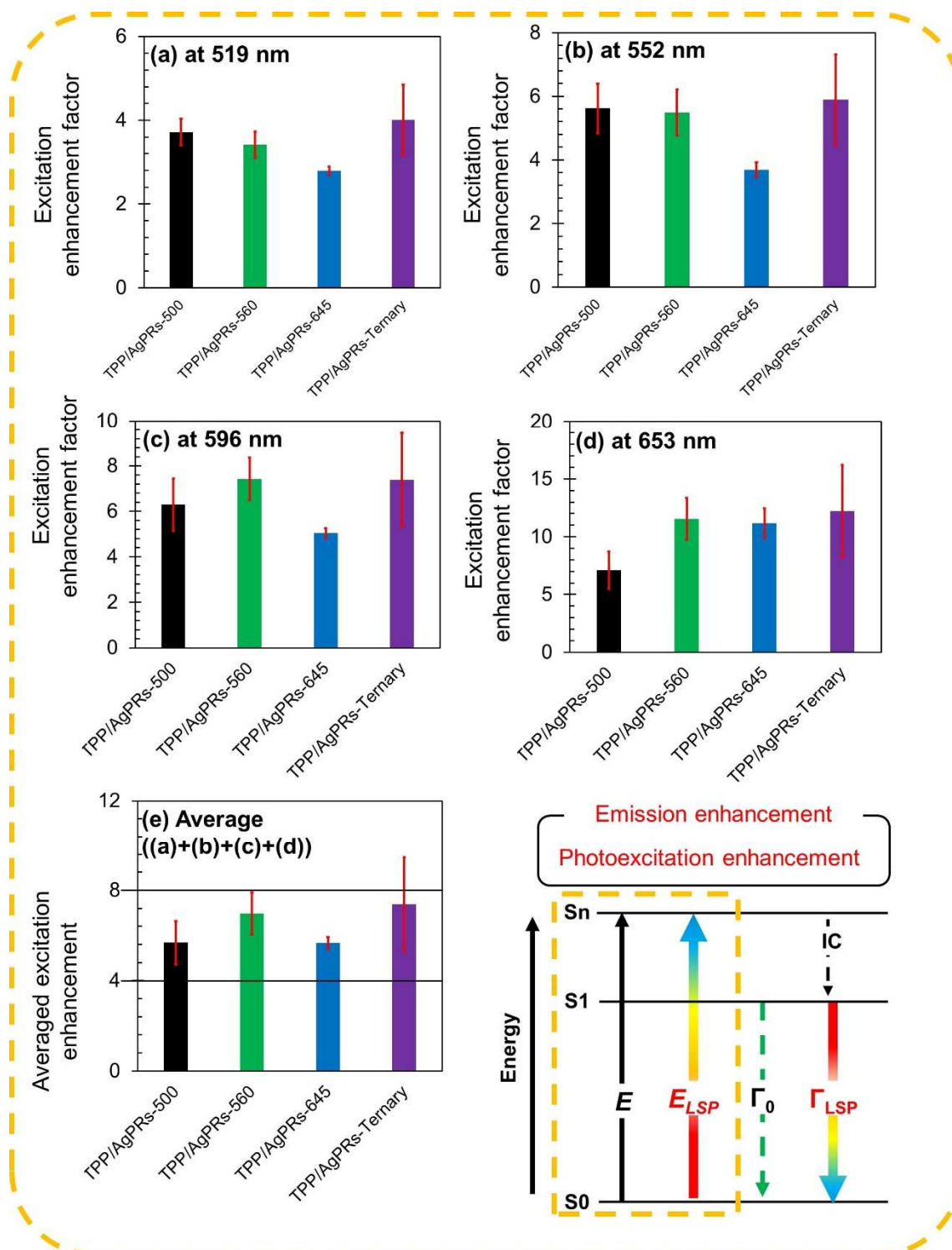
Figure 3-16. Absorption enhancement at **(a)** 519 nm, **(b)** 552 nm, **(c)** 596 nm, **(d)** 653 nm (Q-band wavelengths), and **(e)** average absorption enhancement factors of TPP/AgPRs-500, TPP/AgPRs-560, TPP/AgPRs-645, and TPP/AgPRs-ternary. The red lines indicate the standard deviations for the measurements repeated three times.

3-4. Conclusion

We have succeeded in synthesizing AgPRs with well-defined resonance wavelengths, which can be precisely tuned over a wide visible region. The difference in resonance wavelengths is attributed to the difference in their aspect ratios. The combined use of AgPRs with three different aspect ratios led to the absorption enhancement over the whole Q-bands, which was demonstrated by their extinction, absorption, and scattering spectra. In addition, absorption enhancement factors (up to 7.4 fold) were quantitatively evaluated from the fluorescence excitation spectra, which demonstrated the usefulness of our protocol to produce AgPRs exhibiting precisely-tuned LSP resonance wavelengths in realizing absorption enhancement over the wide visible wavelength region. Thus, the combined use of AgPRs with different aspect ratios have a great potential for enhancing light-matter interaction in a wide wavelength region, which paves the way for the fabrication of high-performance optoelectronic devices including solar cells, photocatalysts, and bio-imaging sensors.

3-5. References

1. Li, X.; Zhou, L.; Hao, Z.; Wang, Q. Q. Plasmon-exciton coupling in complex systems. *Adv Opt Mater* **2018**, *6*, 1800275.

2. Sun, J.; Hu, H.; Zheng, D.; Zhang, D.; Deng, Q.; Zhang, S.; Xu, H. Light-emitting plexciton: exploiting plasmon-exciton interaction in the intermediate coupling regime. *ACS Nano* **2018**, *12*(10), 10393-10402.

3. Munkhbat, B.; Wersall, M.; Baranov, D. G.; Antosiewicz, T. J.; Shegai, T. Suppression of photo-oxidation of organic chromophores by strong coupling to plasmonic nanoantennas. *Sci. Adv.* **2018**, *4*, eaas9552.

4. Gao, M. X.; Zou, H. Y.; Li, Y. F.; Huang, C. Z. General sensitive detecting strategy of ions through plasmonic resonance energy transfer from gold nanoparticles to rhodamine spirolactam. *Anal. Chem.* **2017**, *89*, 1808-1814.

5. Shi, X.; Ueno, K.; Oshikiri, T.; Sun, Q.; Sasaki, K.; Misawa, H. Enhanced water splitting under modal strong coupling conditions. *Nat. Nanotechnol.* **2018**, *13*, 953-958.

6. Antosiewicz, T. J.; Apell, S.P.; Shegai, T. Plasmon-exciton interactions in a core-shell geometry: from enhanced absorption to strong coupling. *ACS Photonics* **2014**, *1*(5), 454-463.

7. Kim, G. M.; Tatsuma, T. Photocurrent enhancement of perovskite solar cells at the absorption edge by electrode-coupled plasmons of silver nanocubes. *J. Phys. Chem. C* **2017**, *121*(21), 11693-11699.

8. Cushing, S. K.; Li, J.; Meng, F.; Senty, T. R.; Suri, S.; Zhi, M.; Li, M.; Bristow, A. D.; Wu, N. Photocatalytic activity enhanced by plasmonic resonant energy transfer from metal to semiconductor. *J. Am. Chem. Soc.* **2012**, *134*(36), 15033-15041.

9. Cai Y.; Wang Z.; Yan S.; Ye L.; Zhu J. Ultraviolet absorption band engineering of graphene by integrated plasmonic structures. *Opt. Mater. Express* **2018**, *8*(11), 3295-3306.

10. Liu T.; Jiang X.; Zhou C.; Xiao S. Black phosphorus-based anisotropic absorption structure in the mid-infrared. *Opt. Express* **2019**, *27*(20), 27619-27627.

11. Cai Y.; Zhu J.; Liu Q. H. Tunable enhanced optical absorption of graphene using plasmonic perfect absorbers. *Appl. Phys. Lett.* **2015**, *106*(4), 043105-1.

12. Melnikau, D.; Govyadinov, A. A.; Sanchez-lglesias, A.; Grzelczak, M.; Nabiev, I. R.; Liz-marzan, L. M.; Rakovich, Y. P. Double Rabi Splitting in a Strongly Coupled System of Core-Shell Au@Ag Nanords and J-aggregates of Multiple Fluorophores. *J. Phys. Chem. Lett.* **2019**, *10*(20), 6137-6143.

13. Zhang Y. F.; Yang D. J.; Wang J. H.; Wang Y. L.; Ding S. J.; Zhou L.; Hua Hao Z.; Wang Q. Q. Multiple hybridized resonance of IR-806 chromonic molecules strongly coupled to Au nanorods. *Nanoscale* **2015**, *7*, 8503-8509.

14. Stete, F.; Koopaman, W.; Bargheer, M. Signatures of Strong Coupling on Nanoparticles: Revealing Absorption Anticrossing by Tuning the Dielectric Environment. *ACS Photonics* **2017**, *4*(7), 1669-1676.

15. Waxenegger, J.; Trugler, A.; Hohenester, U. Plasmonic simulations with the MNPBEM toolbox: Consideration of substrates and layer structures *Comput. Phys. Commun.* **2015**, *193,* 138-150.

16. Rakic, A. D.; Djurisic, A. B.; Elazar, J. M.; Majewski, M. L. Optical properties of metallic films for vertical-cavity optoelectronic devices. *Appl. Opt.* **1998**, *37*(22), 5271-5283.

17. Jin, S.; Sugawa, K.; Takeshima, N.; Tahara, H.; Igari, S.; Yoshinari, S.; Kurihara, Y.; Watanabe, S.; Enoki, M.; Sato, K.; Inoue, W.; Tokuda, K.; Akiyama, T.; Katoh, R.; Takase, K.; Ozawa, H.; Okazaki, T.; Watanabe, T.; Otsuki, J. Precise Control of Localized Surface Plasmon Wavelengths Is Needed for Effective Enhancement of Triplet-Triplet Annihilation-Based Upconversion Emission. *ACS Photonics* **2018**, *5*, 5025-5037.

18. Otsuki J. Supramolecular approach towards light-harvesting materials based on porphyrins and chlorophylls. *J. Mater. Chem. A* **2018**, *9*, 6710-6753.

19. Tuerdi, G.; Nizamidin, P.; Kari, N.; Yimit, A.; Wang, F. Optochemical properties of gas-phase protonated tetraphenylporphyrin investigated using an optical waveguide NH_3 sensor. *RSC Adv.* **2018**, *8,* 5614-5621.

20. Pasternack, R. F.; Collings, P. J. Resonance light scattering: a new technique for studying chromophore aggregation. *Science* **1995**, *269*(5226), 935-939.

21. Melnikau, D.; Esteban, R.; Savateeva, D.; Sanchez-lglesias, A.; Grzelczak, M.; Schmidt, M. K.; Liz-Marzan, L. M.; Aizpurua, J.; Rakovich, Y. P. Rabi splitting in Photoluminescence Spectra of Hybrid Systems of Gold Nanorods and J-Aggregates. *J. Phys. Chem. Lett.* **2016**, *7*(2), 354-362.

22. Ni, W.; Yang, Z.; Chen, H.; Li, L.; Wang, J.; Coupling between Molecular and Plasmonic Resonances in Freestanding Dye-Gold Nanorod Hybrid Nanostructures. *J. Am. Chem. Soc.* **2008**, *130*, 6692-6693.

23. Takeshima, N.; Sugawa, K.; Tahara, H.; Jin, S.; Wakui, H.; Fukushima, M.; Tokuda, K.; Igari, S.; Kanakubo, K.; Hayakawa, Y.; Katoh, R.; Takase, K.; Otsuki, J. Plasmonic Silver Nanoprism-Induced Emissive Mode Control between Fluorescence and Phosphorescence of a Phosphorescent Palladium Porphyrin Derivative. *ACS Nano* **2019**, *13*(11), 13244-13256.

24. Jin, R.; Cao, Y.; Mirkin, C. A.; Kelly, K. L.; Schatz, G. C.; Zheng, J. G. Photoinduced Conversion of Silver Nanospheres to Nanoprisms. *Science* **2001**, *294*, 1901-1903.

25. Jin, R.; Cao, Y. C.; Hao, E.; Metraux, G. S.; Schatz, G. C.; Mirkin, C. A. Controlling

anisotropic nanoparticle growth through plasmon excitation. *Nature* **2003**, *425*, 487-490.

26. Lee, G. P.; Shi, Y.; Lavoie, E.; Daeneke, T.; Reineck, P.; Cappel, U. B.; Huang, D. M.; Bach, U. Light-Driven Transformation Processes of Anisotropic Silver Nanoparticles. *ACS Nano* **2013** *7*(7), 5911-5921.

27. Stamplecoskie, K. G.; Scaiano, J.C. Light Emitting Diode Irradiation Can Control the Morphology ans Optical Properties of Silver Nanoparticles *J. Am. Chem. Soc.* **2010** *132*(6), 1825-1827.

28. Sugawa, K.; Takeshima, N.; Uchida, K.; Tahara, H.; Jin, S. Tsunenari, N.; Akiyama, T.; Kusaka, Y.; Fukuda, N.; Ushijima, H.; Tsuchido, Y.; Hashimoto, T.; Hayashita, T.; Ostuki, J. Photocurrent enhancement of porphyrin molecules over a wide-wavelength region based on combined use of silver nanoprisms with different aspect ratios. *J. Mater. Chem. C* **2015**, *3*, 11439-11448.

29. Zhang, Q.; Li, N.; Goebl, J.; Lu, Z.; Yin, Y.; A Systematic Study of the Synthesis of Silver Nanoplates: Is Citrate a "Magic" Reagent?. *J. Am. Chem. Soc.* **2011**, *133*(46), 18931-18939.

30. Douglas-Gallardo, O. A.; Berdakin, M.; Sanchez, C. G. Atomistic Insights into Chemical Interface Damping of Surface Plasmon Excitations in Silver Nanoclusters. *J. Phys. Chem. C* **2016**, *120*(42), 24389-24399.

31. Underwood, S.; Mulvaney, P. Effect of the Solution Refractive Index on the Color of Gold Colloids. *Langmuir* **1994**, *10*(10), 3427-3430.

32. Anker, J. N.; Hall, W. P.; Lyandres, O.; Shah, N. C.; Zhao, J.; Van Duyne, R. P.; Biosensing with Plasmonic Nanosensors. *Nat. Mater.* **2008**, *7*(6)*, 442-453.

33. Mahmoud, M. A.; Tabor, C. E.; El-Sayed, M. A.; Surface-Enhanced Raman Scattering Enhancement by Aggregated Silver Nanocube Monolayers Assembled by the Langmuir-Blodgett Technique at Different Surface Pressures. *J. Phys. Chem. C* **2009**, *113,* 5493–5501.

34. Wurtz, G. A.; Evans, P. R.; Hendren, W.; Atkinson, H. R.; Dickson, W.; Pollard, R. J.; Zayats, A. V.; Harrison, W.; Bower, C. Molecular Plasmonics with Tunable Exciton-Plasmon Coupling Strength in J-Aggregate Hybridized Au Nanorod Assemblies. *Nano Lett.* **2007**, *7*(5), 1297-1303.

35. Krivenkov, V.; Goncharov, S.; Nabiev, I.; Rakovich, Y. P. Induced Transparency in Plasmon-Exciton Nanostructures for Sensing Applications. *Laser Photonics Rev.* **2019**, 13, 1800176.

36. Chen, M.; Shao, L.; Woo, K. C.; Wang, J.; Lin, H. Q. Plasmonic-Molecular Resonance Coupling: Plasmonic Splitting versus Energy Transfer. *J. Phys. Chem. C* **2012**, *116*(26), 14088-14095.

37. Kang, E. S. H.; Chen, S.; Sardar, S.; Tordera, D.; Armakavicius, N.; Darakchieva, V.; Shegai, T.; Jonsson, M. P. Strong Plasmon-Exciton Coupling with Directional Absorption Features in Optically Thin Hybrid Nanohole Metasurfaces. *ACS Photonics* **2018**, *5*(10), 4046-4055.

38. Zengin, G.; Geshneidtner, T.; Verre, R.; Shao, L.; Antosiewicz, T. J.; Moth-Poulsen, K.; Kall, M.; Shegai, T. Evaluating Conditions for Strong Coupling between Nanoparticle Plasmons and Organic Dyes using Scattering and Absorption Spectroscopy. *J. Phys. Chem. C* **2016**, *120*(37), 20588-20596.

Chapter 4

Conclusion

Conclusion

This thesis investigated the effect of the LSP on the photophysical processes of porphyrins through various spectroscopic measurements. The result obtained in this thesis was summarized as below.

The effect of the LSP of AgPRs on the photophysical process of a phosphorescent Pd-porphyrin derivative, which have the rate of the ISC is nearly 1, was investigated in Chapter 2. The phosphorescent Pd-porphyrin was hybridized with two AgPRs with different aspect ratio. When the LSP wavelength of AgPRs spectrally overlapped with the excitation and the fluorescence wavelength of Pd-porphyrin, very intense fluorescence emission intensity was observed. By measuring the lifetime of the fluorescence, it was found that the lifetime of the excited singlet states of Pd-porphyrin in the presence of AgPRs was shortened compared with that in absence of AgPRs, and this was suggested that a result of the competition of accelerated fluorescence radiation process and intrinsically strong ISC process. Furthermore, the dependence of the spatial distance of AgPRs and polymer layer containing Pd-porphyrin on the emission property was investigated. While fluorescence intensity was maximum at the position which Pd-porphyrin was in close proximity to AgPRs, phosphorescence intensity was maximum when Pd-porphyrin was far from AgPRs. It was demonstrated that observed opposite distance dependences were attributed to the difference in the susceptibility to the metallic quenching, which is ascribed to the emission quantum yield. From the result obtained in Chapter 2, we succeeded in the emissive modes control between fluorescence and phosphorescence of intrinsically phosphorescent Pd-porphyrin by changing the LSP wavelength and the spatial distance.

The optical property of the hybrids comprised of AgPRs and TPP was investigated in Chapter 3. Synthesis method for the AgPRs with precisely-tuned LSP wavelength was developed by controlling the irradiation time and the irradiation wavelength of LED. TPP, which have four absorption peaks corresponding to Q-bands in visible regions ($500 - 700$ nm), was combined with the AgPRs having the LSP wavelength tuned to the Q-bands. Spectral dips were observed at the position, which LSP wavelength overlapped with absorption peaks of TPP, on the extinction spectra. By measuring the absorption and scattering components in the extinction spectra, it was suggested that the dips were attributed to the enhanced absorption phenomenon based on the LSP-exciton interaction. For quantitative evaluation of absorption enhancement, fluorescence spectra of the hybrids combined with TPP and AgPRs were measured. Absorption enhancement up to 7.4-fold based on the LSP-exciton interaction over the visible wavelength regions was

achieved by the combination use of three AgPRs with different LSP wavelength. Towards the realization of the absorption enhancement on wide-wavelength regions, we demonstrated the usefulness of the protocol developed to prepare AgPRs having LSP wavelength precisely tuned.

In this thesis, the effects of LSP resonance on the optical property of porphyrin derivatives was clarified by fabricating the hybrids of AgPRs and porphyrin derivatives. The results, in which demonstrate that the LSP can affect intrinsically strong photophysical process such as ISC, will have an impact and an insight on the complicated photochemical reaction such as photon upconversion via TTA. Moreover, realizing in the absorption enhancement over wide wavelength regions by combination use of different-sized AgPRs will be guidelines for high-performance optoelectronic devices including solar cells, and photocatalysts. Phenomena which has been ever seemed impossible should be possible by exploiting the potential of the LSP resonance.

Publication lists

(As a first author)

(1) **Takeshima, N.**: Sugawa, K.; Tahara, H.; Jin, S.; Noguchi, M.; Hayakawa, Y.; Yamakawa, Y.; Otsuki, J. Combined Use of Anisotropic Silver Nanoprisms with Different Aspect Ratios for Multi-Mode Plasmon-Exciton Coupling. *Nanoscale Res. Lett.* **2020**, *15*, 15.

(2) **Takeshima, N.**; Sugawa, K.; Noguchi, M.; Tahara, H.; Jin, S.; Takase, K.; Otsuki, J.; Tamada, K. Synthesis of Ag Nanoprisms with Precisely-Tuned Localized Surface Plasmon Wavelengths by Sequential Irradiation of Light of Two Different Wavelengths. *Chem. Lett.* **2020**, Just Accepted.

(3) **Takeshima, N.**; Sugawa, K.; Tahara, H.; Jin, S.; Wakui, H.; Fukushima, M.; Tokuda, K.; Igari, S.; Kanakubo, K.; Hayakawa, Y.; Katoh, R.; Takase, K.; Otsuki, J. Plasmonic Silver Nanoprism-Induced Emissive Mode Control between Fluorescence and Phosphorescence of a Phosphorescent Palladium Porphyrin Derivative. *ACS Nano* **2019**, *13*, 13244-13256.

(As a coauthor)

(1) Jin, S.; Sugawa, K.; **Takeshima, N.**; Tahara, H.; Igari, S.; Yoshinari, S.; Kurihara, Y.; Watanabe, S.; Enoki, M.; Sato, K.; Inoue, W.; Tokuda, K.; Akiyama, T.; Katoh, R.; Takase, K.; Ozawa, H.; Okazaki, T.; Watanabe, T.; Otsuki, J. Precise Control of Localized Surface Plasmon Wavelengths Is Needed for Effective Enhancement of Triplet-Triplet Annihilation-Based Upconversion Emission. *ACS Photonics* **2018**, *5*, 5025-5037.

(2) Sugawa, K.; Tsunenari, N.; Takeda, H.; Fujiwara, S.; Akiyama, T.; Honda, J.; Igari, S.; Inoue, W.; Tokuda, K.; **Takeshima, N**.; Watanuki, Y.; Tsukahara, S.; Takase, K.; Umegaki, T.; Kojima, Y.; Nishimiya, N.; Fukuda, N.; Kusaka, Y.; Ushijima, H.; Otsuki, J. Development of Plasmonic Cu2O/Cu Composite Arrays as Visible and Near-Infrared-Light-Driven Plasmonic Photocatalysts. *Langmuir* **2017**, *33*, 5685−5695.

(3) Sugawa, K.: Uchida, K.; **Takeshima, N.**; Jin, S.; Tsunenari, N.; Takeda, H.; Kida, Y.; Akiyama, T.; Otsuki, J.; Takase K.; Yamada, S. Extraordinary enhancement of porphyrin photocurrent utilizing plasmonic silver arrays. *Nanoscale* **2016**, *8*, 15467-15472.

(4) Sugawa, K.; **Takeshima, N.**; Uchida, K.; Tahara, H.; Jin, S. Tsunenari, N.; Akiyama, T.; Kusaka, Y.; Fukuda, N.; Ushijima, H.; Tsuchido, Y.; Hashimoto, T.; Hayashita, T.; Ostuki, J. Photocurrent enhancement of porphyrin molecules over a wide-wavelength region based on combined use of silver nanoprisms with different aspect ratios. *J. Mater. Chem. C* **2015** *3*, 11439-11448.

(5) Sugawa, K.; Ichikawa, R.; **Takeshima, N**.; Tanoue, Y.; Otsuki, J. Development of highly thermoresponsive fluorescent sensors consisting of plasmonic silver nanoprisms and poly(N-isopropylacrylamide) – fluorophore composites. *Photochem. Photobiol. Sci.* **2015**, *14*, 870-874.

(6) Sugawa, K.; Tanaka, D.; Ichikawa, T.; **Takeshima, N.** Development of Plasmon Resonance Sensing Based on Alkylthiol-Coated Triangular Silver Nanoplates on Glass Plates. *J. J. Appl. Phys.* **2013**, *52*, 04CK06.

謝辞